UNIVERSITY OF BEIRA INTERIOR

Engineering

Persistent Gliding Waterframe

The Waterframe Conceptual Project

João Paulo Salgueiro Morgado

Thesis submitted for the degree of Master of Science in

Aeronautical Engineering

(2nd Cycle of Studies)

Supervisor: PhD Miguel Ângelo Rodrigues Silvestre

Covilhã, June 2011

This page has been intentionally left blank
for double side copying

"Try to become not a man of success,
but try rather to become a man of value"
(Albert Einstein)

This page has been intentionally left blank
for double side copying

Acknowledgments

There are many people whom I would like to thank for helping me over the last year in my research and studies that have made this thesis possible. These people have helped me in the classroom, in the laboratory and in all of the general day to day tasks that have occupied my time.

First, I would like to thank to my supervisor, PhD Miguel Silvestre for allowing me the opportunity to work with you. I would like to thank the fact that you received me in your house every week for skype meetings with UST's team. I was always made to feel comfortable and welcomed and I enjoyed each and every interaction I had with you.

Further, I would like to thank those whom I worked with during the project. This obviously includes the University of Saint Thomas team: the professor Christopher Greene, the students Josh Kleven, Matthew Deutsch, Sean Engen, Frances Van Sloun, Jim Giancola, and JB Korte and at last but not the least Engineer Scott Morgan for the opportunity that he gave me to participate in an international project and for everything I learned as a result.

At the same time, I would like to thank to all my friends, especially to Christian, Miguel, Tiago, Joaquim, Ricardo, Luís, Carlos and Andreia for the friendship, kindness, patience and constant support, never letting me give up.

I would also like to thank to laboratory technician, Mr. Rui Paulo, for all the support that you gave me during the prototype construction.

Finally and most importantly, I would like to thank to all my family, especially to my parents and my sisters for everything you did for me and for helping me keep it all in perspective.

Thank You

This page has been intentionally left blank
for double side copying

Abstract

Underwater gliders are autonomous vehicles that profile vertically by controlling buoyancy and move horizontally due to its wings.[14,17] At the top of a bounce, the glider decreases its buoyancy, which causes it to begin to sink. As the glider sinks, the hydrodynamic shape of the exterior (waterframe design) produces horizontal motion. The gilder uses a method of control to adjust pitch and roll as it continues forward. At the bottom of a bounce, the glider becomes more buoyant, which causes it to begin an upward path. Again, horizontal motion is produced by the shape of the waterframe and mainly by wings. When the glider reaches the surface, it will communicate with a ground station, sending out the data it collected during the dive and receiving instructions for its next trajectory.[5]

This type of vehicles can operate over long ranges and are relatively low cost [2] ocean research vehicles, making them the ideal choice for locate potential areas in the ocean that would be suitable for sea farming. The PGW will be equipped with sensors that will monitoring the underwater environment. The data collected from the PGW will help researchers monitor the fish population and even implement sea farming.

The driving customer requirements for the PGW include a four-month continuous operational runtime, the ability to produce a lower cost system than the current competitors, a two-year useful life before refitting, the ability to launch and recover the PGW from a boat or a dock, the ability to reach a maximum depth of 300 meters, the ability to navigate within 1000 meters of the PGW's intended course, and all fluids contained in the PGW must be biodegradable.

This thesis presents the development of the waterframe for small ($75\ kg$, $2{,}00\ m$ long) autonomous underwater vehicle with operating speeds about $0{,}4\ m/s$ and ranges up to$3\ 000\ km$. A half scale prototype was built and performance tests need to be done to evaluate waterframe's performance.

Keywords

AUV, glider, PGW, Persistent Gliding Waterframe, Autonomous glider, underwater vehicle, waterframe design, sea measurements

This page has been intentionally left blank
for double side copying

Resumo

Os planadores subaquáticos são veículos autónomos que se deslocam verticalmente controlando a sua flutuabilidade e se movem horizontalmente devido à presença de asas.[14,17] Quando se encontram à superfície, o planador diminui a sua flutuabilidade, o que faz com que comece a afundar. Enquanto o veículo afunda, a sua forma exterior produz movimento horizontal. O veículo usa um controlo para ajustar o ângulo de picada e de rolamento para se continuar a deslocar na trajectória correcta. Quando o planador atinge o ponto de profundidade máxima, começa a ficar menos denso que a água que o rodeia e mais uma vez a sua forma exterior e principalmente as asas, fazem com que se desloque horizontalmente. Quando regressa à superfície, o planador subaquático pode comunicar com a estação de controlo enviando os dados recolhidos durante o mergulho anterior e receber informações para o próximo mergulho.[5]

Os planadores subaquáticos podem operar durante longos períodos de tempo tendo por isso um grande alcance e um custo de operação relativamente baixo [2], fazendo com que sejam a escolha ideal para identificar, nos oceanos, potenciais locais para aquacultura. O veículo será equipado com sensores que monitorizarão o ambiente subaquático. Os dados recolhidos pelo planador ajudarão os investigadores a monitorizar os cardumes e a implementar a aquacultura.

Os requisitos do cliente para o PGW incluem 4 meses de operação contínua, a capacidade de produzir o veículo a um custo inferior ao dos concorrentes, a capacidade de operar em oceanos, 2 anos de vida útil antes de manutenção, a capacidade de poder ser depositado na água através de um barco ou de uma doca, a capacidade de chegar aos $300\ m$ de profundidade, a capacidade de navegar com um erro máximo de $1000\ m$ em relação à trajectória definida previamente e ainda o facto de todos os fluidos contidos no PGW terem de ser obrigatoriamente biodegradáveis.

Esta dissertação apresenta o desenvolvimento de uma plataforma para um veículo subaquático autónomo, pequeno ($75\ kg, 2{,}00\ m$ de comprimento) com velocidades de operação de cerca de $0{,}4\ m/s$ e alcance de cerca de $3\ 000\ km$. Foi ainda construído um protótipo a metade da escala e é necessário efectuar testes para avaliar a performance da plataforma desenvolvida.

Palavras-chave

Veículo Autónomo Subaquático, Planador, PGW, Planador autónomo, veículo subaquático, projecto conceptual, medições, oceano

This page has been intentionally left blank
for double side copying

Resumo Alargado

Esta tese surgiu no âmbito de projecto com um propósito específico: identificar, nos oceanos, potenciais locais para aquacultura. Esta forma de produção de alimento disponibiliza algumas das proteínas essenciais ao ser humano. O veículo resultante deste projecto estará equipado com um sensor óptico que contará o número de algas numa dada área do oceano. As algas encontram-se na base da cadeia alimentar oceânica e a sua contagem permite que os investigadores estimem e consigam controlar a população de peixes num dado local, ao mesmo tempo que permite ainda que consigam prever mais facilmente mudanças nos cardumes ao longo do tempo. Os dados recolhidos por este veículo irão ajudar os investigadores a implementar a aquacultura.

Os planadores subaquáticos podem operar durante longos períodos de tempo tendo por isso um grande alcance e um custo de operação relativamente baixo, fazendo com que sejam a escolha ideal para a tarefa descrita no parágrafo anterior. O princípio de operação dos planadores submarinos é ilustrado na Figura 1. Nesta figura é ilustrado um ciclo completo de operação de um veículo deste tipo.

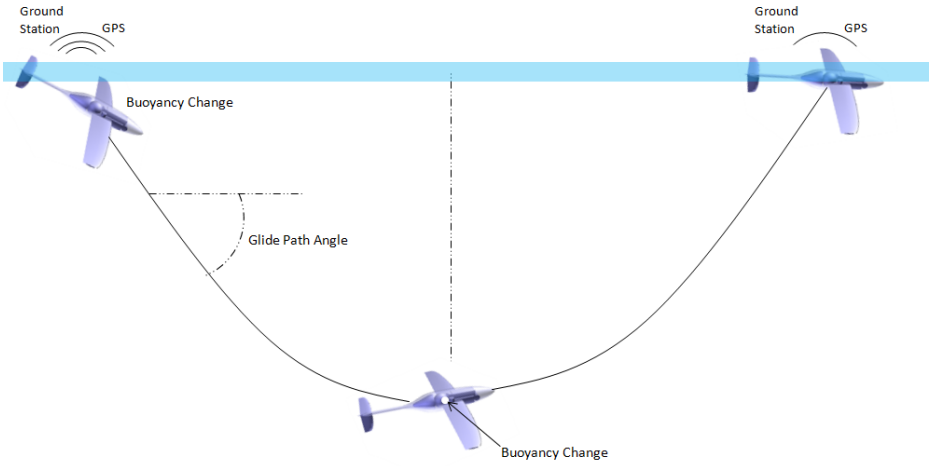

Figura 1 - Esquema de operação de um planador subaquático. [5]

Os planadores submarinos utilizam alterações da sua flutuabilidade para se conseguirem deslocar no plano horizontal. Para o veículo começar a descer fica ligeiramente mais denso que a água que o rodeia e ao iniciar o movimento descendente as asas começarão a produzir sustentação, o que impulsionará o veículo para a frente. Ao atingir a profundidade máxima, o planador fica ligeiramente menos denso que a água que o rodeia, para assim começar uma trajectória ascendente.

Devido à sua forma de converter o movimento vertical em movimento horizontal, os planadores subaquáticos têm um tipo de trajectória muito característica, sendo parecida com uma onda sinusoidal. Quando o veículo retorna à superfície pode então comunicar com a

estação de controlo enviando os dados recolhidos, permitindo ainda receber alterações à missão previamente introduzida.

O trabalho desenvolvido nesta tese de mestrado resulta do trabalho desenvolvido no 1º ano do projecto cujo principal objectivo foi projectar conceptualmente a plataforma que albergará todos os sistemas e sensores necessários à operação do veículo.

Todo o trabalho foi desenvolvido em cooperação com a equipa da Universidade de Saint Thomas, nos Estados Unidos da América e com o Engenheiro Scott Morgan, sendo estes responsáveis pelo resto dos subsistemas presentes na Figura 2.

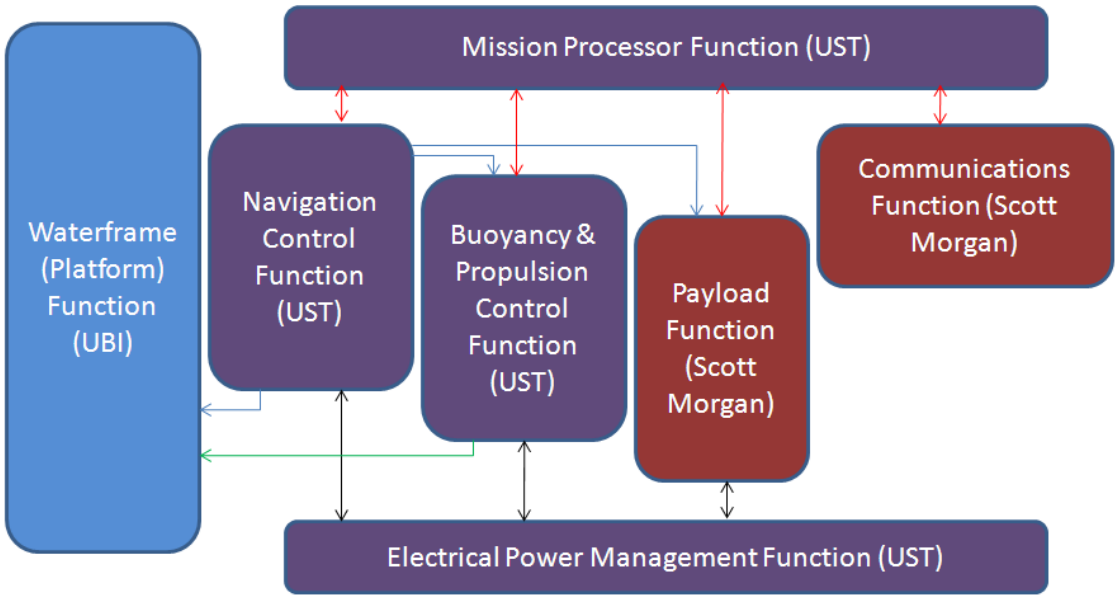

Figura 2 - Diagrama de funcionamento do projecto do PGW.

O trabalho desenvolvido nesta dissertação está, como se pode observar, na parte da *"Platform Function"*, ou seja, desenvolver uma plataforma que consiga albergar todos os sistemas necessários ao desempenho da missão.

Como este é um projecto a 5 anos, dos quais este foi apenas o 1º, o objectivo principal passou por um projecto conceptual com a adequada selecção dos conceitos aplicáveis, passando pelo cálculo de um ponto de projecto e depois pela definição geométrica do veículo em si. Foram ainda calculados os coeficientes de estabilidade do veículo, para permitir o estudo do seu controlo e estabilidade.

No final obteve-se uma plataforma optimizada, que cumpria os requisitos do projecto e foi ainda construído um protótipo a metade da escala para testes de performance a efectuar futuramente em piscina.

Table of Contents

List of Figures

This page has been intentionally left blank
for double side copying

List of Charts

This page has been intentionally left blank
for double side copying

List of Tables

This page has been intentionally left blank
for double side copying

Nomenclature

A_f → frontal area of vehicle $[m^2]$

AR → aspect ratio

AR_{fin} → fin aspect ratio

b_{fin}→ fin span

b → wing span $[m]$

B_x → center of buoyancy coordinate along xx

B_y → center of buoyancy coordinate along yy

B_z → center of buoyancy coordinate along zz

c_{d_0} → airfoil parasite drag coefficient

$c_{d_{airfoil}}$ → airfoil drag coefficient

$c_{d_{0_{waterframe}}}$ → waterframe parasite drag coefficient

$c_{d_{total}}$ → waterframe total drag coefficient

c_{p_l} → pressure coefficient lower surface

c_{p_u} → pressure coefficient upper surface

c_{fin} → fin chord

c_h → horizontal tail volume coefficient

c_l → lift coefficient

c_p → pressure coefficient

c_{root} → wing root chord

c_{tip} → wing tip chord

c_v → vertical tail volume coefficient

c_{wing} → wing mean chord[m]

d_{total} → total number of cycles

D → drag force $[N]$

dh → difference between initial and final depths

E_{dive} → energy spent per dive $[J]$

$E_{specific}$ → specific energy

E_{total} → total energy necessary for maximum range

e → Oswald factor

G_x → center of gravity coordinate along xx

G_y → center of gravity coordinate along yy

G_z → center of gravity coordinate along zz

g → gravitational acceleration

$h_{maximum\ depth}$ → maximum depth (surface was considered h=0)

h_1 → Initial depth

I_{xx} → moment of inertia of PGW $[kg * m^2]$

I_{xy} → moment of inertia of PGW $[kg * m^2]$

I_{xz} → moment of inertia of PGW $[kg * m^2]$

I_{yy} → moment of inertia of PGW $[kg * m^2]$

I_{yz} → moment of inertia of PGW $[kg * m^2]$

I_{zz} → moment of inertia of PGW $[kg * m^2]$

L/D → glide ratio

l_{dive} → distance traveled per dive cycle $[m]$

l_h → horizontal tail arm from center of gravity $[m]$

l_v → vertical tail arm from center of gravity $[m]$

l → distance traveled $[m]$

L → lift force $[N]$

n_s → number of spheres

p_∞ → freestream static pressure

p_c → roll rate$[rad/s]$

p → static pressure

q → dynamic pressure

R → range $[m]$

r → yaw rate $[rad/s]$

r_{body} → body radius

Re_{exp} → exponential Reynolds number for Mark Drela model

Re_{ref} → reference Reynolds number for Mark Drela model

Re_V → volume Reynolds number

Re → Reynolds number

S_{fin} → individual fin area

S_h → horizontal tail area $[m\text{^}2]$

S_{tail} → tail area $[m\text{^}2]$

S_v → vertical tail area $[m\text{^}2]$

S → wing area $[m\text{^}2]$

t_{dive} → time per dive cycle

t_{total} → total time for maximum range

t → airfoil thickness

u_0 → variation of speed along the x-axis

v_∞ → freestream velocity

V_{body} → body volume

$V_{buoyancy}$ → buoyancy volume $[m\text{^}3]$

v_c → variation of speed along the y-axis

$v_{horizontal}$ → horizontal velocity

v_{max} →maximum velocity $[m\ /\ s]$

v_{min} → minimum velocity $[m\ /\ s]$

V → half of buoyancy volume $[m\text{^}3]$

v → velocity of vehicle $[m\ /\ s]$

W → maximum propulsive force $[N]$

w → variation of speed along the z-axis

x/c → position of station

X_{CoG} → position of center of gravity in x-axis

x_t → maximum thickness point

Y_{CoG}→ position of center of gravity in y-axis

Z_{CoG}→ position of center of gravity in Z-axis

γ→ trajectory angle [°]

λ →taper ratio

μ → dynamic viscosity of seawater $[Pa * s]$

ν → kinematic seawater viscosity $[m\text{^}2/s]$

ρ → density of seawater $[kg\ /\ m\text{^}3]$

This page has been intentionally left blank
for double side copying

1 - Introduction

1.1 Motivation

Some three-quarters of the Earth's surface is covered by water and only about 0.1% of oceans bottoms have been explored.[1]

Historically, the ocean bottoms has been mainly observed using instruments lowered from research ships or, later, suspended from moorings. The relatively high cost of these observation platforms has limited their number and, consequently, the spatial and temporal density at witch oceans has been observed.[2]

To solve this problem began to be developed the Autonomous Underwater Vehicles (AUVs) and in particular the Autonomous Underwater Gliders.

With this vehicles it is now possible for the scientists make more complex studies on topics such as the effect of metals, pesticides and nutrients on fish abundance, reproductive success and ability to feed or on contaminants such as chemicals such as chemicals or biological toxins that are transported in particulate form and become incorporated into living organisms (plankton, bivalves, fishes) or become deposited in bottom sediments.[3,4]

This vehicle, however, has a different specific purpose: locating potential areas in the ocean that would be suitable for sea farming. These farms would provide sources of protein to nations that are in need of food. The PGW will be equipped with an optical sensor that counts the number of blue-green algae in a given area of the ocean. Blue-green algae are at the bottom of the oceanic food chain and counting them allows researchers to estimate and track the fish population in given locations, and make predictions for changes in populations over time. The data collected from the PGW will help researchers monitor the fish population and effectively implement sea farming.[5]

1.2 Objective

The objective of this work is developing the waterframe for a low cost, effective, efficient sea glider, autonomous underwater vehicle (AUV) that can be produced in mass quantities.

1.3 Overview

Chapter 1 provides the motivation for the development of this vehicles and the objective of this thesis.

Chapter 2 presents a brief historic development of underwater vehicles and their applications. In addition presents a competing product review and some scientific research like airfoil design, wing design and possible fuselage shapes.

Chapter 3 shows a table with customer requirements, which should be guaranteed in all design process.

Chapter 4 provides some specific concepts as initial study to begin the design of a new vehicle.

Chapter 5 demonstrates how was calculated the design point and the performance specifications of the vehicle.

Chapter 6 shows the final geometry and dimensions of the different subparts of the vehicle.

Chapter 7 provides the stability coefficients calculation for the designed vehicle.

Chapter 8 shows the construction of different parts of half scale prototype.

2 - Bibliographic Review

2.1 Underwater Vehicles

2.1.1 History

To understand the development process of underwater vehicles we shall first explore previous research conducted in development of this type of vehicles.

Underwater vehicles were invented to address scientists frequent need to monitor underwater areas over long periods of time. This job, like we saw before, was very expensive when were used ships or even manned submersibles. [6]

The first research in this area resulted from the need to study arctic under ice profiles in the late 1950s. Murphy *et al (1957)* was developed "*Special Purpose Underwater Research Vehicle*" (SPURV) in the Applied Physics Laboratory at the University of Washington. This underwater vehicle was machined by Boeing from a forging 7078-T6 aluminum alloy. [4]

The SPURV was operated at $2{,}2\ m/s$ for close to 6 hours. The vehicle had a maximum depth of$3\,000\ m$, could communicate acoustically with the surface and was autonomously at constant pressure, between two depths, or a constant climb or dive angle.

The French Research Institute for Exploitation of the Sea, IFREMER, designed and developed Epulard in 1976, and deployed it for the first dive in 1980. This vehicle also was acoustically controlled and had a maximum depth of $6\,000\ m$. Epulard successfully completed about 300 dives between 1980 and 1990.

The vehicle was capable to maintain a constant altitude above the ocean bottom by dragging a cable.[7]

In the end of 1970s at Naval Ocean Systems Center was developed the *"Advanced Unmanned Search System"* (AUSS). This vehicle was launched a first time in 1983 and completed over 114 dives up to a depth of $6\ km$. [8]

The AUSS was $5{,}2\ m$ long, $0{,}8\ m$ in diameter had silver zinc batteries and it had an acoustic communication system that transmitted video images through the water. The vehicle was compact and portable, easily fitting on an offshore supply boat. The center section of vehicle was a cylindrical graphite epoxy pressure hull with titanium hemispherical ends. The free flooded forward and aft end fairings and structure were made of Spectra, a nearly buoyant composite.[9]

Busby's et al. wrote Undersea Vehicle Directory, where they mentioned that there were six operational AUVs and an additional 15 others under construction.

In the early of $90s$ the interest in UAVs began to significantly pick up and many others vehicles were developed.

The Massachusetts Institute of Technology's Sea Grant AUV lab developed six Odyssey vehicles during the early 90's. These vehicles displaced $160\ kg$, could operate at $1{,}5\ m/s$ for up to six hours, and were rated to $6\,000\ m$. Odyssey vehicles were operated under ice in

1994, and to a depth of $1{,}4\ km$ for 3 hours in the open ocean in 1995. [10] Odyssey vehicles were also used in support of experiments demonstrating the Autonomous Ocean Sampling Network during this period [11]. The schematic of odyssey is represented on Figure 2-1.

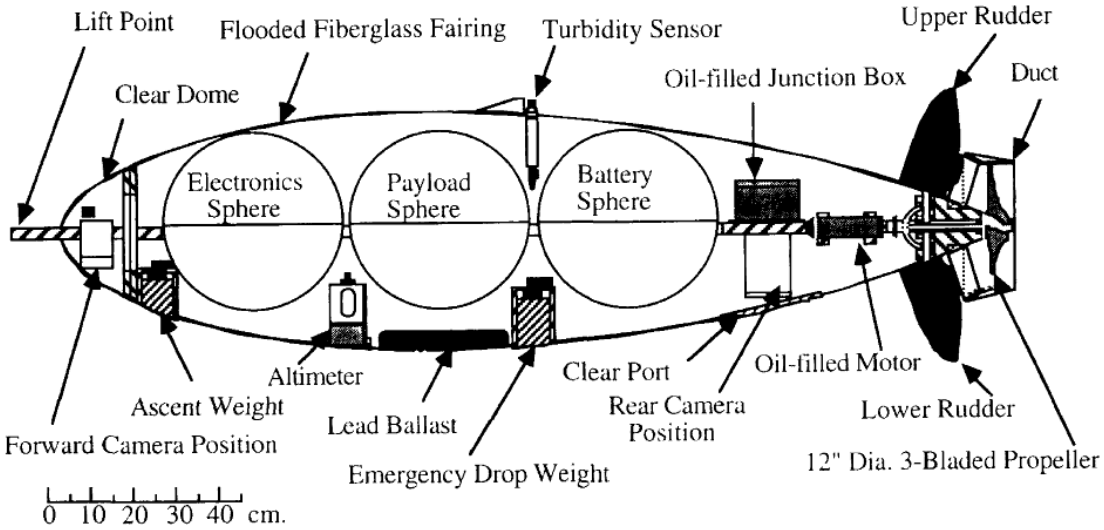

Figure 2-1 - Schematic of Odyssey. The outer faired surface is a low drag form. A ducted propeller minimizes fouling. Steering is by cruciform control surfaces.

In the early 90's the Woods Hole Oceanographic Institute (WHOI) created the "*Autonomous Benthic Explorer*" (ABE). The ABE was the first vehicle completely independent of the surface vessel and capable of covering large areas of underwater terrain.

ABE had a gross weight of $500\ kg$ and made approximately 80 dives to the deep seafloor. Typical dives lasted about $16 - 34$ hours depending on the instrument payload and the bottom terrain. Later, were made some modifications that included a multibeam sonar (SM2000), which was used on a recent survey of the Explorer Ridge. [12]

At the same time, in South Hampton Oceanography Center was developed the first vehicle prepared for long duration mission. The AUTOSUB is a long range, deep diving, autonomous underwater vehicle. It displaces $1700\ kg$ can travelling at $1{,}5\ m/s$ and has 6 days operation time. It has 271 completed missions and travelled about $3600\ km$. Long mission lasted 50 hours and Stub travelled $260\ km$. [13]

In the late 90's WHOI introduced REMUS, an AUV displacing $36\ kg$, to support scientific objectives. It could operate for 20 hours at a speed of $1.5\ m/s$ at up to $100\ m$ depth. Hundreds of people have been successfully trained in the use of REMUS vehicles. It is not possible to determine how many missions have been performed by REMUS. [8]

The second half of the 1990's saw increasing funding and support of the glider concept from the Office of Naval Research, in part as an element of the AOSN initiative. This led to three programs to design and develop oceanographic gliders: the Slocum glider at WRC, Seaglider at University of Washington, and Spray at SIO. Within the last ten years, these groups have developed these underwater gliders and deployed them in large-scale

oceanography projects. These three glider designs are now approaching the end of their development phase [14]. Gliders also show great potential in other applications. Recent studies show exciting possibilities for glider performance and future designs. [15]

The year 2002 saw the first commercial sales of gliders. These electric Slocum gliders sold by WRC to WHOI are the first to be operated by a group that had not built the glider themselves. Early operations by the WHOI Glider Lab took place in Buzzards Bay, off Cape Cod, Massachusetts. In January 2003 that laboratory, directed by David Fratantoni, deployed three Slocum Electric gliders in operations from a vessel in the Bahamas. Tests of a thermally driven Slocum glider were conducted by WRC concurrently. [3]

In Japan, the $1.4m$ long, $45\ kg$ ALBAC was designed as a one-profile glider with a maximum depth of 300m. It used wings to control its motion through the water on descent, and on reaching its destination depth, dropped a weight to return, gliding upwards to the surface. [16]

2.1.2 Underwater Gliders - A particular type of underwater vehicles

Henry *Stommel* envisioned a world ocean observing system based on "a fleet of small neutrally-buoyant floats called Slocums" that "migrate vertically through the ocean by changing ballast, and they can be steered horizontally by gliding on wings at about a 35 degrees angle . . . During brief moments at the surface, they transmit their accumulated data and receive instructions . . . Their speed is generally about $0{,}5\ knot$." [2]

An underwater glider is a type of buoyancy propelled, fixed wing underwater vehicle without external active propulsion.[17] They alternately reduce and expand displaced volume to dive and climb through the ocean. Unlike floats, gliders additionally carry wings and control their pitch attitude to effectuate a horizontal speed component through the ocean.[14]

Buoyancy control, coupled with hydrodynamic lift is a natural choice for a platform designed to both profile and traverse the stratified ocean where gradients are near vertical and the tilt of surfaces is of key importance. Sensible sampling dictates glide slopes steep compared to isopleths, hence ocean gliders need not attain the shallow slopes of sail planes in the atmosphere.[14]

Gliders must have both long range and high endurance to be an effective alternative to ships. Glider economy stems from long range small size, remote control, and modestly priced data communication. Their small size allows them to be launched from a small boat and recovered few months later for reuse.

Range and endurance are highly dependent on mission objectives and the operating environment. Typically, in battery powered gliders, $80\% - 85\%$ of available energy is intended to power and only $15\% - 20\%$ is devoted to control, sensors and other systems.[2]

The high pressure pumps used to change buoyancy are usually inefficient at low pressure, so that deeper dives result in much longer range. Deeper dives also tend to encounter less current on average, which means an increased range over the ground.

The ratio between horizontal speed and vertical speed (glide slope) equals lift over drag and is typically 2 to 4, much less than for an aeronautical glider but comparable with NASA Space Shuttle.[18]

Nowadays, underwater gliders are entirely autonomous, despite their operation can be controlled with two-way satellite communications.[16] When it is given a set of mission parameters, gliders follow them until they are changed or mission ends.

2.1.3 Applications

The first application of underwater gliders, and the inspiration for their development, has been oceanographic data collection. The importance of understanding the oceans and their role in the planet's ecosystem cannot be overstated. Progress in oceanography depends in part on the gathering of scientific data from the oceans. Because of the distributed nature of ocean dynamics, data is needed over a wide temporal and spatial range. Progress in oceanography depends in part on the gathering of scientific data from the oceans. Because of the distributed nature of ocean dynamics, data is needed over a wide temporal and spatial range.

Gliders can be used in remote sensing for physical, chemical and biological oceanography by a low operating cost. [3]

The underwater gliders are inexpensive, offer a superior scientific sampling (depending of the installed sensors, they can do a large variety of measures over a long period of time). They may also be operated in coordinated groups and easily launched and recovered from an ocean going ship or even from a dock that has access to the world's oceans.

Some alternative methods to the underwater gliders are the use of ships, the use of fixed moorings or even the use of drifters, but ships are expensive to operate and are limited in number and availability. Fixed moorings just give data around a fixed location, while drifters cannot choose their path through the ocean.

The characteristic saw tooth motion gliders make is also well suited to oceanographic sampling. Variations of ocean water properties are generally much stronger in the vertical than horizontal directions, making vertical sampling important in oceanographic applications. For this reason, propeller driven AUVs and towed arrays are often flown in a vertical saw tooth pattern for data collection.

A typical mission of an underwater glider includes repeatedly surveying an area of the ocean over a long period or maintaining their position against ocean currents.

Oceanographic sampling also calls for the deployment of groups of gliders. In summer 2003, as part of the Autonomous Oceanographic Sampling Network II (AOSN II) experiment,

seventeen gliders were deployed in the Monterey Bay, California, over a six-week period. [19]

As part of the experiment, the network of gliders performed adaptive sampling missions for specific purposes including updating and evaluating forecast models. This application made use of the gliders as a re-configurable sensor array and took advantage of the available data from the sampling network to plan glider trajectories. [19]

Some examples of other underwater gliders applications can be easily achieved. Military applications such as tactical oceanography and maritime reconnaissance that is some quiet different from oceanographic science for which they were invented. Military applications include use the vehicles as communications gateways or navigation aids. Gliders can also be operate in both deep ocean and coastal environments. [20]

Because they do not have thrusters and use internal actuators, gliders are very quiet. This is very useful for military applications, because quieter vehicles are more difficult to be detected by the enemy.

2.2 Competing Products Review

In this section will be described the designs of existing gliders which some of them are similar to PGW project objectives. This is intend to show the present state of the art in underwater gliders and to guide the development of this glider design.

Three buoyancy driven autonomous underwater gliders, Slocum, Spray and Seaglider have been developed and deployed in the United States of America.

Spray was developed from Scripps Institution of Oceanography (SIO), Seaglider from University of Washington and Slocum from Woods Hole Oceanographic Institution.

In Japan, at the University of Tokyo have been developed an underwater glider called ALBAC. This vehicle is driven by a drop weight instead of a ballast system. [21]

At "*École Nationale Supérieur D'Inginiéurs*", in France was developed a vehicle whose name is STERNE. STERNE is a hybrid vehicle with both ballast control and a thruster. [22]

2.2.1 Spray

The Spray underwater glider was developed at Scripps Institution of Oceanography, is meant to fill the need for a relatively long-lived vehicle to observe ocean physics and biology. In trying to define the general circulation, or climate variability like the El Niño-Southern Oscillation (ENSO), mesoscale variability is the main source of competing noise. For biological communities the mesoscale represents an often-dominant perturbation to be observed. The main confusing noises in describing the mesoscale are quasi-diurnal phenomena like the diurnal cycle, internal tides, inertial waves, and weather events. To describe the typical seasonal state, or to define typical relations occurring on the mesoscale, it is necessary to observe many mesoscale realizations, which translates to years of operation.

The design missions for spray glider are a combination of three archetypes: time series, transects, and roving assistants to research cruises.

The Spray oceanographic glider is two meters long and has a mass of $51\ kg$. Spray has a range about to $7000\ km$ at $0{,}27\ m/s$. It uses lithium batteries, which have better energy density and performance than alkaline batteries. [23] Spray has a cylindrical pressure hull with two wings and a vertical tail. The hull employs a finer entry shape than the Webb Research Corporation glider hull, which has about 50% higher drag. [23] A flooded fairing forms the rear of the hull and houses the external oil-filled bladder for the ballast system.[3]

This underwater glider is optimized for long-duration, long-range, deep ocean use where the emphasis is on energy efficiency. Spray oceanic glider employs a high-pressure wobble-plate reciprocating pump and external bladders in the same hydraulic configuration as ALACE floats. [24] GPS and satellite communication antennas are housed in a wing that is rolled vertical during communication like is shown in Figure 2-2.

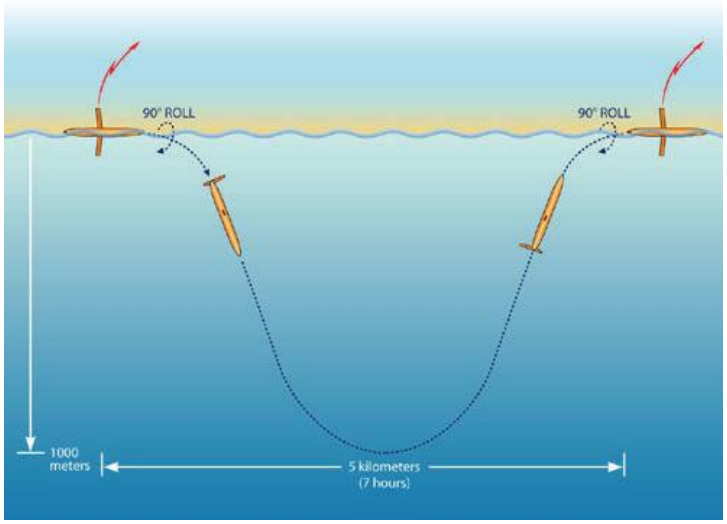

Figure 2-2 - Spray's method of travel (Spray 2008b) [4]

The vertical stabilizer houses an emergency-recovery antenna. Scientific sensors may be mounted on the hull or aft of the pressure hull in the flooded compartment which supports the vertical stabilizer.

Glide control in Spray is achieved using two internal moving masses: one for pitch and other for roll. The pitch battery pack has a range of travel of $0{,}1\ m$ and moving vehicle's center of gravity.[3] The roll actuator is also a battery pack, but located in the nose of the vehicle and can rotate 360 degrees, as we can see in Figure 2-3.

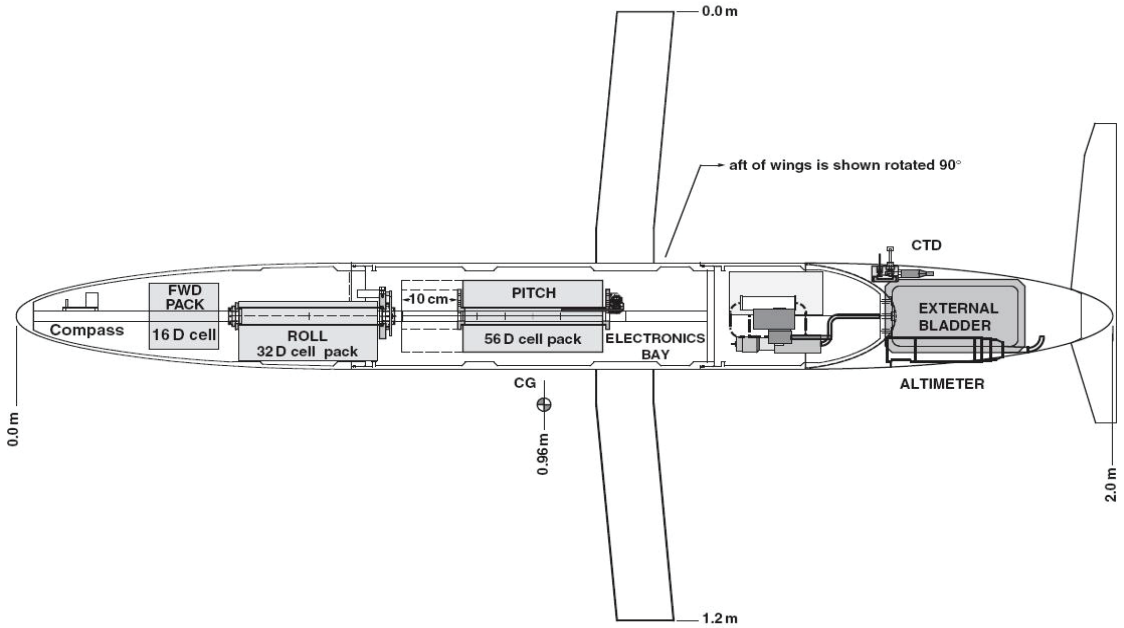

Figure 2-3 - Spray Schematics (Spray 2008b) Forward of the wings is a top of view, aft is a view from the port side. The hull is formed by three pieces. Separate battery packs are moved to control pitch and roll. Antennas are enclosed in a wing that is rolled vertical on the surface. An aft flooded section houses hydraulic bladders and some science sensors. [4]

To maneuver, Spray is initially starts by rolling. This gives a horizontal component to the lift vector and induces vehicle starting sideslip in the plane of the wing in the direction of the buoyant force. The horizontal component of lift provides the centripetal force for turning while sideslip acting on the vertical stabilizer produces the yaw moment needed to change vehicle heading. For example, to turn right during descent phase, the right wing is dropped, like a conventional airplane, which generating a lift component to the right that drives the vehicle to the right. Sideslips down and to the right acts on the vertical stabilizer causing the nose to yaw to the right. To turn right in ascent the glider is rolled oppositely by dropping the left wing.

2.2.2 Slocum Battery

The Slocum Battery was developed from Webb Research Corporation and it is comprised of three main separate hull sections in addition to two wet sections located fore and aft. The cylindrical hull sections are made in $OD\ 6061\ T6$ aluminum alloy chosen due to its simplicity, economy, and expandability. The nose end cap is a machined pressure resistant elliptical shape, and the tail cap a truncated cone to allow for penetrator surface.

Slocum has fixed wings, with one meter span. The wing sections are flat plate and they are made in composites and are easily replaced. [25] The wings are swept 45 degrees because in all operations, particularly coastal work, there is a risk of entraining weed on the wings causing major degradation in gliding performance. [25]

The tail has $0{,}3\,m$ long and houses the antenna for GPS and communications. Horizontal tail surfaces are not required since pitch stability is provided by the wings, which are mounted aft of the center of buoyancy.[26]

This glider is electrically powered, its operational envelope includes a $200\,m$ depth capability and a projected $30\,days$ endurance, which translates into approximately $1000\,km$ operational range with a $0{,}4\,m/s$ fixed horizontal speed and $0{,}2\,m/s$ vertical speed.

The Slocum Glider has $1{,}8\,m$ long, $0{,}21\,m$ in diameter and his mass is approximately $52\,kg$. It maneuvers through the ocean in sawthooth-shaped gliding trajectory. It is controlled by two different methods. The pitch and roll are controlled by translating and rotating the internal battery packs. [4] A rudder controls the turning rate and the pitch and the buoyancy ate the surface are aided by the inflation of a bladder.

The glider has two onboard computers, a control computer and a science computer. Navigation sensors on the glider measure heading, pitch, roll, depth, sliding mass position and the piston drive position. These readings are recorded and processed by the control computer. Vehicle position at the surface is determined by a GPS receiver. Note that while submerged the glider velocity and horizontal position are not sensed because of the difficulty in measuring these states. [3]

The Slocum glider can be programmed to navigate in various ways. For a typical mission scenario the glider navigates to a set of preprogrammed waypoints specified by the operator. A mission file with these waypoints, desired glide path angles, speed, and other parameters, may be transmitted to the glider before the start of the mission. The glider is then capable of operating autonomously and navigating with dead reckoning and closed-loop pitch and heading control.

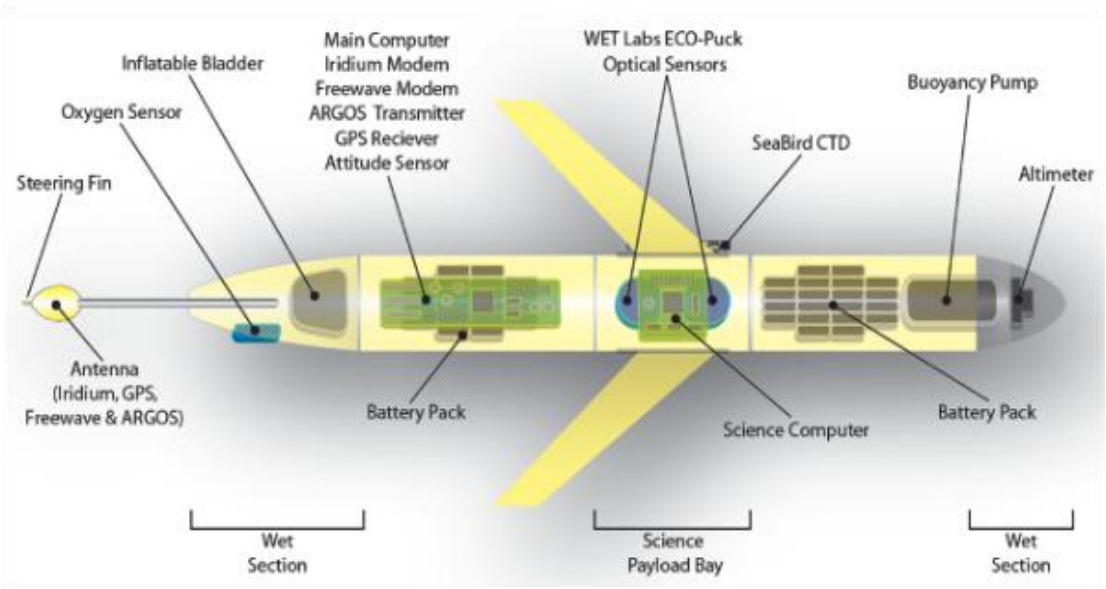

Figure 2-4 - Slocum Schematics. [25]

2.2.3 Slocum Thermal

The Slocum Thermal glider was developed and optimized for long duration missions. The Slocum thermal glider harvesting the energy needed for its propulsion from the ocean's temperature gradient.

In missions with electric-powered gliders, 60-85% of the energy is consumed into propulsion. [2,4] A thermal-powered glider may have a range $3-4$ times that of a similar electric powered vehicle. [4]

Slocum Thermal propulsion depends on the volume change associated with melting a material with a freezing point in the range of ocean temperatures. In warm surface waters the working fluid is heated, melts and expands. This expansion compresses an accumulator where energy is stored. Descent is initiated by transferring fluid from an external bladder to an internal reservoir. At temperatures colder than freezing point of fluid used, the freezing contraction draws fluid out of the internal reservoir into the heat exchanger. For ascent, energy stored in the accumulator does the pressure-volume work and the cycle repeats. This method of propulsion can be better understood on Figure 2-5. The heat exchange volume is inside tubes that run the vehicle's length (see Figure 2-6) and provide a large surface area for rapid heat flow.

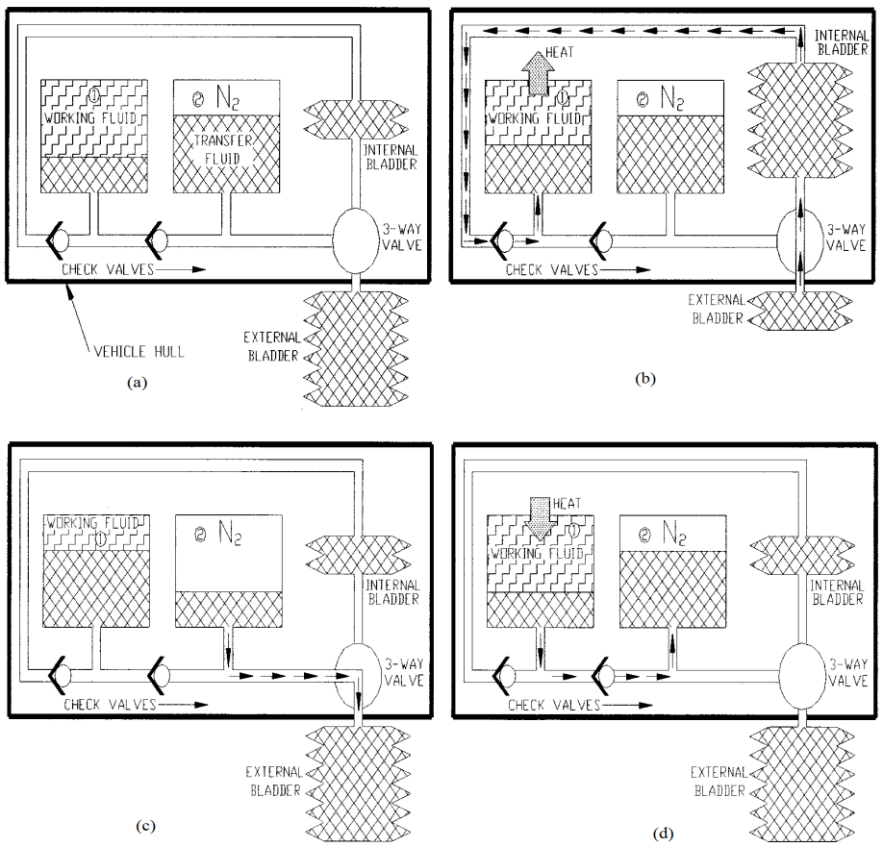

Figure 2-5 - Slocum's thermodynamic cycle. (a) Equilibrium conditions at surface before descent. (b) Descent with heat flow to water. (c) Beginning of ascent. (d) Ascent, heat flowing from water, returned to equilibrium as in (a). [26]

Slocum Thermal is controlled by changing the position of the center of gravity with respect to the center of buoyancy, thus controlling both pitch and roll. As in Slocum Battery, roll results in a yaw moment thus steering the glider. The main battery is eccentrically mounted and supported on a carriage equipped with pitch and roll actuators. Most of the pitch moment is generated by the movement of fluid in the main buoyancy changer, and the moment due to controlled movement of the battery is used for fine adjustment of pitch angle. [26]

The outer shape of the Slocum Thermal is very similar to Slocum Battery, which was previously described. Maximum depth of Slocum Thermal is $1200\ m$ and his horizontal speed is close to $0{,}25\ m/s$ at $40°$ dive angle. The vehicle weights approximately $50\ kg$ in air, and has a maximum diameter of $0{,}21\ m$.

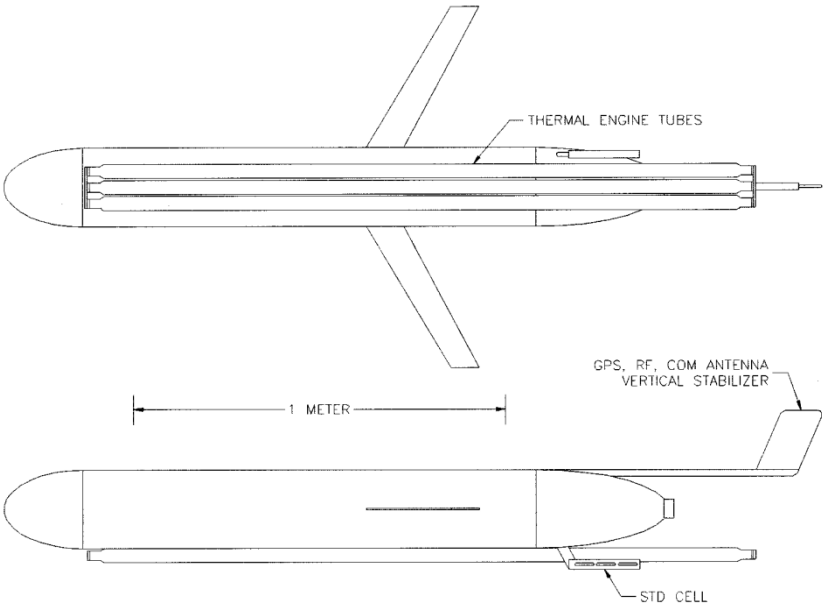

Figure 2-6 - Outer shape of Slocum Thermal Glider. [26]

2.2.4 Seaglider

Seaglider was developed at University of Washington Applied Physics Lab, and its purpose is doing extended oceanographic sampling missions. Seaglider is enclosed in a hydrodynamic fiberglass fairing supporting wings, a vertical stabilizer and trailing antenna staff. His hull is made up of an internal pressure hull and an external fairing. The fairing is $1{,}8\ m$ long with $0{,}3\ m$ maximum diameter and is free flooding. The fairing is a low-drag hydrodynamic shape and retains a laminar boundary layer forward of this maximum-diameter point. Due to different design philosophy used than other gliders, its shape is derived from a low drag laminar flow shape used by the U.S. Navy in target drones. The shape was designed to reduce pressure drag by developing a favorable pressure gradient at the rear of the vehicle. It is possible to see the fairing shape in Figure 2-7. [3]

It has a range of $6000\,km$ and has a mass of $52\,kg$ in air. A curious aspect is that Seaglider has an internal isopycnal hull, which is a hull with same compressibility as seawater. This special hull reduces the ballast pumping requirements: "this feature extends vehicle range by as much as fifty percent over a conventional stiff hull" [27].

The Seaglider has a fixed wing with one meter span and vertical tail fins located above and below the body. The vehicle efficiently maintains position in weak currents by pitching to near vertical and using minimal buoyancy forcing.

Buoyancy control is provided by ALACE's hydraulic system. Movement of internal masses controls gliding and pitches the vehicle forward to raise the trailing antenna mast during communication and navigation. The wing is so far aft that the turning dynamics are opposite that of Spray. In descent phase, to turn right, the vehicle's left wing is dropped so that lift on the wing drives the stern to left, overcoming lift off the vertical stabilizer, and initiating a turn to the right. Hydrodynamic lift on the side slipping hull produces the centripetal force to curve the course. However, in ascent phase a roll to the left side produces a left turn. [2]

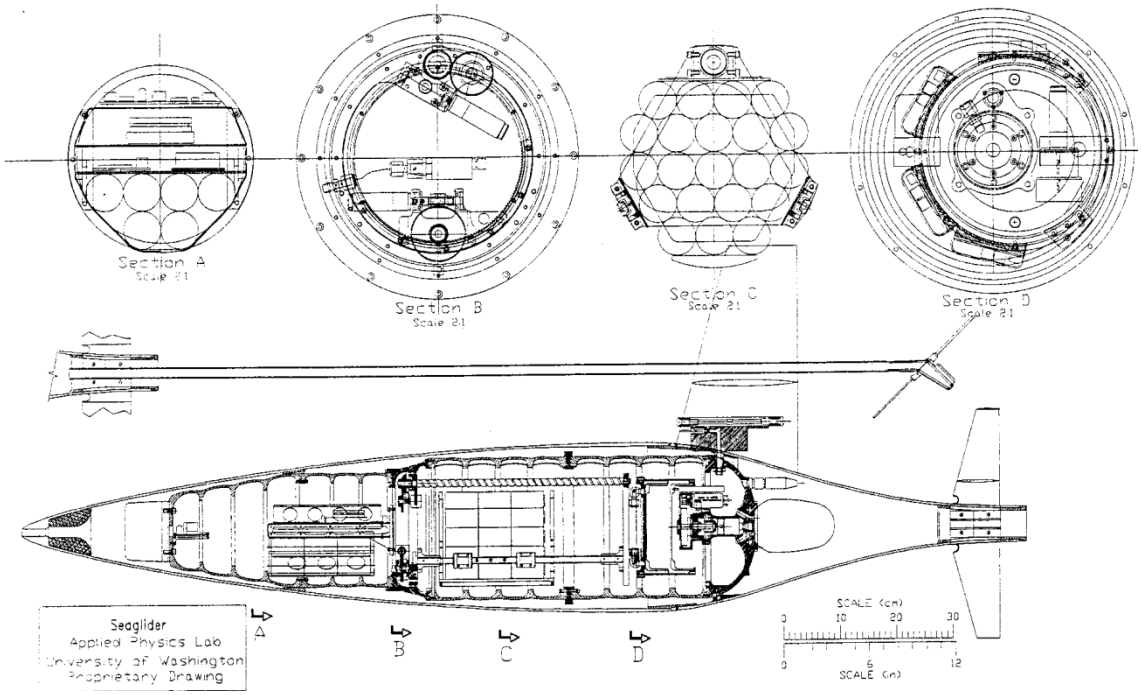

Figure 2-7 - Schematic design of Seaglider. The Bottom shows a side view with the wing shape provided above for reference. The antenna mast is shown separately above the fairing and pressure hull. Four cross sectional views at an expanded scale are shown at the top of the figure.[27]

2.2.5 ALBAC

The ALBAC was designed and constructed in 1992 in Sugura Bay, Japan. The glider was developed at the University of Tokyo in the laboratory of Tamaki Ura for oceanographic measurement of water column and from sea bottom observation. [21] This design is notable because it is a shuttle type glider designed to conduct dives from a ship and does not have a

buoyancy control system. ALBAC is driven by a drop weight which it carries on one downward glide and then releases to ascend back to the surface, conducting a single trip to depth between deployment and retrieval.

To control the attitude and trajectory, an actuator system displaces the location of the center of gravity longitudinally and laterally by moving a weight like Seaglider. Because it has no ballast pump, ALBAC carries batteries to power only its instruments and actuators.

The ALBAC has fixed wings and a vertical and horizontal tail. Since it has wings ALBAC can move horizontally without consuming energy of batteries by gliding up to 20 degrees down from the horizontal plane. It is $1{,}4\,m$ long, weighs $45\,kg$, and can dive to depths of $300\,m$ at speeds of $0{,}5\,to\,1\,m/s$. It has horizontal tail fins which change angle at inflection from downwards to upwards gliding, a feature not present in other gliders. The wings and tail are larger in comparison to the body than on Slocum, Spray or Seaglider.

ALBAC carries flight sensors including compass, depth, pitch, roll, and a propeller-type water speed indicator.

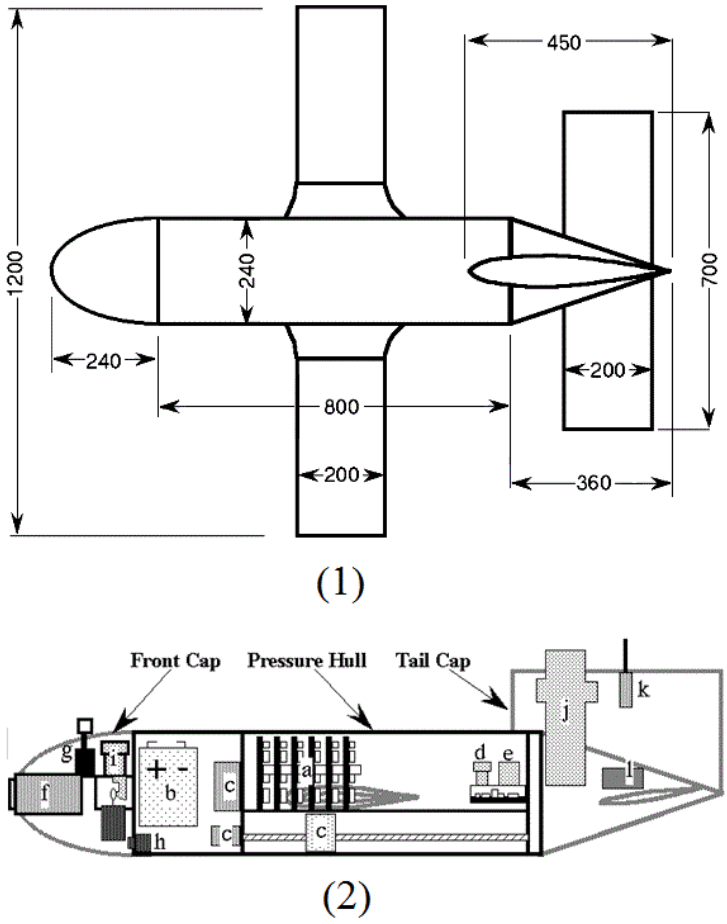

Figure 2-8 - (1)-Top view of ALBAC with the general dimensions. **(2)-** ALBAC schematic. a)CPU, b)Power Supply, c)Actuators, d)Gravity Sensor, e)Magnetic Sensor, f)Ranging Sensor, g)Velocity Sensor, h)Depth Sensor, i)Deballastor, j) Transponder, k)Thermistor, l)Tail Angle Trigger.[21]

2.3 Airfoil Design

The airfoil shape variation has deterministic effect on the aerodynamic coefficients. The ideal shape of an airfoil depends mainly on the angle of attack, Reynolds number, Mach number, surface roughness and fluid turbulence. [28]

Some airfoils are designed to produce low drag (and may not be required to generate lift at all) while other airfoils may need to produce low drag while producing a given amount of lift. In some cases, the drag does not really matter - it is maximum lift that is important.

In this section will be presented the influence of different parameters in airfoil performance as well as some different airfoil design methods.

2.3.1 Airfoil Geometry

The geometry of an airfoil can be characterized by its both upper and lower surfaces coordinates, but there are a few more parameters that can be used to describe and characterize an airfoil such as: nose radius, maximum camber, and maximum thickness, position of maximum camber and position of maximum thickness. In Figure 2-9 it is possible observe all of these parameters which allow the characterization of airfoils.

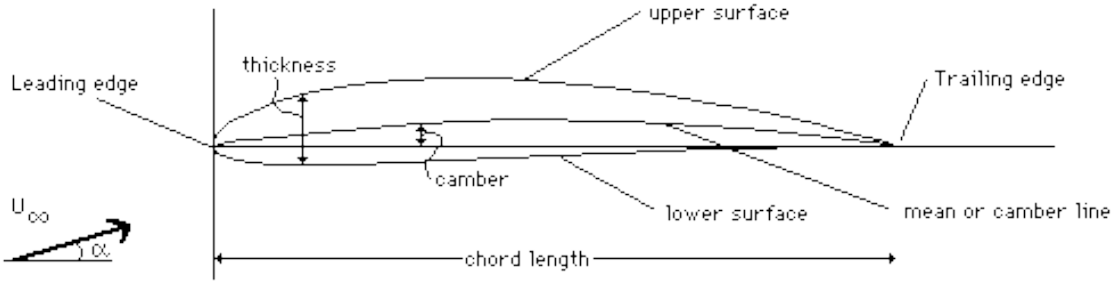

Figure 2-9 - Airfoil Geometry. [29]

2.3.2 Airfoil pressure distributions and performance

The performance of airfoils can be easily studied by reference to the distribution of pressure over the airfoil. This distribution is usually given by:

$$c_p = \frac{p - p_\infty}{\frac{1}{2}\,\rho\, v_\infty^2} \qquad 2.3\text{-}1$$

Pressure coefficient (c_p) is the difference between local static pressure and freestream static pressure, nondimensionalized by the freestream dynamic pressure. [29]

This coefficient is ever lower than 1 and depends on the geometry of the airfoil that being analyzed. On Chart 2-1 is presented a plot of $c_p \; vs \; {}^{x}/_{c}$. ${}^{x}/_{c}$ varies from 0 (at leading edge) to 1 (at trailing edge).

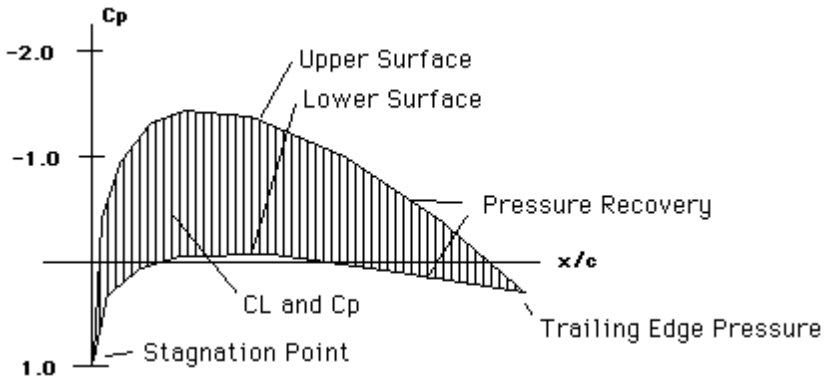

Chart 2-1 - Typical c_p distribution. c_p is plotted "upside-down" with negative values (suction), higher on the plot. This is done so that the upper surface of a conventional lifting airfoil corresponds to the upper curve. [29]

At upper surface pressure is lower (usually is plotted higher) than on the lower surface, but it does not have to be. Sometimes, the lower surface carries a positive pressure (usually plotted lower) but in Chart 2-1 is possible observe some suction present near the midchord.

The region of pressure distribution is called the pressure recovery region. In this region pressure increases from its minimum value to the value at the trailing edge. This region is also known as the area of adverse pressure gradient and this adverse pressure gradient is associated with boundary layer transition and possible separation if the gradient is to severe.

For a symmetric airfoil and angle of attack, $\alpha = 0$, c_p is maximum at leading edge and its value is about 1. For infinitely thin sections $c_p = 0$ at the trailing edge.

With c_p distributions we can achieve c_l, which are given by:

$$c_l = \int c_{p_l} - c_{p_u} \, d \; {}^{x}/_{c} \qquad 2.3\text{-}2$$

The performance of an airfoil is directly related to the shape of pressure distribution as indicated on the Chart 2-2.

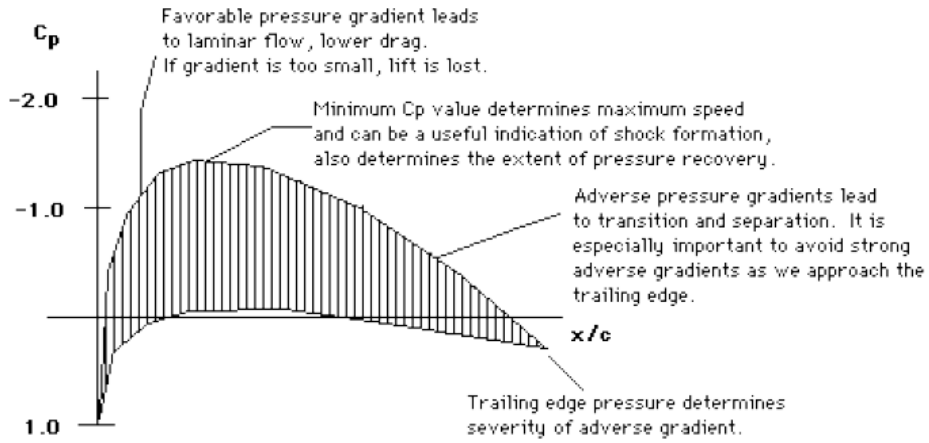

Chart 2-2 - Shape of pressure distributions on an airfoil. [29]

2.3.3 Airfoil Design philosophies

In the past, airfoils were designed experimentally. A designer engineer would build a model based on experience, place it in a wind tunnel, record the results, and make some adjustments to the airfoil model if it did not perform satisfactorily. Often, these airfoils were classified into several families that could be placed into a catalogue of airfoils. The engineer would then choose the appropriate airfoil or airfoils for a vehicle based on the recorded experimental data.

Nowadays, with computers this process has changed significantly. An engineer can make custom airfoils at almost any design condition, can simulate the wing planform to calculate its performance.

There are two main approaches used for custom airfoil design: direct design or inverse design. [30]

The direct airfoil design methods involve the specification of section geometry and the calculation of pressure and performance. The simplest form of direct airfoil design consists of starting with an assumed airfoil (such as NACA airfoil), determining the characteristic of the section and fixing the existing problems. This process is repeated until there is no major problem with the section. [29]

Inverse design, in other hand, uses the target pressure distribution as an objective function. The basic idea behind a variety of methods of inverse design is to specify the desired c_p distribution and use the least squares difference between the actual and target c_p's as the objective. [29]

2.4 Wing Geometry

There are many issues that can affect the performance of wings. In this section will be presented some of that aspects and will be explained how each one changes the performance of the wings.

2.4.1 Aspect Ratio

Aspect Ratio is defined as the span squared divided by the area as shown in Eq. 2.4-1.

$$AR = \frac{b^2}{S} \qquad 2.4\text{-}1$$

This affects directly the slope of the lifting curve $\frac{\partial c_l}{\partial \alpha}$. The larger the aspect ratio the more nearly does the lift slope approaches the theoretical maximum for an infinitely long wing. [32] This happens because a wing with a high aspect ratio has tips farther apart than an equal area wing with low aspect ratio. Therefore, the amount of the wing affected by the tip vortex is less for a high aspect ratio wing than for a low aspect ratio wing and the strength of the tip vortex is reduced.

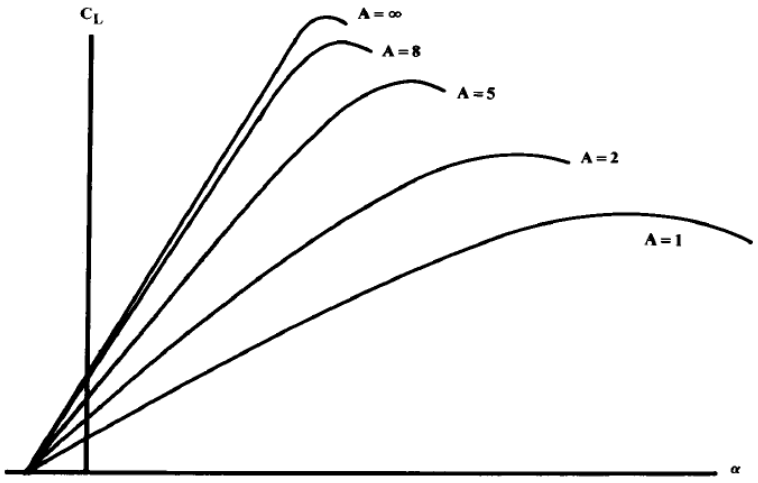

Figure 2-10 - Effect of aspect ratio on lift. [30]

2.4.2 Wing Sweep

Wing sweep is usually used to reduce the adverse effects of transonic and supersonic flow. But PGW project, neither transonic nor supersonic flows are a problem due to the extra low speeds of the vehicle.

Other consideration about wing sweep is that wing sweep improves stability. A swept wing has a natural dihedral effect. In many cases is necessary to use negative dihedral to avoid excessive stability. [30]

2.4.3 Wing Taper Ratio

This is the ratio between the tip chord and the centerline root chord.

$$\lambda = \frac{c_{tip}}{c_{root}} \qquad 2.4\text{-}2$$

Taper affects the lift distribution along the wing's span. As proven by the Prandtl [31] wing theory, minimum drag due to lift occurs when the lift is distributed in an elliptical fashion.

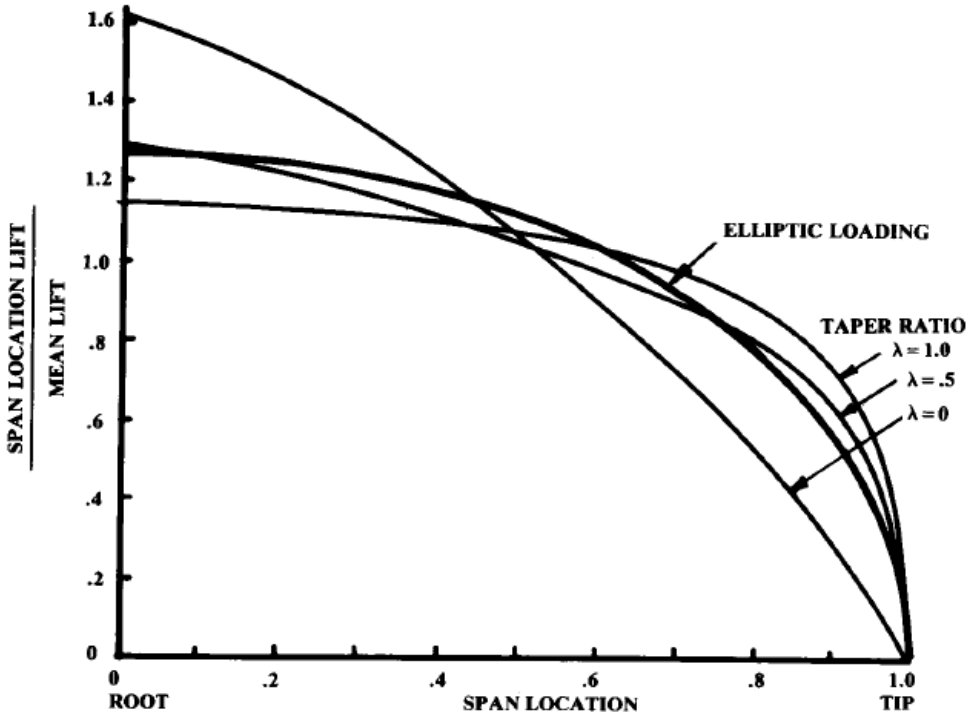

Figure 2-11 - Effects of taper on lift distribution. [30]

An elliptical wing planform is difficult and expensive to build. The easiest wing planform to build is an untapered rectangular wing $(\lambda = 1)$. However, the untapered wing has a constant chord along the span and so has excessive chord towards the tip. [32] When compared with an elliptical wing, an untwisted rectangular wing has about 7% more drag due to lift. [30]

2.4.4 Wing Incidence

Wing incidence angle is the pitch angle of the wing with respect to the fuselage. Usually, this angle is chosen to minimize drag at some operating conditions.

The incidence angle is chosen such that when the wing is at correct angle of attack for the selected design condition, the fuselage is at angle of attack for minimum drag. [32]

If we have a variable wing incidence angle, we can use angle's change as a way to provide vehicle control.

2.5 Low Drag Shapes

To maximize the performance of the vehicle is absolutely essential that its drag is as lower as possible. There are many issues that can affect the performance of the vehicle and the fuselage shape is one of the most important subjects. In this section some methods to design low drag shapes are analyzed.

2.5.1 Axisymmetric Bodies

One of the possible ways to reduce drag is increasing the laminarization of the boundary layer, which plays an important role in aerodynamic aircraft design [33] and also in hydrodynamic of underwater vehicles.

For the aerodynamic design of three-dimensional fuselages with low skin-friction drag, laminar bodies of revolution are often used as a basis. [33]

One of the major problems on underwater bodies design is laminar to turbulent transition. This is a complex and yet not fully understood phenomenon.

A correct theoretical model calculation of the controlled transition process is only possible with direct numerical simulations by solving the complete unsteady Navier Stokes equations. [33]

J. S. Parsons and R.E. Goodson developed a shape for axisymmetric bodies for minimum drag for an incompressible flow.[35]

The fact that extensive laminar flow can exist in the ocean environment at these high Reynolds numbers is in itself significant.[35] The geometry that they developed provides a laminar flow until 70% of total length, which produces lower drag than turbulent flow.

Eriksen [14] describes the University of Washington Applied Physics Laboratory (UW/APL) laminar-flow shape that involves a free-flooding hydrodynamic shroud around the pressure case.

In 1995, Webb [36] carried out pool tests of a glider hull designed by WRC. These tests were intended to confirm performance calculations such as those above, but the results were not consistent enough to define the hull drag to better than about 50%.

Some studies to compare the different shapes drag were performed. On Figure 2-12 it is possible to observe 4 cross sections of low drag shapes and on Figure 2-13 is presented the drag measured for each shape.

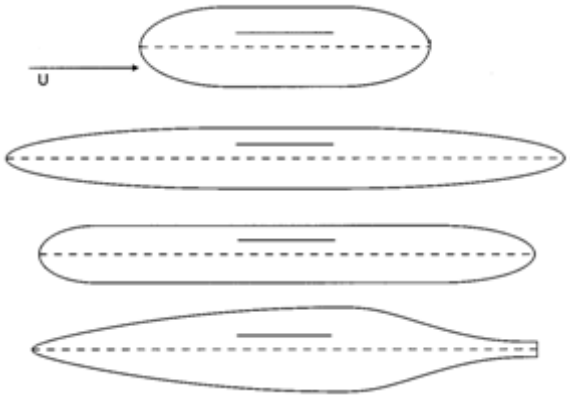

Figure 2-12 - Cross sections of the four models used for drag tests and schematic of mechanism used to measure drag. The shapes are, from top to bottom, fat ellipsoid, the slender ellipsoid, the WRC prototype, and the UW/APL glider. Horizontal lines inside each figure show the volume-based length$L = V^{1/3}$. [23]

The study concluded that all the shapes have approximately constant drag coefficients except the laminar-flow form. The slender ellipsoid has the smallest of the constant drag coefficients, with (based on frontal cross section is $0{,}26$). The WRC shape is higher by 50% and the fat ellipsoid higher by 500%. The drag coefficient for the UW/APL shape decreases as and has approximately the same drag as the slender ellipsoid at, which for full size vehicles corresponds to a speed near $0{,}3\ m/s$. [23]

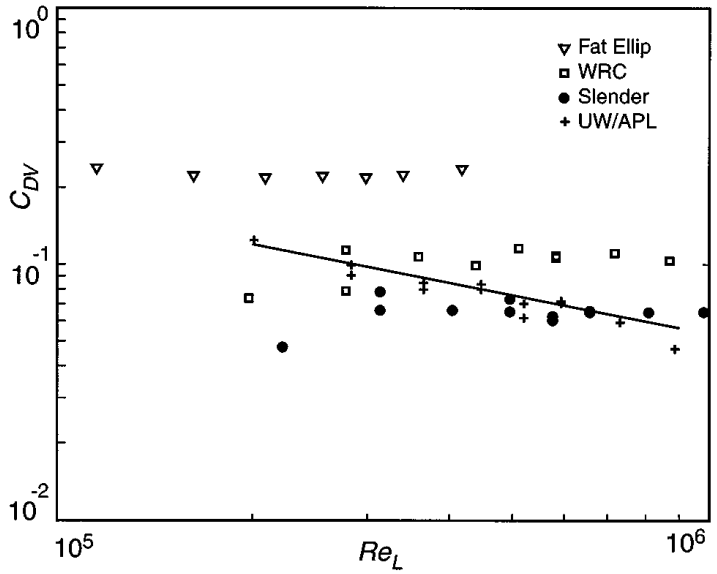

Figure 2-13 - Measured drag coefficients, based on the useful-volume-based area, for the four half-scale models showed on Figure 2-12. Unlike all the scale models, the full-scale UW/APL model had wings that should make its drag higher than the hull-only models.[23]

This page has been intentionally left blank
for double side copying

3 - Customer Requirements

Since the objective of this thesis is develop a new vehicle with collaboration of University of Saint Thomas and Scott Morgan it is necessary to define the requirements to start the design process.

The initial requirements of the project can be observed on Table 3-1.

Table 3-1 - Project Requirements

*1	The PGW shall be capable of autonomous operation for a minimum period of 4 contiguous months before periodic maintenance is required to be performed.
2	The PGW shall be capable of surviving in an ocean environment.
*3	The PGW shall be able to transmit a distress code if caught and unable to surface by normal propulsion.
4	The PGW shall be launched and recovered from an ocean going ship or from a dock that has access to the world's oceans.
*5	The PGW shall be designed for a deployed useful life of 2 years for the navigation systems.
6	The PGW shall be designed for a deployed useful life of 5 years for the waterframe before refitting.
*7	The PGW shall be designed for a deployed useful life of 2 years for the power subsystem.
*8	The PGW shall be able to navigate to a minimum accuracy of 1000 meters left or right of the desired programmed course upon returning to the surface after a dive of 300 meters.
*9	The PGW shall, upon surfacing, determine its position latitude and longitude, speed progressing forward and determine a new trajectory for the next bounce.
*10	In the event that negative progress be possible by the PGW, a message shall be passed to the command and control element requesting a new heading allowing forward progress in the given conditions.
**11	The PGW shall be capable of bidirectional Line of Sight communications up to 20 kilometers from 2 Pi radians while station keeping at the surface.
**12	The PGW communications shall be secured by the use of hopping waveform communications, and secure command and control protocols.
**13	The PGW shall have a sailfin that provides for an isotropic antenna for communications.
**14	The PGW antenna shall be a color that is highly visible and easily recognized as a manmade object to be steered away from by all ships within ¼ nautical mile.
*15	The PGW shall be capable of powering all of the systems for at least 4 months.
*16	Any expendable fluid used in the propulsion system shall be bio-degradable.

* Part of UST's design
** Part of Scott Morgan's design

This page has been intentionally left blank
for double side copying

4 - Problem Definition and Concepts Identification

In this chapter will be identified the applicable concepts to solve specific problems.

A requirements review is necessary to fix the problems and identify possible solutions to solve it.

4.1 Dive and Climbing - L/D problem

As said above, the vehicle should be capable to traveling the largest distance possible in one dive cycle. At the same time, the vehicle needs to return the surface when it finds itself at the point of maximum depth. To solve this problem we identified 3 possible concepts.

4.1.1 Symmetric Airfoil

This concept consists in a simple symmetric airfoil like "NACA-00" series or even a flat plate, which can generate lift with the same L/D in both descending and ascending phases. With this type of airfoil the wings are symmetrical and able to glide in both upward and downward phases with same lift, producing a symmetrical trajectory.

The main disadvantage of these type of airfoils is the lower L/D compared with cambered airfoils. In Figure 4-1 we can see an illustration of this type of airfoils and resultant lift force direction in both descent and ascent phases.

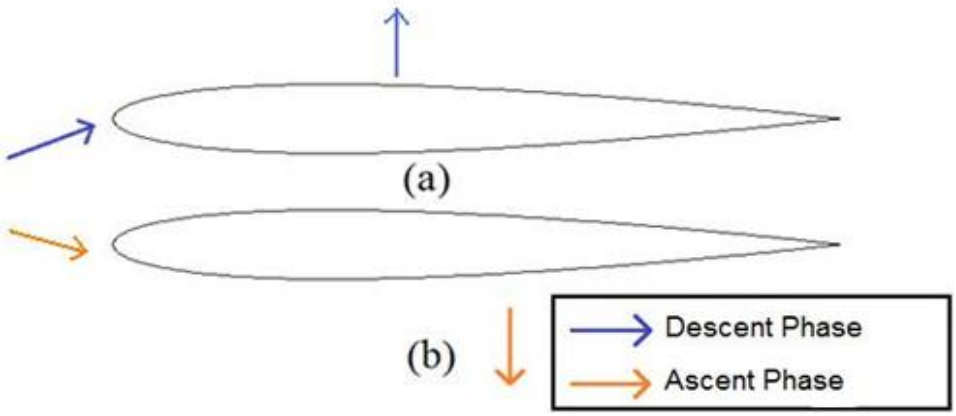

Figure 4-1 - Symmetric airfoil concept to solve L/D problem.

4.1.2 Fixed Camber Airfoil

This concept consists in an asymmetrical airfoil which is generally more efficient than the symmetric airfoils. Therefore, the major benefit of this group of airfoils is that they have higher L/D coefficient compared with symmetric airfoils. The major problem of this concept is, when the vehicle arrives at maximum depth and start climbing, it should be capable of rolling the wings (or somehow invert the flight) and make the profile look like in Figure 4-2 (b) for ascent phase.

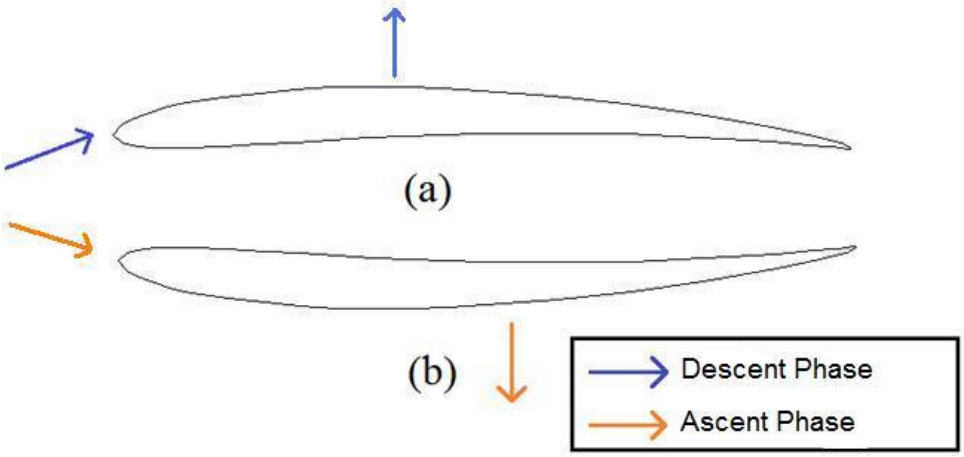

Figure 4-2 - Asymmetric airfoil concept to solve L/D problem.

4.1.3 Concept Selection

Although the Fixed Camber airfoil is more efficient, it was decided to use a Symmetric airfoil, mainly due to lower complexity in its implementation.

With this concept, the PGW does not need to swivel to make symmetric trajectories, and if a new airfoil is developed, the performance of the glider will not be greatly affected.

4.2 Body Shape

Other problem that was found is related with body shape. There are 2 principal solutions to solve the problem. The vehicle can be flying wing shaped or may have a fuselage shape like torpedoes and additional wings to produce necessary lift.

4.2.1 Flying Wing

This configuration provide an additional increment of the L/D ratio due to the following factors inherent in this configuration such as higher Reynolds numbers on the wing with chords twice as large as those of the conventional configuration.

The major benefit of this configuration is the absence of horizontal tail with corresponding friction and induced drag penalty; [36]

It is possible to improve the total L/D ratio about 20% as against the conventional layout.

The main problem with this configuration is the limitation in total internal volume and consequently would be necessary a bigger vehicle compared with the conventional configuration.

4.2.2 Torpedo Shaped Fuselage

This configuration consists of a fuselage like a torpedo with additional wings which produce required lift.

The greatest benefit of this type of configuration is the supplementary internal volume allowing solid wings which are simpler to build than wings with ribs and a spar.

On the other hand, this configuration has a higher total drag than flying wing configuration.

4.2.3 Concept Selection

The chosen concept was torpedo shaped fuselage, since it provides some extra space, and the vehicle can be smaller than a flying wing shape with same internal volume.

This decision take into account the previous concept selection, since building a stable flying wing with a symmetric airfoil would be complicated.

4.3 Wing Vertical Position

In case of decide to make a glider with a torpedo shaped fuselage, is necessary to decide the vertical position of wing, since it can change the performance of the vehicle.

To solve this problem it was decided to place the wing as mid-wing configuration, since is the most simple solution and allows using any concepts previously described.

Even in case of entire vehicle swivel, this configuration is the most favorable configuration and it is simpler to control the vehicle for symmetric trajectory.

4.4 Stability

In this subsection, it will be introduced the identified concepts for the stability of the vehicle. Stability is very important to ensure that vehicle can perform the mission without any troubles and can maneuver properly.

4.4.1 Longitudinal Stability

For longitudinal stability it was identified the use of a horizontal tail, which is a simple way to counteract the moment generated by the wings.

The associated problems to using a tail are higher seaweed accumulation and increased total drag of the vehicle when compared with the configuration without horizontal tail.

4.4.2 Lateral-Directional Stability

A simple way to control yaw moments and supply the necessary later-directional stability is adding vertical tail. In spite of increases total drag of the glider such as horizontal tail concept, this is the simplest concept that was found to provide necessary later-directional stability to the vehicle.

4.4.3 Concept Selection

It was decided to use a "Y" tail, due to lower interference drag when compared with a conventional tail. The vertical fin bellows the "V" provides some extra area for later-directional stability.

4.5 Waterframe Control

Other problem that was identified during project development was the way to control the waterframe to ensure that it can easily avoid obstacles and will maintain the correct trajectory. It was identified 3 different concepts to waterframe's control, which will be explained next.

All of these concepts require experimental validation to ensure that they will work correctly.

4.5.1 Tail Position Change

On first situation of tail position change, there may be two bladders located as shown on Figure 4-3. These bladders could be attached to the tail boom and can be flooded or drained to change incidence of the tail, and with this modification of tail's incidence the vehicle can be controlled.

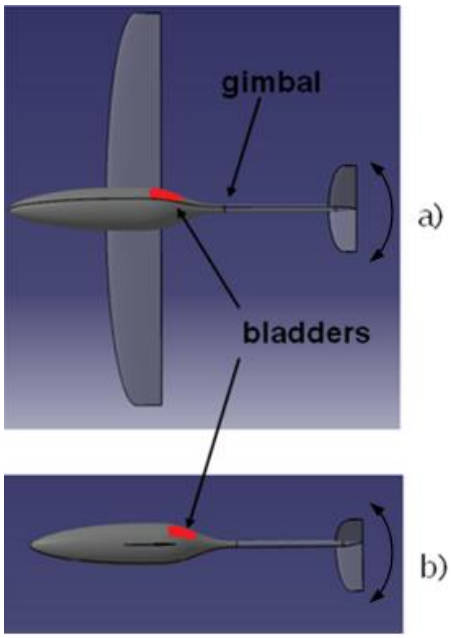

Figure 4-3 -Possible concept to waterframe control - a) Top View b) Side View.

On Figure 4-3 - a) the bladder is located on side of the fuselage and provides the modification of position on horizontal plane. On Figure 4-3 - b) bladder is located on top of the fuselage and provides control on the vertical plane.

Instead of using bladders to change the incidence of tail it is also possible to use a servo, maintaining the operating principle as explained above.

On the other hand, it is possible to make the tail spin around its axis in place of change its incidence.

The tail may spin until $180\,°$ and thus make the configuration completely symmetric on both descending and ascending phases. This concept is illustrated on Figure 4-4.

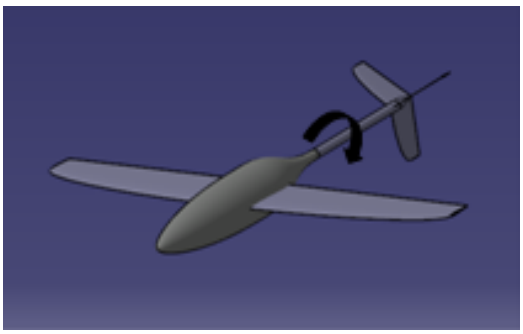

Figure 4-4 - Another of possible concepts to waterframe's control.

4.5.2 Wing Incidence Change

This concept use the change in incidence of wing instead the change in tail's incidence. As shown on Figure 4-5 if a servo is attached to wing's spar, the incidence of the wing can be easily modified.

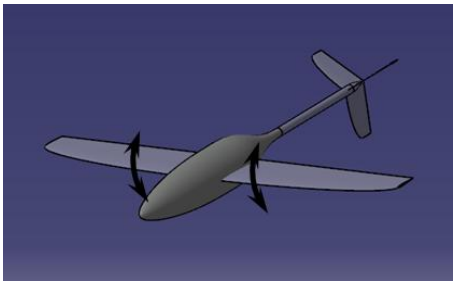

Figure 4-5 - Concept of Wing's incidence modification.

This modification in incidence of wing will modify the c_m coefficient and provide the necessary control to waterframe.

The major advantage of this concept is that the angle between the fuselage and freestream can be adjusted making that the drag produced by the fuselage is minimum, while wings generate the necessary lift.

4.5.3 Concept Selection

As it said before, all of these concepts need experimental validation, and cannot be decided that will be used before then.

Prototype construction should have taken this into account, to allow testing of different waterframe control concepts.

4.6 Buoyancy Volume

At this point of the project, a single spherical tank, positioned on the center of gravity is the best found solution to solve this problem due to its simplicity and facility to implement. The spherical tank is the best solution since the angle of PGW does not affects the center of gravity of internal liquid. If the tank is cylindrical, in case of high angles of attack, the center of gravity of liquid changes, and consequently, the center of gravity of entire vehicle also changes, which could be an additional problem to stabilize and control the PGW.

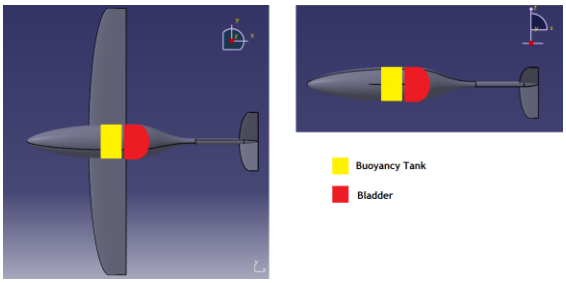

Figure 4-6 - Possible position for buoyancy tank and bladder.

4.7 Materials

Other problem that needed to be solved is related with materials. Some of possible materials that can be used for build a vehicle were identified and its main properties are presented on the next subsections.

4.7.1 Metals

The most common example in this family of materials are the aluminum alloys. Some of specific aluminum alloys was already used to build other similar vehicles. For example, the 6061-T6 Aluminum Alloy was used on all hull sections of Seaglider.

This aluminum is especially adequate to withstand pressures to $1000\ dbar$. [27]

On the other hand metals are more susceptible to corrosion in maritime environments and they are hard to mold and work to make complex shapes like wings.

4.7.2 Cement Reinforced Plastic and Ceramics

Cement Reinforced Plastic has a high bulk modulus, and consequently the volume variation with depth is very small.

However, this type of material needs a higher structural volume than plastic reinforced fibers to ensure that structures are not too breakable. [37]

Besides what was said before, cement reinforced plastic has a higher density than seawater which can be harmful. We need a material with a density close to the sea water to avoid the need of floats or ballast since they are dead weights and take up needed space.

Ceramics are very similar to the cement and generally have the same advantages and disadvantages of require a higher structural volume than fibers reinforced plastic.

4.7.3 Fibers Reinforced Plastic

This type of materials has the advantage of their density being very similar to the density of seawater. Usually, plastics are very resistant to corrosion and are easier to work

and molding and also have the great advantage of require a smaller structural volume when compared with cement or ceramics.

Despite all advantages of this type of material, they usually have a lower bulk modulus than cement reinforced plastic or even ceramics.

4.7.4 Material Selection

At this point it is not possible to choose the best materials for PGW application. A closer and detailed analysis is required to ensure that the best material is chosen. The most recent developments into materials should be taken into account and due this some research is necessary to select the best one.

5 - Design Point

In this chapter will be presented the calculations done to achieve the design point. Due this is an iterative process, and as it will be possible to observe over this chapter, many iterations were done until achieve the final optimized point.

5.1 Spreadsheet Implementation

To begin the design process, it was decided to implement a Microsoft Excel spreadsheet. With this spreadsheet, it is need to arbitrate an initial glide ratio. After that, it is also need to fix the lift coefficient, wing aspect ratio, total range, half buoyancy volume, maximum depth of dive, initial depth of dive, flight speed and Oswald wing factor. The necessary coefficients are calculated with its equations, which are described along this chapter in their own sub-sections. With fixed c_l and calculated c_d, a macro iterates the value of L/D and all other values are updated.

For example, to understand the spreadsheet operation, will be explained the first iteration. It was decided to fix $c_l = 0{,}4$, $R = 3000\,km$, $AR = 6$, $dh = 300\,m$, $h_1 = 0\,m$ and $v = 0{,}5$. First calculated parameter is the airfoil parasite drag, presented in Eq. 5.1-1, which was obtained from Mark Drela model's. [34]

$$c_{d_{airfoil}}(c_l, Re) = (0{,}2522 * c_l^3 - 0{,}1511 * c_l^2 + 0{,}0267 * c_l + 0{,}0088) * \left(\frac{Re}{Re_{ref}}\right)^{Re_{exp}} \quad \text{5.1-1}$$

$Re_{ref} \rightarrow 1{,}20 * 10^5$

$Re_{exp} \rightarrow -0{,}5$

As initial guess for frontal area (A_f) was considered the area of a circle with the same radius than body. To calculate the body radius, was considered an equivalent set of 5 spheres, and their radius were calculated according Eq. 5.1-2.

$$r_{body} = \sqrt[3]{\frac{\frac{3}{4} * \left(\frac{V_{body}}{n_s}\right)}{\pi}} \quad \text{5.1-2}$$

And A_f can be calculated as:

$$A_f = \pi * r_{body}^2 \quad \text{5.1-3}$$

With initial guess of L/D it is possible to obtain the trajectory angle, and make possible to calculate the necessary lift force by the Eq.5.1-4.

$$L = \cos\left(atan\left(\frac{1}{\frac{L}{D}}\right)\right) * W \quad \text{5.1-4}$$

Since the necessary lift force was calculated, it is possible to calculate the wing area by Eq.5.1-5.

$$S = \frac{2 * L}{c_l * \rho * v^2} \quad 5.1\text{-}5$$

From this, it is possible to calculate the wing span and wing chord by Eq. 5.3-1 and Eq. 5.3-2, respectively.

Also, as c_d was previous calculated with Eq. 5.1-1 and with a fix c_l it is possible calculate the waterframe parasite drag coefficient:

$$c_{d_{0_{waterframe}}} = 1{,}3 * c_{d_{airfoil}} + 0{,}06 * \frac{A_f}{S} \quad 5.1\text{-}6$$

With this $c_{d_{0_{waterframe}}}$ and the same fixed c_l it is possible to calculate total c_d for waterframe:

$$c_{d_{total}} = c_{d_{0_{waterframe}}} + \frac{c_l^2}{\pi * AR * e} \quad 5.1\text{-}7$$

Since the $c_{d_{total}}$ was calculated, the new L/D can be calculated to update the results. This is done by a visual basic macro, which make the initial arbitrated value of L/D converge to the calculated L/D.

To obtain refined results, it is need to draw some graphs and evaluate the influence of the given parameters in each others.

To start the calculations, it is need to take into account the initial customer requirements. Thus, the most relevant was selected and are presented into Table 5-1.

Table 5-1 - Customer Initial Requirements

Initial Requirements	
Maximum Depth	300 $[m]$
Distance to travel	3 000 $[km]$
Maximum period of time	120 $[days]$

Starting from customer requirements, presented in Table 5-1, it was calculated the minimum speed for PGW:

$$v_{min} = \frac{3\,000\,000}{120 * 24 * 3600} \approx 0{,}3\ \frac{m}{s} \quad 5.1\text{-}8$$

Arbitrarily, if the PGW covers the same distance in one month (30 days), his speed will be:

$$v_{max} = \frac{3\,000\,000}{30 * 24 * 3600} \approx 1{,}2 \frac{m}{s} \quad 5.1\text{-}9$$

5.2 Glide Ratio

One of the most important parameters that need to be calculated is glide ratio. This parameter is extremely important to give a notion about vehicle's performance.

Other important thing that is necessary to take into account is the size of vehicle. It is necessary to discover how the size of vehicle affects the energy needed since the vehicle has to be as efficient as possible. Some calculations were performed in Microsoft Excel™ spreadsheet and the first graph that was obtained was Chart 5-1.

Obviously, these results are dependent on assumptions like Reynolds influence on wing section or parasite drag coefficient among many other assumptions that were made.

With this chart it was possible to conclude that the necessary battery volume to complete the full range of $3000\,km$ is determinant for value of total internal volume of vehicle. In worst case the necessary battery volume is 6 times the total buoyant volume and on average battery volume represents 3 times the total buoyancy volume.

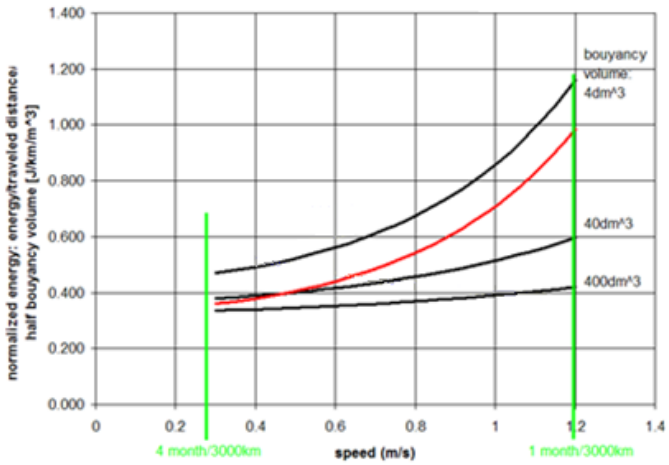

Chart 5-1 - Initial calculations to defining the size of vehicle. This graph was obtained with an Aspect Ratio of 5 and red curve shows aspect ratio doubled to 10.

The results presented on Chart 5-1 are far from refined but give a notion on the influence of buoyancy volume and speed on an effectiveness parameter.

To continue the calculations, the needed volume for different systems was discussed and Table 5-2 was obtained.

Table 5-2 - Required volume for each subsystem.

Subsystem	Volume $[dm^3]$
Navigation	2,311
Power	20,293
Propulsion	4,804
TOTAL	**27,409**

The table presented above takes some assumptions into account and as first guess of subsystems volume, is far to the final value of necessary volume.

Later, the necessary internal volume was updated and was fixed in values presented on Table 5-3.

Table 5-3 - Updated necessary space for each subsystem.

Subsystem	Volume $[dm^3]$
Navigation	1,339
Control	1,045
Power	5,901
Propulsion	19,461
Payload	6,000
Communications	0,05
TOTAL	**33,796**

The variation of the L/D with buoyancy volume it's illustrated on the Chart 5-2. Although not the best L/D area, it was decided choose the smaller buoyancy volumes illustrated on Chart 5-1 since as it was previously presented on Table 5-3 the necessary volume of the body is about $0{,}03\ m^3$and as explained before, the volume for the battery was calculated as 3 times the buoyancy volume. Thus the buoyancy volume is close to $0{,}006\ m^3$.

The range of selected values for half of buoyancy volume is between $0{,}001 < V_{buoyancy} < 0{,}003$ as shown in Chart 5-2.

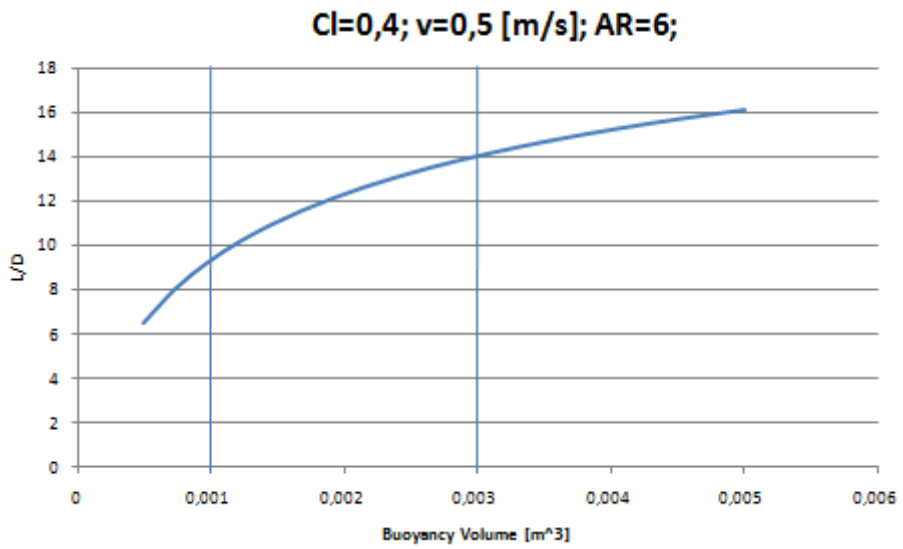

Chart 5-2 - L/D variation due to increasing buoyancy volume. The values on xx axis represent half buoyancy volume.

To select the range of possible speeds, were did variations of speed, and the corresponding L/D variations were analyzed. The remaining parameters were kept constant with its previous values.

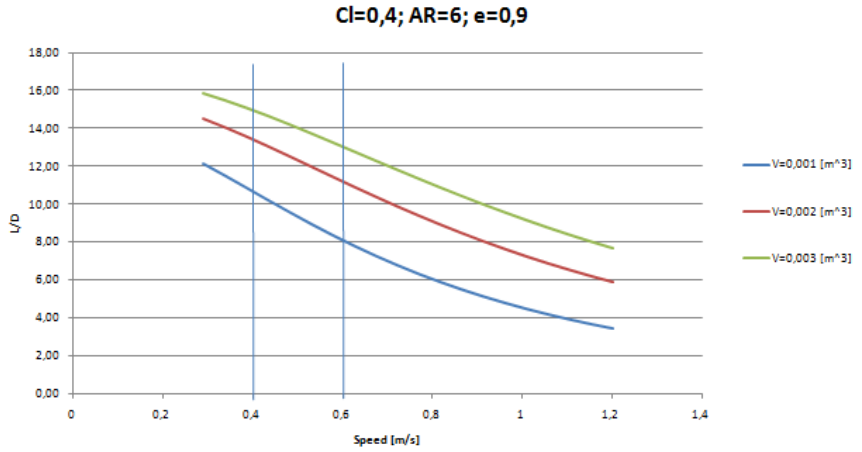

Chart 5-3 - Glide Ratio vs Speed. The values are obtained for a 3 different values of buoyancy volume: $\boldsymbol{2dm^3}$ $(\boldsymbol{V = 0,001})$, $\boldsymbol{4\ dm^3}$ $(\boldsymbol{V = 0,002})$, $\boldsymbol{6\ dm^3}$ $(\boldsymbol{V = 0,003})$

In a first analysis of Chart 5-3 the area with highest glide ratio is located between $0{,}4 < v < 0{,}6\ m/s$, but we need to conjugate this information with specific energy to select the best range of values.

Another parameter that can help to select an adequate design point, is the energy spent per unit of length traveled. It is possible calculate the energy spent for one dive cycle, and its distance. Energy for one dive cycle can be obtained from:

$$E_{dive} = 2 * V * (\rho * g * h_{maximum\ depth}) \qquad 5.2\text{-}1$$

To obtain the forward distance traveled in a dive, just need the L/D and difference between depths (dh):

$$l_{dive} = 2 * \left(dh * \frac{L}{D}\right) \qquad 5.2\text{-}2$$

To obtain the energy spent by unit of length traveled, it is necessary divide the first one by the other:

$$E_{specific} = \frac{E_{dive}}{l_{dive}} \qquad 5.2\text{-}3$$

The Chart 5-4 was obtained for the same range of values of speed:

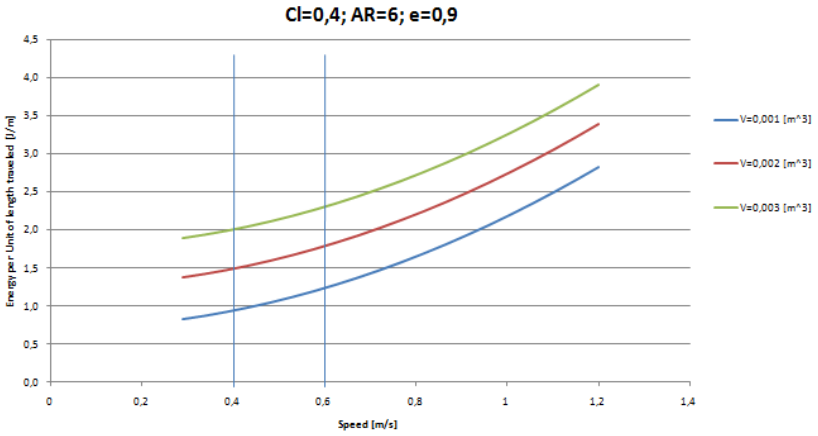

Chart 5-4 - Variation of Specific Energy due to speed variation.

Analyzing Chart 5-4 together with Chart 5-3, it follows easily that the best range of values to speed is between $0{,}4\ m/s$ and $0{,}6\ m/s$. On this range the glide ratio is higher, while the specific energy consumption is lower.

It was decided limit the lower value at $0{,}4\ m/s$ to ensure that PGW can meet the distance requirements with a margin of time.

If the value of buoyancy volume was fixed in $4\ dm^3$, and curves for different speeds are drawn, best range of values to c_l can easily determined. Thus, analyzing the Chart 5-5 , it is possible conclude that for the same values of c_l high glide ratios occur for lower speeds.

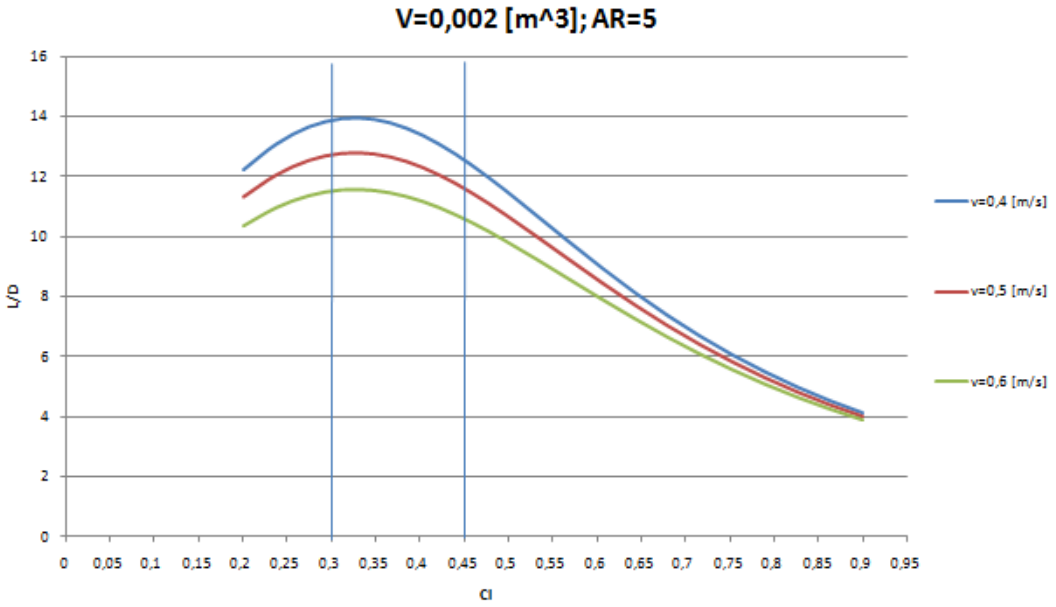

Chart 5-5 - Glide Ratio for different values of speed. The values were obtained for a fix buoyancy volume of $\boldsymbol{4\ dm^3}$.

Analyzing the chart, easily conclude that the best range of values for c_l is $0{,}30 < c_l < 0{,}45$. These values are acceptable, even for a symmetric airfoil. The values lower than $c_l = 0{,}3$ were not considered once they are too low.

5.3 Wing Size

To continue the design process, it was needed to determining the influence of wing area on the glide ratio. Thus, as a way to start, it was decided draw a chart where it can be possible see the influence of wing's aspect ratio on the L/D.

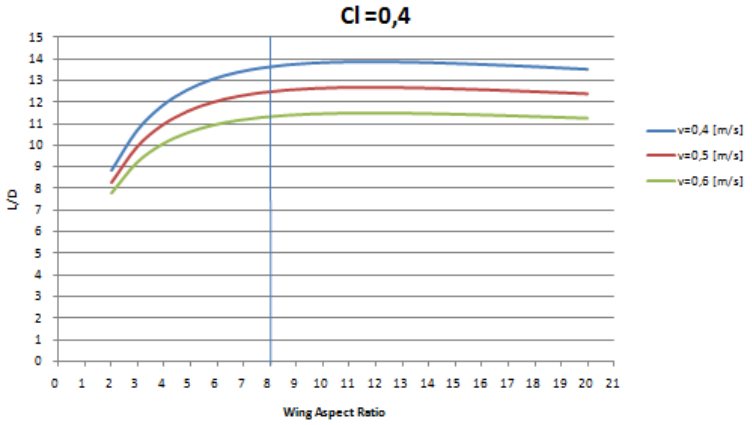

Chart 5-6 - Influence of wing's aspect ratio on glide ratio, for 3 different values of speed.

With a careful observation of Chart 5-6 easily conclude that for an aspect ratio of 8, the vehicle has almost maximum glide ratio. It is important to maximize the glide ratio, but the wings cannot be too long, to avoid that it is getting caught on the seaweed.

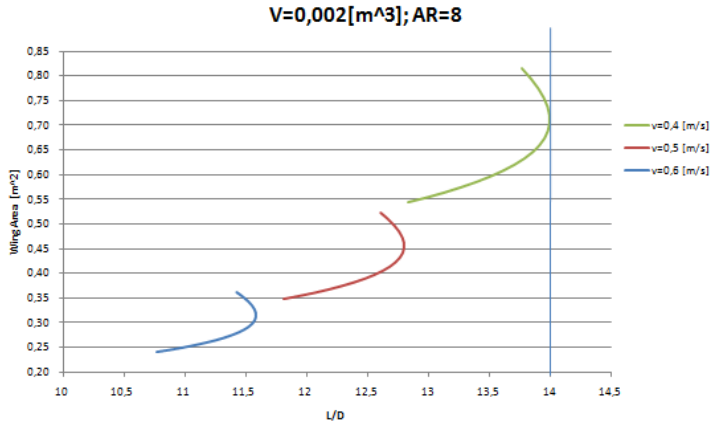

Chart 5-7 - Influence of L/D on wing area.

The Chart 5-7 notice that a maximum glide ratio occurs for a wing area about $0{,}70\ m^2$ for $v = 0{,}4\ m/s$. After decided the wing area we can calculate the wing span, and wing chord:

$$b = \sqrt{AR * S}$$
$$b = \sqrt{8 * 0{,}70} = 2{,}37\ m \qquad \text{5.3-1}$$

Wing mean chord can be determined by the next equation:

$$c = \frac{b}{AR}$$
$$c = \frac{2{,}37}{8} = 0{,}30\ m \qquad 5.3\text{-}2$$

To accurate the initial value of c_l, it is possible draw a chart with constant aspect ratio, and find the c_l for best L/D. The aspect ratio of 8 was fixed and variations in c_l between $0{,}30$ and $0{,}45$ was done.

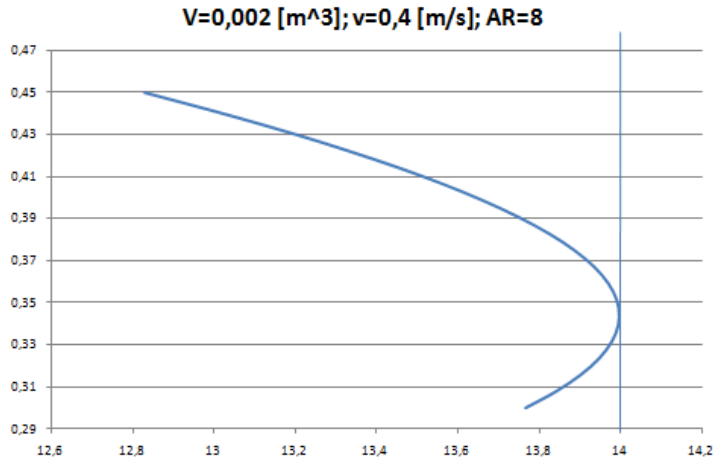

Chart 5-8 -c_l vs Glide Ratio. This chart allow us determining the c_l for a specific glide ratio.

Combining the information presented on Chart 5-8 it is possible conclude that the value of c_l for best glide ratio is close of $c_l = 0{,}34$.

When the previous values were fixed on spreadsheet, the specific design point emerged. On Table 5-4 are presented the main characteristics for this design point.

Body Volume was fixed as the necessary volume to accommodate all needed systems with some extra free space.

Table 5-4 - Main characteristics of design point.

Design Point	
Aspect Ratio (AR)	8
Lift Coefficient (c_l)	$0{,}34$
Wing Area (S)	$0{,}70\ m^2$
Wing Span (b)	$2{,}37\ m$
Wing mean chord (c)	$0{,}30\ m$
Total PGW Volume	$76{,}702\ dm^3$
Specific Energy	$1{,}48\ J/m$

5.4 Airfoil Design

Due to the extra low speed of PGW, the Reynolds number is also very low, and a special family of airfoils is required. As shown on Section 2.3 there are some different methods to design airfoils. This specific airfoil need to be symmetric and need to generate a certain amount of lift with a drag as low as possible. To start an airfoil design, we need to calculate the airfoil Reynolds number:

$$Re = \frac{\rho v c}{\mu} = \frac{1026 * 0{,}4 * \ 0{,}3}{1{,}31 * 10^{-3}} \approx 9{,}50 * 10^{4} \qquad 5.4\text{-}1$$

Trough previous research was discovered some airfoils that are able to operate at this Reynolds number with low drag. The process begins by importing the airfoils to software, and draws some airfoil drag polars. Analyzing the Figure 5-1 easily concludes that the best base airfoil was *Boeing Vertol VR9*.

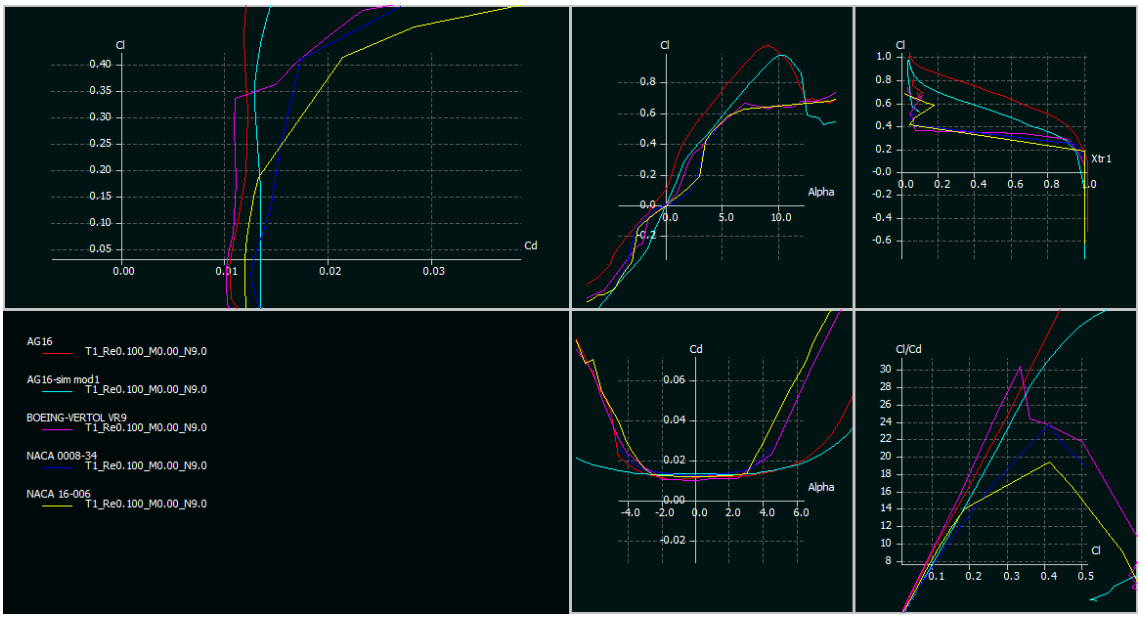

Figure 5-1 - Base Airfoil Drag Polars. Some of the used airfoils are not symmetric, but we can modify them and make them symmetric.

The major problem of the Boeing Vertol VR 9 is that the airfoil is not symmetric although the maximum c_l with a low drag is close of $c_l = 0{,}34$. As a way to continue the airfoil design, need to make Boeing Vertol VR9 airfoil symmetric, doing a mirror from the upper surface.

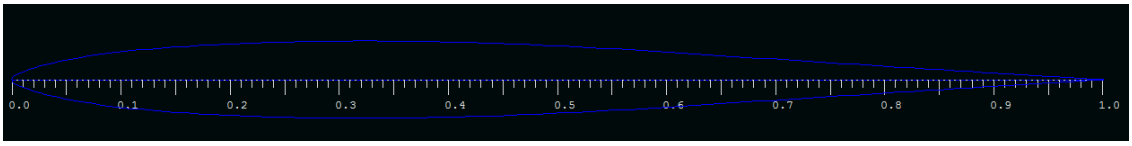

Figure 5-2 - First iteration to obtain an optimized airfoil. In this step it was just changed the original airfoil and make it symmetric.

Optimizing the airfoil, it is possible to have an airfoil with low drag for a $c_l = 0,34$ and lower values. Our final optimized airfoil is:

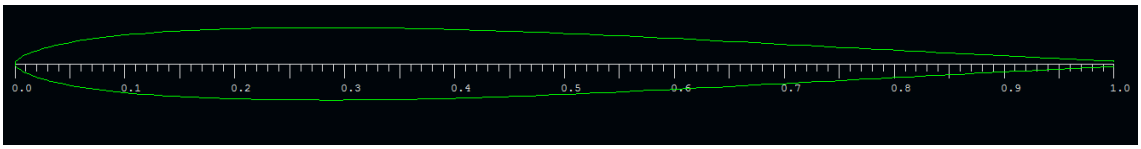

Figure 5-3 - Final optimized airfoil.

This airfoil is a symmetric airfoil with a $6{,}50\ \%$ thickness located at $28{,}2\%$ of airfoil chord.

Note that the trailing edge of final developed airfoil has some thickness, to facilitate the production, since it is impossible machining infinitesimal thickness.

The final airfoil drag polar are presented on Figure 5-4 and Figure 5-5:

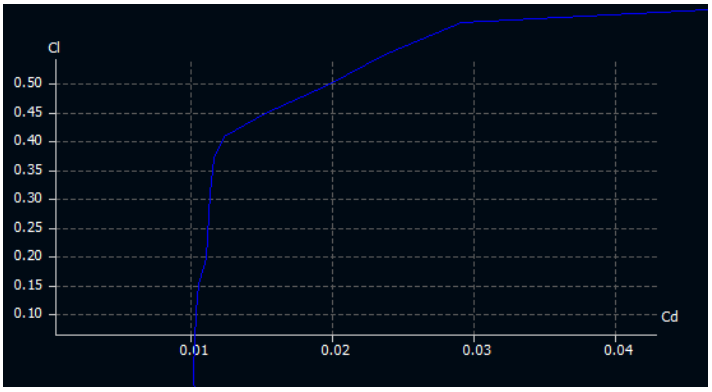

Figure 5-4 - Drag Polar for final airfoil.

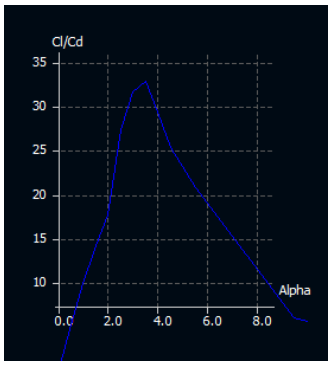

Figure 5-5 - L/D of final airfoil.

Summarizing the airfoil main characteristics of the airfoil was obtained the Table 5-5:

Table 5-5 - Airfoil Characteristics.

Airfoil Characteristics	
Airfoil Reynolds Reference Number (Re)	$9{,}50 * 10^4$
Thickness (t)	6,50 %
Maximum thickness point (x_t)	28,20 %
Minimum drag	0,0102
Alpha for minimum drag	0°
Drag for $c_l = 0,34$	0,0115
Maximum c_l	0,81
Alpha for maximum c_l	15°
Maximum L/D	32,8
c_l corresponding to maximum L/D	0,41
Alpha for maximum L/D	3,5°

The coordinates of final airfoil can be achieved on Appendix I.

After optimized the airfoil, its drag polar was exported for Microsoft Excel and a chart for determining the equation of parasite drag of airfoil was drawn.

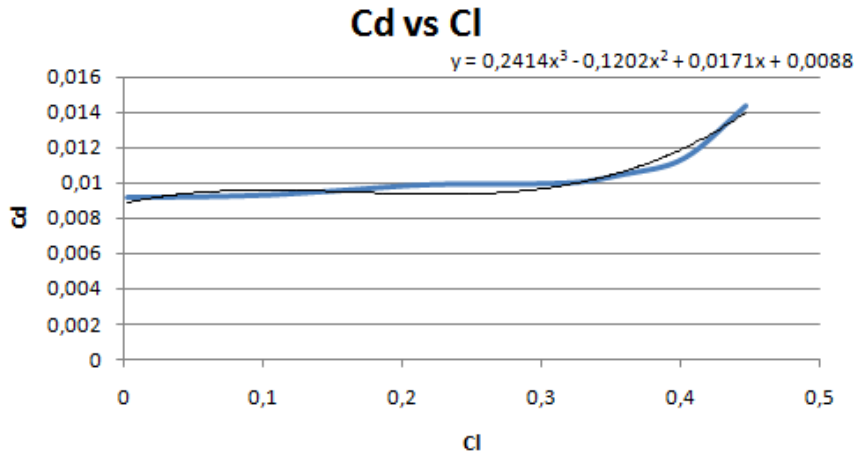

Chart 5-9 - Drag polar of optimized airfoil. This chart only represents the lowest drag area.

After implemented the equation on spreadsheet, and do all calculations again, the results were more accurate. Thus, as this process is an iterative process, the results presented in Table 5-6 were optimized using this parameter.

After fixed previous values, it is possible to calculate some extra parameters and build a table with technical features of the glider.

Lift force is given by:

$$L = cos\left(\tan^{-1}(\frac{1}{L/D}\right) * W \quad \text{5.4-2}$$

Drag force results from:

$$D = \frac{W * cos\left(\tan^{-1}(\frac{1}{\frac{L}{D}}\right)}{\frac{L}{D}} \quad \text{5.4-3}$$

Maximum propulsive force needed is given by:

$$W = Vg\,\rho \quad \text{5.4-4}$$

Trajectory angle was calculated from:

$$\gamma = \tan^{-1}\left(\frac{L}{D}\right) \quad \text{5.4-5}$$

Horizontal speed was obtained from:

$$v_{horizontal} = v * \cos(\gamma) \quad \text{5.4-6}$$

Forward distance traveled per cycle (descent and ascent phases) is given by:

$$l_{dive} = \frac{L}{D} * dh \quad \text{5.4-7}$$

Time per cycle was calculated using the formula:

$$t_{dive} = \frac{l_{dive}}{v_{horizontal}} \quad \text{5.4-8}$$

Total number of cycles is given by:

$$d_{total} = \frac{R}{l_{dive}} \quad \text{5.4-9}$$

Total time for mission completion was calculated from:

$$t_{total} = \frac{R}{v_{horizontal}} \quad \text{5.4-10}$$

Specific Energy was obtained from:

$$E_{specific} = \frac{2\,V\,\rho\,g\,dh}{l_{dive}} \quad \text{5.4-11}$$

Necessary energy for total range was calculated using the formula:

$$E_{total} = E_{specific}\,R \quad \text{5.4-12}$$

Table 5-6 - PGW Energetic and Hydrodynamic Performance

Energetic and Hydrodynamic Performance	
Lift Force during dive	20,08 N
Drag Force during dive	1,48 N
Maximum Propulsive Force	20,13 N
Horizontal Speed	0,399 m/s
Forward travel per cycle	8 112,43 m
Trajectory angle	4,23 °
Time per Dive[(1)]	5,66 $hours$
Number of dives	368
Total time for range completion [(1)]	87 $days$
Energy for range	4 452 543 J
Energy per unit length traveled	1,48 J/m

[(1)] - The calculated times not counting with any recharge time or data upload.

5.5 Tail Sizing

Tails are little wings. Much of the previous discussion concerning wings can also be applied to tail surfaces.

To begin tail sizing some calculations are needed. The horizontal tail area primarily refers to balancing of the moment created by the wing. To calculate the required area to provide the adequate force to balancing the moment produced by the wing was used the tail volume coefficient method. Since the force due to tail lift is proportional to the tail area, the tail effectiveness is proportional to the tail area times the tail moment arm. This method has been used for initial estimation of tail size. The horizontal tail area is given by:

$$S_h = \frac{c_{wing}\, S\, c_h}{l_h} \qquad 5.5\text{-}1$$

For a vertical tail, the wing yawing moments which must be countered are most directly related to the wing span. This means that vertical tail area is given by:

$$S_v = \frac{S\, b\, c_v}{l_v} \qquad 5.5\text{-}2$$

Note that moment arms l_v and l_h is commonly approximated as the distance from the tail quarter-chord to the wing quarter-chord.

The tail volume coefficients both vertical and horizontal need to be assumed. Thus, it was assumed $c_h = 0{,}5$ and $c_v = 0{,}04$.

The chosen concept was a "Y" tail shape. The required tail area is given by:

$$S_{tail} = S_h + S_v \quad 5.5\text{-}3$$

To decide the necessary tail arm, a chart representing the influence of tail arm length into tail area was drawn.

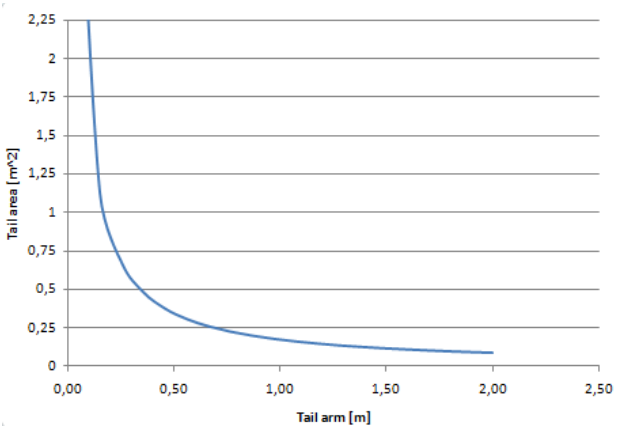

Chart 5-10 - Influence of tail arm length into tail area

It was decided to fix the tail arm at $1{,}3$ due to lower area needed to perform a stable PGW. The area needed for an arm of $1{,}3\ m$ is about $0{,}132\ m^2$.

After chosen the arm and consequently the required area, as tail has 3 surfaces, the area for each fin was determined by:

$$S_{fin} = \frac{S_{tail}}{3} \quad 5.5\text{-}4$$

It was fixed the aspect ratio of the tail in 2, and since the area for each fin and its aspect ratio is defined, it is possible to calculate its chord and its span.

The span of the fin is given by:

$$b_{fin} = \sqrt{AR_{fin} * S_{fin}} \quad 5.5\text{-}5$$

After determined span, it is easily to determine the fin's chord by the equation:

$$c_{fin} = \frac{b_{fin}}{AR_{fin}} \quad 5.5\text{-}6$$

The main characteristics of tail are presented on table Table 5-7.

Table 5-7 - Tail Sizing.

Fin Dimensions	
Arm	$1{,}3\ m$
Fin Span	$0{,}300\ m$
Fin Chord	$0{,}150\ m$
Fin Aspect Ratio	2
Tail Area	$0{,}132\ m^2$

6 - Critical Design Review

After calculate the performance of the vehicle, it is need to decide the fuselage, wings and tail shapes. As part of an ongoing process the final geometry of the components of the vehicle are dependent of the options taken previously.

In this chapter will be presented the final geometry of fuselage, wings and tail with their respective drawings.

6.1 Fuselage

Due to the low Reynolds number of the fuselage, an efficient hydrodynamic shape is required to obtain a performance as high as possible.

A buoyancy-powered vehicle expends energy against hydrodynamic drag, differential compressibility between the vehicle and seawater, and ocean stratification.

Even at slow speeds expected to the PGW, the drag is the most important, by far. To counteract this constraint, it was adopted a low drag shape developed by Jerome Parsons.[35]

To start fuselage design we need to calculate the Reynolds number as function of enclosed volume. Thus:

$$Re_V = \frac{v_\infty V_{body}^{1/3}}{\nu} = \frac{0{,}4 * 0{,}077^{1/3}}{1{,}05 * 10^{-6}} \approx 1{,}65 * 10^5 \qquad 6.1\text{-}1$$

Due to small difference between glider Reynolds number and Reynolds number showed on base paper, it was decided to use the same geometry for the fuselage of the vehicle.

To draw the fuselage on CAD software it was used a Microsoft Visual Basic Macro that allows points importation for CATIA® V5R19.

The coordinates on CATIA® has shown on the Figure 6-1 and they are present on Appendix II.

Figure 6-1 - Fuselage points in CATIA obtained from Excel.

The resultant shape of the body of the vehicle can be seen on Figure 6-2.

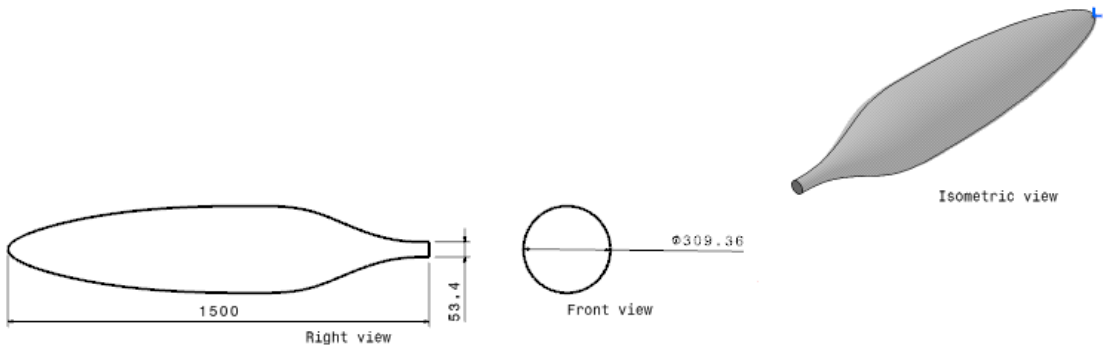

Figure 6-2 - Fuselage shape. All measures are in millimeters.

To attach the tail at the fuselage, it was necessary develop a tail boom, that is represented on Figure 6-3. This boom is a constant diameter, with necessary length and can be used to house an antenna.

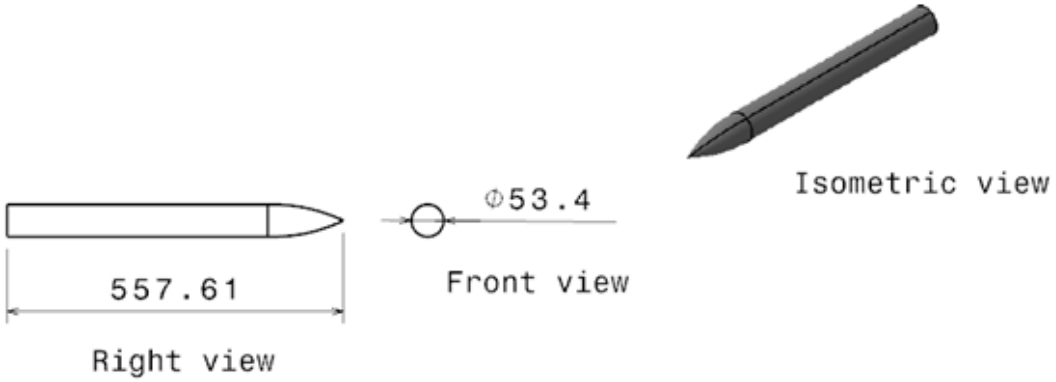

Figure 6-3 - Tail boom geometry. All measures are in millimeters.

6.2 Wings

As it seen before it was decided to use a mid-wing since it allows a symmetrical configuration in both descent and ascent phases.

Minimum induced drag occurs when lift is distributed in an elliptical fashion - i.e. elliptical wing planform without twist or sweep. But elliptical wings in low Reynolds vehicles has not an elliptical lift distribution, because the airfoil change its performance for different chords and this is not an ideal shape for wings which operating in low Reynolds environments. In elliptical wings at low Reynolds environments, parasite drag increases more (due to the low Reynolds wing tip) than induced drag decreases, so, it was adopted a mixture between elliptical and rectangular wing shape. Wing has a taper ratio $\lambda = 0{,}5$, to take the benefits of elliptical wing and at the same time, will be easier and simple to build. The straight trailing edge makes the wing acts as if it has swept, creating dihedral effect, which is useful for lateral stability.

The main characteristics of the wing are presented on Table 6-1.

Table 6-1 - Characteristics of the wing

Wing's Dimensions	
Mean chord	300 mm
Tip chord	150 mm
Root chord	332,62 mm
Wing Span	2370 mm
Aspect Ratio	8
Wing Area	0,700 m^2

The chord distribution along span was obtained from:

$$c(y) = \frac{c_{wing} + c_2(y)}{2} \qquad 6.2\text{-}1$$

Where:

$$c_2(y) = \sqrt{c_{root}^2 * \left(1 - \frac{y^2}{\left(\frac{b}{2}\right)^2}\right)} \qquad 6.2\text{-}2$$

$$c_{root}^2 = 332{,}67\ mm$$

$$b = 2370\ mm$$

The chord distribution was calculated to allow that wing can have the same area as an elliptical wing but with better lift distribution shape than elliptical wing.

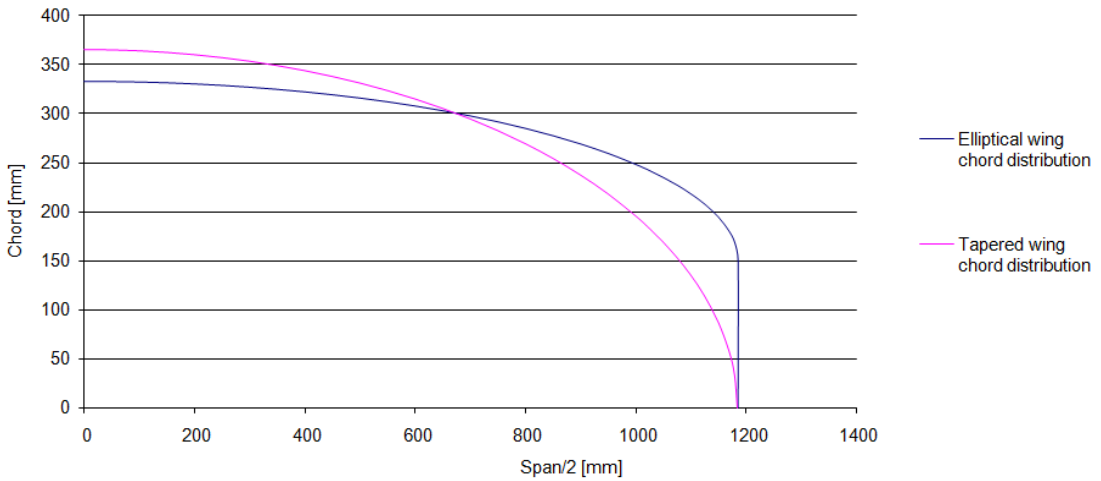

Chart 6-1 - Comparison of elliptical wing chord distribution and tapered wing with the chord distribution presented on Equations 6.2-1 and 6.2-2.

To enable the drawing of the wing on CATIA® a spreadsheet was created to calculate the airfoil coordinates for the calculated medium chord $c_{wing} = 300\ mm$. These points were

copied to the same macro that was used to import fuselage points and they were imported to CATIA as can be noticed on Figure 6-4.

Figure 6-4 - Wing root airfoil coordinates.

At the same time the leading edge points were calculated according the Equation 6.2-3.

$$x_n(y) = c(y) - c_{root} \qquad 6.2\text{-}3$$

The resultant negative value of the Equation 6.2-3 represents the offset of the point from origin.

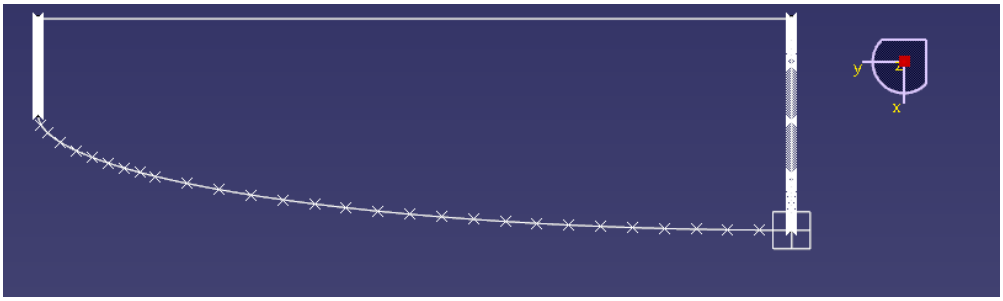

Figure 6-5 - Wing points from Excel.

Once imported all points together with spline, it is only necessary to do a multi-section body where root and tip airfoils are profiles, and leading edge and trailing edge are guidelines.

The result of this process can be observed on Figure 6-6.

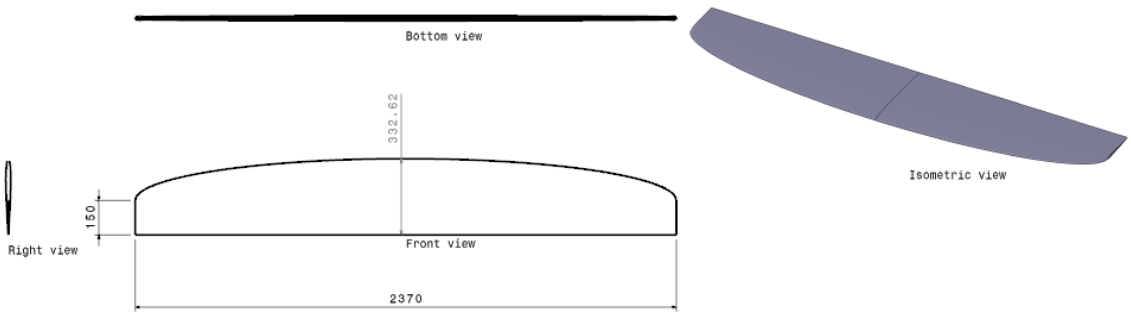

Figure 6-6 - Geometry of wing and its dimensions. All measures are in millimeters.

The trailing edge of the wings is at $881{,}55\ mm$ from the nose of the fuselage, making it coinciding both trailing edge and maximum thickness point of the fuselage.

6.3 Tail

It was decided to adopt a "Y" tail, as explained before, because this tail has to lower dihedral effect and vertical fin will improve later-directional control.

When compared with a conventional tail, the "Y" tail has a lower interference drag which is good for performance of the vehicle that is the main objective of the project.

The airfoil used on tail is the same that was developed for wing since it is symmetric and thin.

The tail chord distribution along the span of the fin is also the same that was used on wings. On Figure 6-7 it is possible to observe the tail shape and its dimensions.

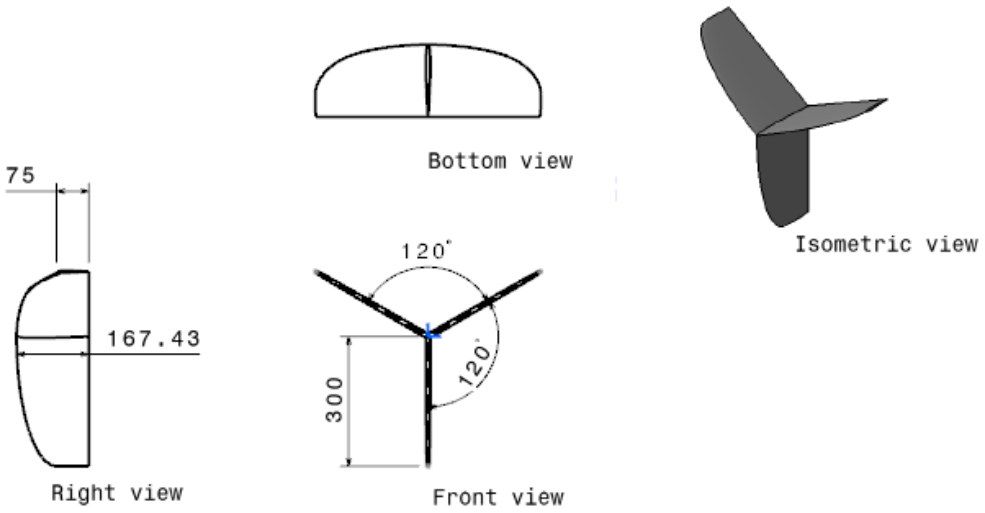

Figure 6-7 - Geometry of tail and its dimensions. All measures are in millimeters.

Main characteristics of the tail are shown on Table 5-7 and can be easily observed in the figure above. The process to obtain the tail on CATIA® was very similar to the wing drawing process.

This page has been intentionally left blank
for double side copying

7 - Stability Coefficients Calculation

To implement and guarantee vehicle's control is necessary the calculation of stability coefficients. To calculate the stability coefficients of the vehicle it was used an open source software named XFLR5.

7.1 Determination of Center of Gravity and moments of inertia

Before starting the calculations of stability coefficients, the moments of inertia and the position of center of gravity were determined.

The most reliable way to determine the position of center of gravity is drawing the vehicle on CATIA and uses a specific tool present on CATIA®.

This tool also provides the moments of inertia around center of gravity or even at some other point defined by user.

To make possible the determination of center of gravity, the vehicle was drawn only with its outer shape (completely solid inside) and a material with a density of $1000\ kg/m^3$ was applied to it.

The measure can be observed on Figure 7-1.

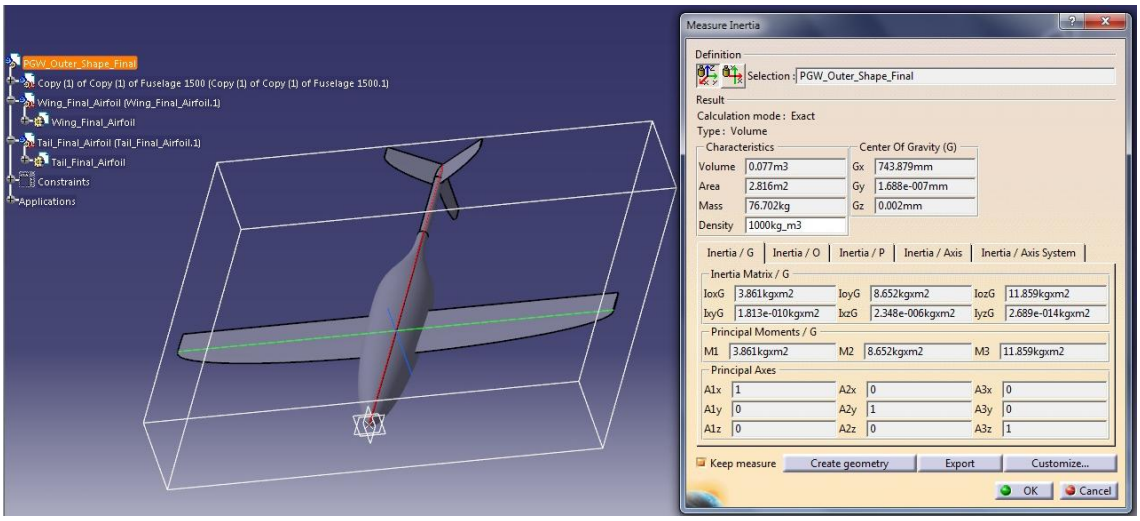

Figure 7-1 - PGW measurement of position of center of gravity.

Relevant data is summarized on Table 7-1, Table 7-2 and Table 7-3.

Table 7-1 - Main parameters of vehicle.

Characteristics of the vehicle	
Volume $[m^3]$	0,077
Mass $[kg]$	76,702
Wet Area $[m^2]$	2,816

Table 7-2 - Center of buoyancy coordinates. The origin of axis system is the point located on the nose of the fuselage of the vehicle as can be seen on the Figure 7-1.

Center of Buoyancy	
$B_x\ [mm]$	743,88
$B_y\ [mm]$	$1{,}688 * 10^{-7}$
$B_z\ [mm]$	0,002

The moments of inertia around center of gravity, which coincides with center of buoyancy, were also determined with this CATIA® tool. Their values are presented on Table 7-3.

Table 7-3 - Values of Moments of Inertia.

Moments of Inertia	
$I_{xx}\ [kg * m^2]$	3,861
$I_{yy}\ [kg * m^2]$	8,652
$I_{zz}\ [kg * m^2]$	11,859
$I_{xy}\ [kg * m^2]$	$1{,}813 * 10^{-8}$
$I_{xz}\ [kg * m^2]$	$2{,}348 * 10^{-6}$
$I_{yz}\ [kg * m^2]$	$2{,}689 * 10^{-14}$

7.2 Wing and Body axis sign conventions

The lift and drag coefficients are given in wind axis. In version that was used (up to 3.1) calculations have been performed using a small angles approximation, which means that the wind and body axis were the same.

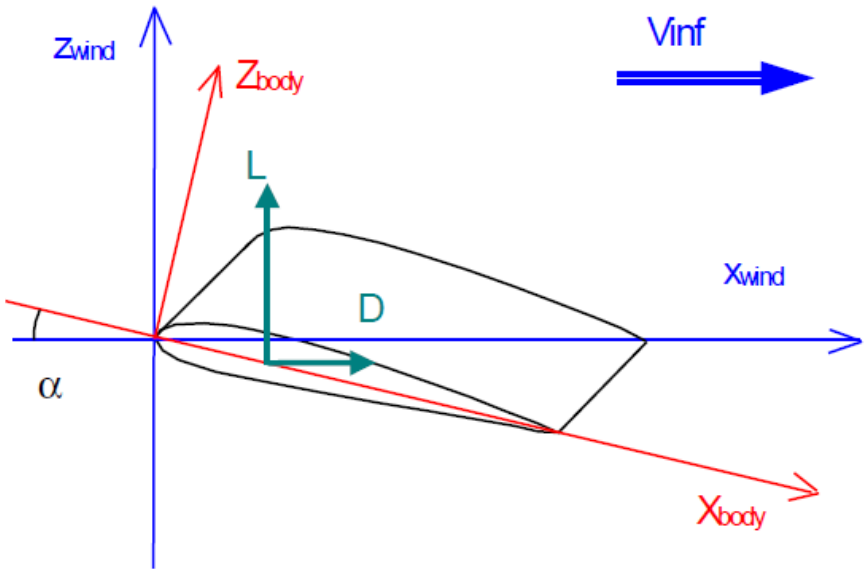

Figure 7-2 - Wing and body axis [38]

"The most common aeronautical convention defines the roll as acting about the longitudinal axis, positive with the starboard wing down. The yaw is about the vertical body axis, positive with the nose to starboard. Pitch is about an axis perpendicular to the longitudinal plane of symmetry, positive nose up." [38]

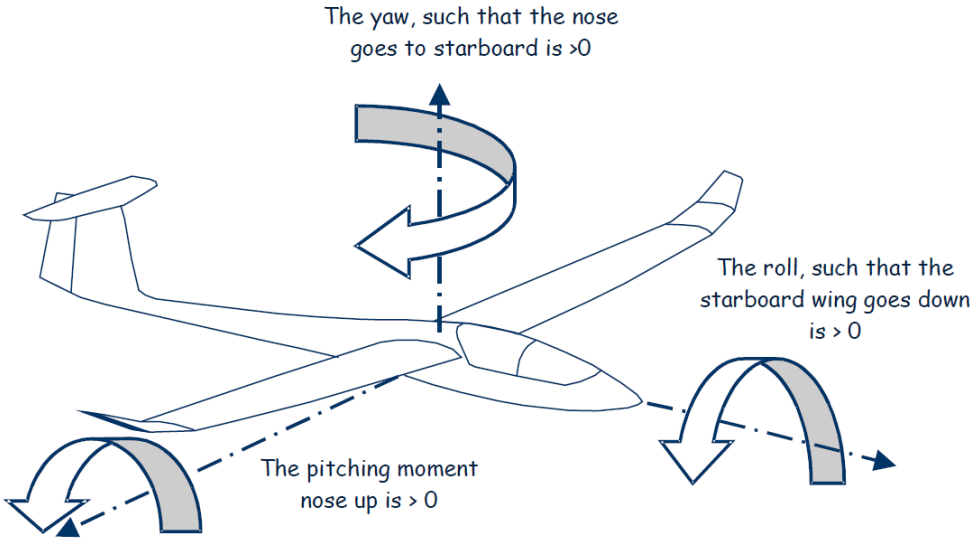

Figure 7-3 - Moment sign convention. [38]

7.3 Wing Definition

This software uses either one of three methods, each having its own advantages, and all having some usage restrictions.

The first is the Lifting Line method, derived from Prandtl's wing theory. The second is the Vortex Lattice method. The third is a 3D panel method. The originality of the implementations is their coupling with XFoil calculation results to estimate the viscous drag associated with the wing, although this is done in a different manner depending on the method.

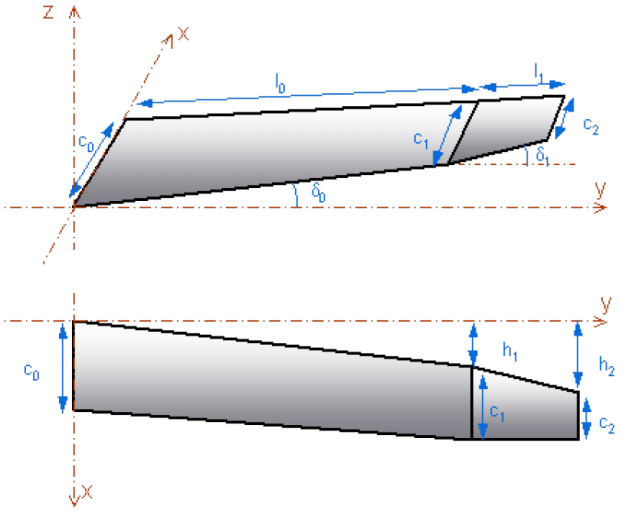

Figure 7-4 - Wing definition. [38]

The wing of the vehicle was defined as a group of panels, as illustrated on Table 7-4, with an offset from the origin. The origin of the axis, in XFLR5, corresponds to the position of center of gravity.

Table 7-4 - Wing panels definition.

No. of Panel	y $[mm]$	c $[mm]$	Leading Edge offset $[mm]$
1	0	332,62	−194,12
2	300	326,67	−188,17
3	500	315,57	−177,07
4	600	307,48	−168,98
5	700	297,35	−158,85
6	800	284,72	−146,22
7	900	268,80	−130,3
8	1000	247,98	−109,48
9	1025	241,64	−103,14
10	1050	234,65	−96,15
11	1075	226,84	−88,34
12	1100	217,92	−79,42
13	1125	207,37	−68,87
14	1150	194,06	−55,56
15	1170	178,96	−40,47
16	1180	166,76	−28,26
17	1185	150,00	−11,5

The span of the wing is defined as:

$$b = 2 * \sum y_{max} \qquad 7.3\text{-}1$$

For ease of interpretation, the wing is shown developed on a horizontal planform, both in the wing design dialog box and in the 2D view. Only the 3D view gives a realistic representation of the geometry. This software has an option on which only needs to define one wing and the software make a symmetry for the other wing.

The reference area for all wing aerodynamic coefficients is the main wing's area.

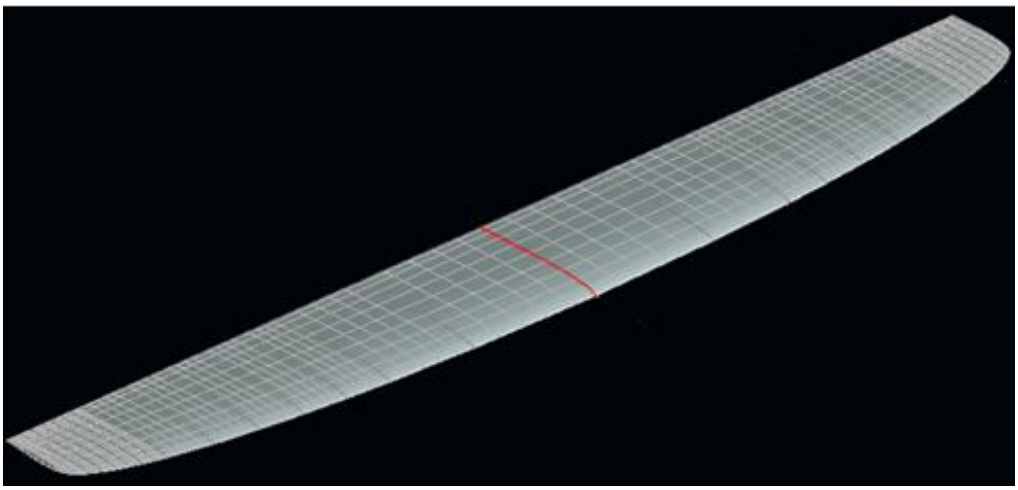

Figure 7-5 - Wing geometry on XFLR5.

7.4 Body Definition

To facilitate the edition process, the software allows that the control points can be edited in a text file and imported to the XFLR5, rather than being defined directly in XFLR5.

As the body of vehicle is an axisymmetric body, it is possible calculate the coordinates of the body's sections.

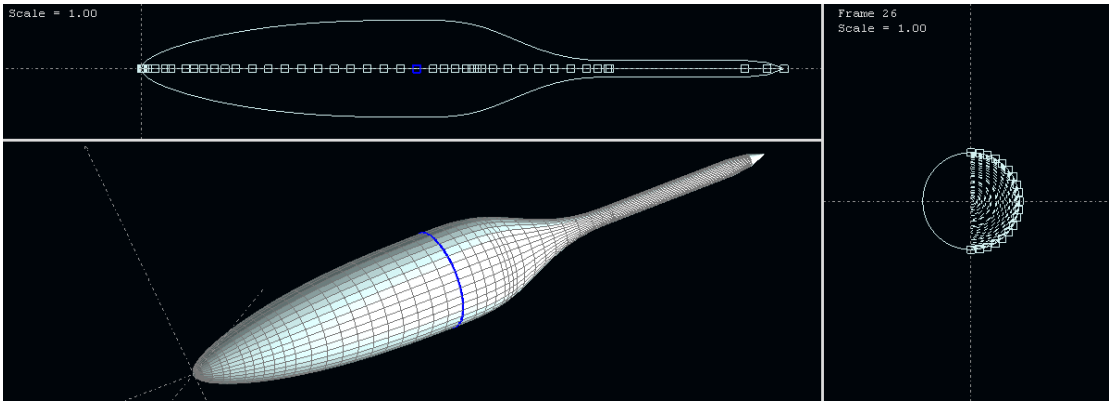

Figure 7-6 - Body definition on XFLR5.

The body was defined as a group of 46 cross sections with 19 control points each and points were defined on a *txt file first and then imported to the XFLR5.

The control points were joined by flat panels since their spacing is small, and splines make the sections slightly non-circular.

After defined the body, an offset of $743{,}89\ mm$ was given to it to matching the axis origin with the position of center of gravity.

7.5 Tail Definition

The tail was defined as an elevator with $30°$ dihedral angle and a vertical fin. The method to define tail geometry is very similar to the wing's method. The tail panels definition is presented on Table 7-5.

Table 7-5 - Tail definition on XFLR5. The offset of the leading edge was calculated to keep the distance between quarter chord of wing and quarter chord of tail fin equal to $\mathbf{1,3}\ \boldsymbol{m}$. This coordinates are valid to the horizontal tail (with 30° dihedral) and also for vertical fin.

No. of Panel	y $[mm]$	c $[mm]$
1	0	167,43
2	20	167,22
3	40	166,60
4	60	165,56
5	80	164,08
6	100	162,14
7	120	159,71
8	140	156,75
9	160	153,19
10	180	148,94
11	200	143,89
12	220	137,84
13	240	130,46
14	260	121,11
15	270	115,29
16	280	108,18
17	290	98,67
18	295	91,80
19	298	85,66
20	300	75,00

After defined all fins, the aspect of the vehicle and its characteristics on XFLR5 is showed on Figure 7-7.

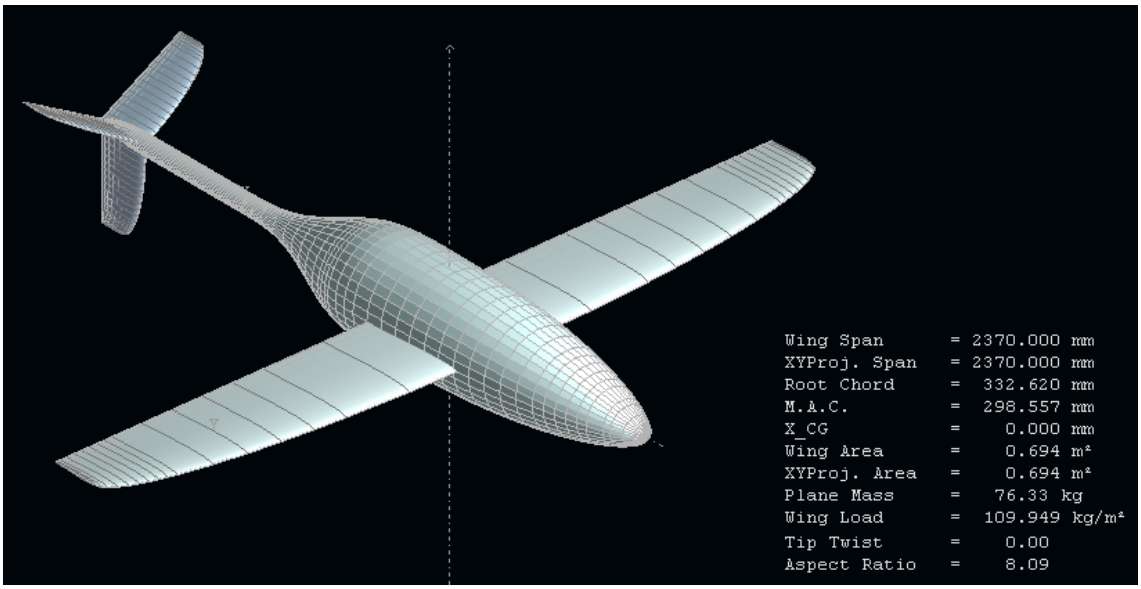

Figure 7-7 - Aspect of glider on XFLR5.

7.6 Stability Analysis

XFLR5 follows the method proposed by Etkin [39] and due this, longitudinal and lateral dynamics are independent and were evaluated separately.

Three different reference frames come into consideration in stability analysis: the geometric axes, the body, axes and the stability axes. These refer to any frame which is fixed to the body, and is therefore not an inertial frame of reference. The convention adopted by this software is showed on the Figure 7-8:

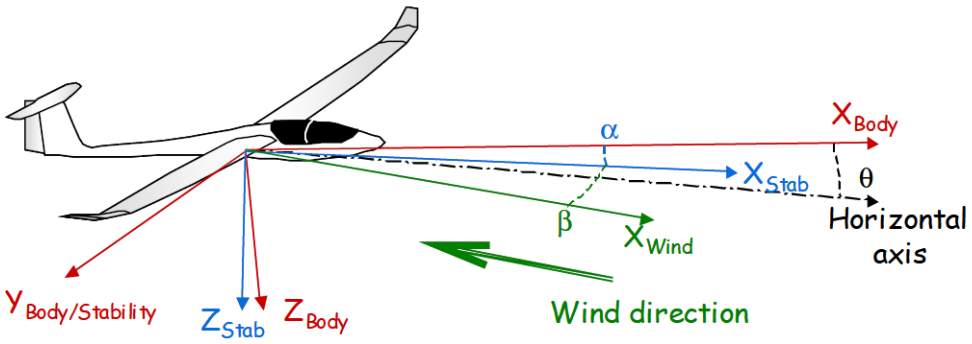

Figure 7-8 - Convention of body and stability axes adopted by XFLR5. [38]

About body axes:

- the X'-axis is aligned with the fuselage nose;
- the Z'-axis is in the plane of symmetry, and points downwards;
- the Y'-axis is perpendicular to the XZ-plane and points starboard.

About geometric axes:

- the X-axis is aligned "backwards"

- the Z-axis is in the plane of symmetry, and points upwards;
- the Y-axis is perpendicular to the xz-plane and points starboard.

About stability axes:

- the x-axis is the projection of the velocity vector on the body's xz-plane; this axis therefore points forward
- the z-axis points downwards;
- the y-axis points starboard
- the point of origin of the frame is the plane's centre of gravity CoG.

Note that XFLR5 performs all calculations in stability axes. The definition of non dimensional derivatives is:

$$C_{L_\alpha} = \frac{Z * w * u_0}{q * S} \quad \text{7.6-1}$$

$$C_{L_q} = \frac{Z * q * 2 * u_0}{q * S * c_{wing}} \quad \text{7.6-2}$$

$$C_{m_\alpha} = \frac{M * w * u_0}{q * S * c_{wing}} \quad \text{7.6-3}$$

$$C_{m_q} = \frac{\frac{2 * u_0}{c_{wing}}}{q * S * c_{wing}} \quad \text{7.6-4}$$

$$C_{Y_\beta} = \frac{Y * v_c * u_0}{q * S} \quad \text{7.6-5}$$

$$C_{Y_p} = \frac{Y * p_c * 2 * u_0}{q * S * b} \quad \text{7.6-6}$$

$$C_{Y_r} = \frac{Y * r * 2 * u_0}{q * S * b} \quad \text{7.6-7}$$

$$C_{L_\beta} = \frac{L_c * v_c * u_0}{q * S * b} \quad \text{7.6-8}$$

$$C_{L_p} = \frac{L_c * p_c * \frac{2 * u_0}{b}}{q * S * b} \quad \text{7.6-9}$$

$$C_{L_r} = \frac{L_c * r * \frac{2 * u_0}{b}}{q * S * b} \quad \text{7.6-10}$$

$$C_{n_\beta} = \frac{N * v_c * u_0}{q * S * b} \quad \text{7.6-11}$$

$$C_{n_p} = \frac{N * p_c * \frac{2 * u_0}{b}}{q * S * b} \quad \text{7.6-12}$$

$$C_{n_r} = \frac{N * r * \frac{2 * u_0}{b}}{q * S * b} \quad \text{7.6-13}$$

Were performed two types of analysis. In the first type, the response of the vehicle for a given mass and speed was analyzed, and an output file with some coefficients (like

$c_L, c_D, c_m,$ …) for each angle of attack was created. On the second type analysis the stability of the vehicle was performed and stability coefficients were calculated. All of these coefficients present on output files are on Appendix III.

The position of center of gravity used on this analysis was 20% of wing chord, since it is a possible position to make a stable "flight".

Before to start a complete vehicle's analysis it is necessary to calculate, separately, the airfoil performance from wing tip Reynolds number to wing root Reynolds number. An analysis between $-10\,° \leq \alpha \leq 10\,°$ was performed and the charts presented on Figure 7-9 were obtained.

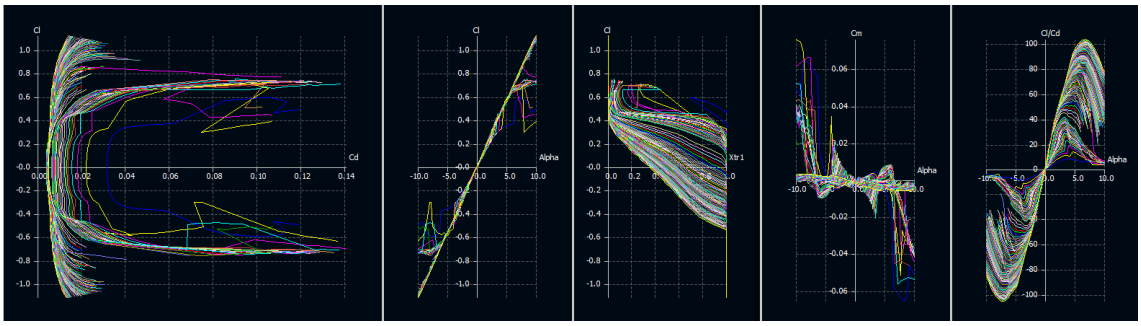

Figure 7-9 - Polars of vehicle's airfoil.

On the first analysis a mixture between 3D panels and VLM evaluated the response of the vehicle for a given speed of $0{,}4\ m/s$. On Table 7-6 is possible to observe the inputs of the analysis. This was a viscous analysis with wing planform as reference area and span for aerodynamic coefficients calculations.

Table 7-6 - Inputs of first type of analysis.

Analysis Inputs	
Vehicle Mass $[kg]$	76,329
Speed $\left[\frac{m}{s}\right]$	0,4
X_{CoG} $[mm]$	0,000
Z_{CoG} $[mm]$	0,000
ρ $\left[\frac{kg}{m^3}\right]$	1026
υ $\left[\frac{m^2}{s}\right]$	$1{,}05 * 10^{-6}$

As we can see on Figure 7-10, which was obtained for an angle of attack $\alpha = 5°$, the pressure coefficient is higher on wings and tail leading edges. The green lines up the wings and tail fins represent the lift generated by these surfaces. The yellow lines represent the

induced drag and the pink lines represents the viscous drag. The pink lines up the wings and tail represent the trasition of laminar flow to turbulent flow. Purple lines represent the free stream and it is possible to observe the wing tip vortex and some instabilities near the aft section of the fuselage.

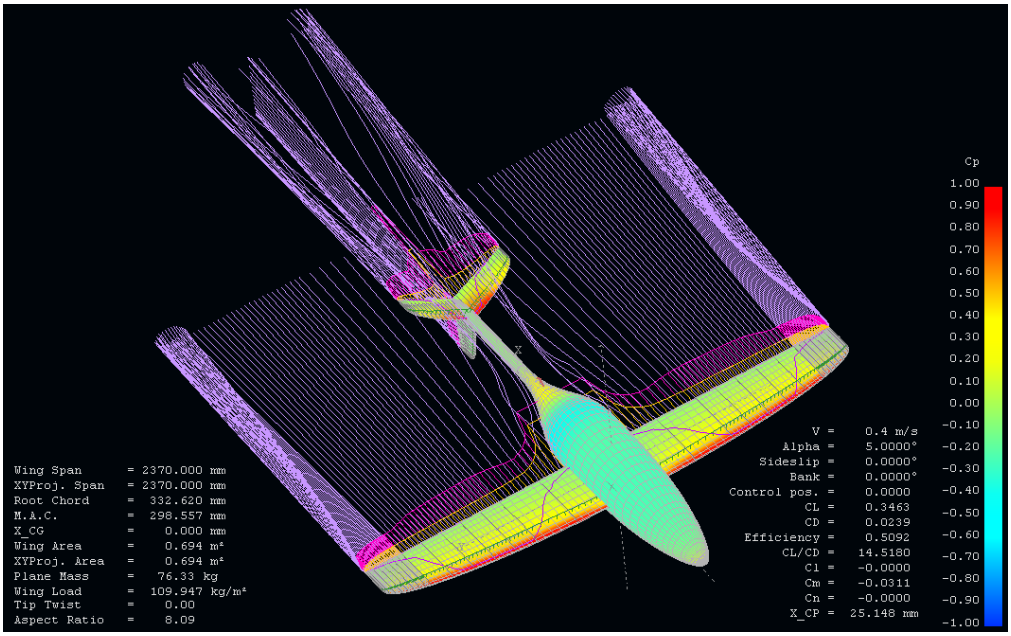

Figure 7-10 - Glider simulation on XFLR5.

To perform the stability analysis to achieve the remaining coefficients was necessary some extra input parameters which are showed on Table 7-7 was needed to calculated the aerodynamic coefficients.

Table 7-7 - Input parameters for aerodynamic coefficients calculation.

Analysis Inputs	
Vehicle Mass $[kg]$	76,33
Center of gravity $[X_{CoG}, Y_{CoG}, Z_{CoG}]$	[0,00 0,00 0,00]
I_{xx} $[kg * mm^2]$	$3{,}861 * 10^6$
I_{yy} $[kg * mm^2]$	$8{,}652 * 10^6$
I_{zz} $[kg * mm^2]$	$1{,}19 * 10^7$
I_{xz} $[kg * mm^2]$	2,35
ρ $\left[\frac{kg}{m^3}\right]$	1026
υ $\left[\frac{m^2}{s}\right]$	$1{,}05 * 10^{-6}$

The other parameters of this analysis were very similar to the analysis presented above. To balance the weight, software found a speed around $28\,m/s$ and due this was necessary to calculate the airfoil performance to this speed. This may have happened because the software is open source and have used the density of air instead the density of sea water, which was introduced as an input.

Nevertheless, as aerodynamic coefficients are non dimensional the speed does not influence their values. Even so, other simulations were done to ensure that aerodynamic coefficients were being calculated correctly.

As explained before, XFLR5 performs longitudinal and lateral stability calculations independent and separately. Thus, the resulting non dimensional coefficients are presented on Table 7-8 and Table 7-9.

Table 7-8 - Non Dimensional Longitudinal Coefficients

Non Dimensional Longitudinal Coefficients	
c_{x_u}	$-0{,}010409$
c_{x_α}	$0{,}0046062$
c_{z_u}	$-9{,}921 * 10^{-7}$
c_{L_α}	$4{,}0723$
c_{L_q}	$8{,}1583$
c_{m_u}	$0{,}00096105$
c_{m_α}	$-2{,}7209$
c_{m_q}	$-18{,}004$

Table 7-9 - Non Dimensional Lateral Coefficients

Non Dimensional Lateral Coefficients	
c_{Y_β}	$-0{,}39569$
c_{Y_p}	$-\ 0{,}021858$
c_{Y_r}	$0{,}46426$
c_{l_β}	$-0{,}00014417$
c_{l_p}	$-\ 0{,}52494$
c_{l_r}	$0{,}0013944$
c_{n_β}	$0{,}22109$
c_{n_p}	$0{,}012025$
c_{n_r}	$-\ 0{,}25828$

7.7 Performance Estimation

After drawing the vehicle, and perform the coefficients calculations, it is possible to estimate the performance of the vehicle.

When comparing Chart 7-1 with Chart 5-8 it is possible to conclude that values obtained from Microsoft Excel were unsophisticated, since doesn't consider the exact shape of the vehicle, or the interference drag between wings and fuselage.

Although, the value obtained from Microsoft Excel was lower than obtained from XFLR5.

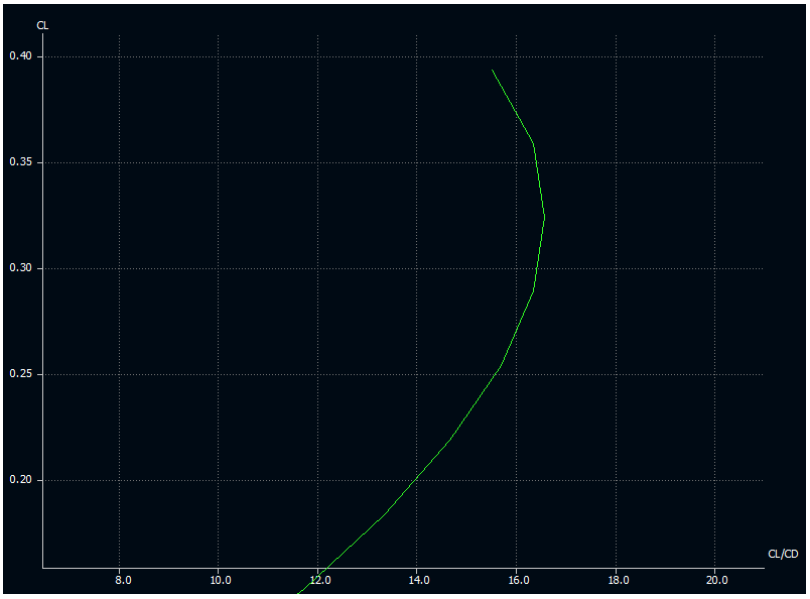

Chart 7-1 - Estimation of performance obtained from XFLR5.

This page has been intentionally left blank
for double side copying

8 - Prototype Construction

In this chapter will be explained the procedure used to build the prototype. The wings and tail have a very similar building method, as will be showed. The fuselage and tail boom followed a different building method, which will be explained later.

8.1 Wings and Tail

8.1.1 Wings

The first parts to be worked are wings. It was some difficulties due to its thinness and also due to the materials used to build the moulds.

The plugs of wings were machined using a 3-axis CNC machine. It was used blocks of Medium Density Fiberboard also known as MDF as support to machining the plugs.

The aspect of plugs after machining is showed on Figure 8-1. Were machined upper and lower surfaces to allow building a closed mold on a later stage of wings construction.

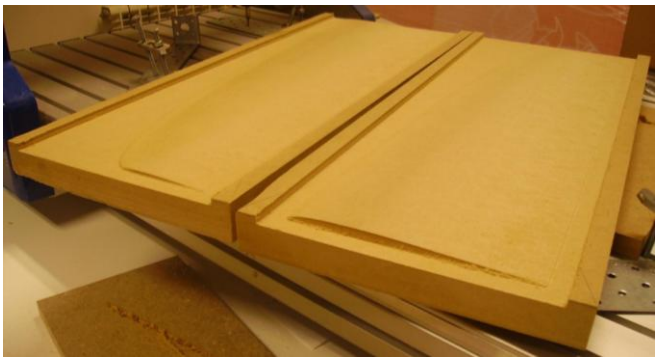

Figure 8-1 - Aspect of machined wing plugs.

As the finishing given by the CNC machine is poor, some extra handwork needed to be done. First of all, the plugs were varnished to waterproof the wood and allow a later painting. Later, the plugs were sanded and painted until the any roughness disappears. The appearance of plugs at the end of this stage is showed on Figure 8-2.

Figure 8-2 - Aspect of the plug after painting.

Following the wings construction and with the wing plugs ready to build the moulds, the pugs were prepared as we can show in Figure 8-3 and plaster moulds were did.

Figure 8-3 - Plug prepared to receive the plaster for mould construction.

As always happens, the first correct mould only came after a few attempts. The first ones had some difficulty in properly mold releasing or had some porosities which made them unsuitable. The appearance of final moulds can be observed on Figure 8-4.

Figure 8-4 - Final plaster moulds.

After releasing 2 moulds correctly, it was necessary put some realize gel into them and put them together so that they can be filled with resin which can be observed in Figure 8-5.

Figure 8-5 - Filling the wing's mould with resin.

Initial idea was build plaster wings or even concrete wings, but the higher fragility of these materials prevented the construction of the wings with this materials. Later, it was decided to do the wings in resin. It was used epoxy resin and the realized wings can be observed on Figure 8-6.

Figure 8-6 - Released resin wing

Some extra handwork to finish the wings was needed, but on Figure 8-7 can be observed an intermediate appearance of the wing.

Figure 8-7 - Intermediate aspect of the wing. Corrections on trailing edge were applied to make it smooth and constant.

8.1.2 Tail

The tail's construction method was very similar to the wing's construction method. As is possible to observe in Figure 8-8, the plaster moulds for tail are smaller than wing's moulds but very similar to the wing's plaster moulds.

Figure 8-8 - Tail's plaster moulds.

The molds were filled also with resin and the fins which were obtained, were glued to tail boom.

8.2 Fuselage

To build the fuselage of the vehicle it was decided to use oak-wood, since it simple to get it and it has a high density.

To begin the construction work, it was needed to glue the different parts and an inner hole, to accommodate extra ballast, was opened.

The appearance of glued planks is showed on Figure 8-9.

Figure 8-9 - Appearance of glued planks. On the image on the left is possible to watch all planks glued, and in the image on the right is showed the hole inside to accommodate extra ballast.

After glued all planks, the resulting block was machined on a lathe until obtain the correct shape. The process is illustrated on the next figures.

Figure 8-10 - Initial machining of the fuselage.

After the block of wood is perfectly rounded, it was necessary give to it the shape of the fuselage. It was handwork as it is possible to observe on Figure 8-11. This figure presents the intermediate shape of the fuselage.

Figure 8-11 - Illustration of handwork during fuselage machining, and on the right, the intermediate shape of the fuselage.

In the Figure 8-11, on the right, is possible to observe the apparatus for giving the correct shape to fuselage. The horizontal white shape worked as holder of the cutting tool, preventing the tool to go further than necessary.

To verify the final shape, it was cut an outside shape of fuselage, and with a visual inspection allowed the small corrections. This method is illustrated on

Figure 8-12 - Comparison between ideal shape and handwork machined shape. The small gaps present in this figure were eliminated later.

The fuselage final shape can be observed on Figure 8-13.

Figure 8-13 - Final machined shape of fuselage.

After the final form of the fuselage had been obtained, the fuselage was cut to allow access to the inner hole which carries needed ballast. To finish the fuselage, nose need to be rounded and tail boom need to be built and attached to fuselage.

The machining process of tail boom was very similar to the fuselage, just on a smaller scale than fuselage. Final obtained boom can be observed on Figure 8-14.

Figure 8-14 - Final machined tail boom

9 - Conclusions & Recommendations

9.1 - Conclusions

- An efficient, low drag waterframe for application on PGW was successfully designed respecting the constraints of the project.

- A symmetric airfoil for application in low Reynolds operation as is the case of PGW was simultaneously developed and can be used in its wings.

- The stability coefficients were calculated for different wing incidence angle and were included in control algorithm as way to attest the PGW stability.

9.2 - Recommendations

- The construction of prototype parts should be finished and assembled to perform necessary tests.

- Regarding to testing, some pool tests should be performed to verify the effective control due to changes in incidence angle of wings.

- Looking forward for this project, the waterframe materials should be defined and internal structure should be dimensioned, respecting the operation environment and PGW expected loads due to the maximum depth requirements.

This page has been intentionally left blank
for double side copying

10 - References

[1]-Ross, C., *A conceptual design of an underwater vehicle*, University of Portsmouth, Ocean Engineering 33, USA, 2006.

[2]-Davis, R. *et al*, *"Autonomous Buoyancy-Driven Underwater Gliders"*, Institution of Oceanography, La Jolla, USA, 2002.

[3]-Graver, J., *"Underwater Gliders: Dynamics, Control and Design"*, Princeton University, USA, 2005.

[4]-Wood, S., *"Autonomous Underwater Gliders"*, Florida Institute of Technology, USA.

[5]-Kleven, J., *et al "Persistent Gliding Wateframe (PGW) - Final Report"*, University of Saint Thomas, Minnesota, USA, 2011.

[6]-http://oceanexplorer.noaa.gov/technology/subs/abe/abe.html - last visit in 04/11/2010

[7]-D. L. Endicott *et al*, *"Epulard: deep bottom surveys now with acoustic remote controlled vehicle, first operational experience", Technical Report*, Proceedings of Oceans 81, Boston, USA, 1981.

[8]-Alt, C. *"Autonomous Underwater Vehicles - Autonomous Underwater Lagrangian Platforms and Sensors Workshop"*, Woods Hole Oceanographic Institution, USA, 2003.

[9]-http://www.globalsecurity.org/intell/systems/auss.htm - last visit in 04-11-2010

[10]-Bellingham, J., *et al, "A small long range autonomous vehicle for deep ocean exploration*", Proceedings of the 2nd International Offshore and Polar Engineering Conference, Pp 148-155, San Francisco, USA, 1992.

[11]-Curtin, T., *et al "Autonomous oceanographic sampling networks"*. Oceanographics 6 (3): 86 – 93, 1993.

[12]-http://dsg.whoi.edu:90/ships/auvs/abe_description.htm - last visit in 06/11/2010

[13]-http://www.noc.soton.ac.uk/nmf/usl_index.php?page=as - last visit in 04/11/2010

[14]-Eriksen, C., *"Autonomous Underwater Gliders - Autonoumous and Lagrangian Platforms and Sensors (ALPS) Workshop"*, School of Oceanography, University of Washington, Seattle, USA, 2003.

[15]-Jenkyns, S., *et al*, *"Underwater Glider System Study. Technical report"*, Office of Naval Research, USA, 2003.

[16]-Griffits, G., *et al, "Undersea Gliders",* ECOR Specialist Panel on Underwater Vehicles, Journal of Ocean Tevhnology, USA, 2007.

[17]-http://www.naoe.eng.osaka-u.ac.jp/naoe/naoe7/MUG.html - last visit in 05/11/2010

[18]-Rudnick, D., *et al, "Underwater Gliders for Ocean Research" Mar. Technol. Soc. J.*, vol. 38, 2004.

[19]-Fiorelli, E., *et al "Multi-auv control and adaptive sampling in monterey bay*", Proc. IEEE Autonomous Underwater Vehicles 2004: Workshop on Multiple AUV Operations, Sebasco, 2004.

[20]-Griffiths, G., *"Technology and Applications of Autonomous Underwater Vehicles*", London, UK, 2003.

[21]-Kawaguchi, K., *et al*, *"Development of shuttle type AUV 'ALBAC' and sea trials for oceanographic measurement*", *Journal of the Society of Naval Architects of Japan*, Vol. 178, pp. 657-665, Japan, 1995.

[22]-Moitie, R., *et al, "Guidance and control of an autonomous underwater glider*", Proc. 12th Int. Symposium on Unmanned Untethered Submersible Tech., Durham, Netherlands, 2001.

[23]-Sherman, J., *et al, "The Autonomous Underwater Glider "Spray" ",* IEE Journal of Oceanic Engeneering, Vol. 26, USA, 2001.

[24]-Davis, R., *et al, "The Autonomous Lagrangian Circulation Explorer (ALACE)",* J. Atm. Oceanic Tech., Vol. 9, pp 264-285, 1991

[25]-SLOCUM, Operations Manual, Version 1.6, 01/11/2005, Webb Research Corporation

[26]-Webb, D., *et al "SLOCUM, an underwater glider propelled by environmental energy"*, IEEE Journal of Oceanic Engineering, Special Issue on Autonomous Ocean Sampling Networks, Vol. 26, pp 447–452, 2001.

[27]-Eriksen, C., *et al, "Seaglider - a long range autonomous underwater vehicle for oceanic research",* IEEE, Journal of Oceanographic Engineering, Vol. 26, 2001.

[28]-P. B. S. Lissaman, "Low Reynolds Number Aerofoils ", Annual review of Fluid Mechanics, AeroVironment Inc., California, USA, 1983

[29]-Kroo, I., *"Applied Aerodynamics: A Digital Textbook"*, Version 5.0, Desktop Aeronautics Inc., Stanford, USA, 2007

[30]-Borer, N., *"Design and Analysis of Low Reynolds Number Airfoil"*, Final Project, USA

[31]-Prandtl, L., and Betz, A., *Vier Abhandlungen zur Hydro- und Aerodynamik*, Gottingen, Germany, 1927.

[32]-Stinton D., *"The Design of the Airplane",* Second Edition, Loughborough University of Technology, AIAA Education, USA.

[33]-B. H. Carmichael. *Personal Aircraft Drag Reduction.* Published by the author, 1996.

[34]-Drela, M., "XFOIL: An Analysis and Design System for Low Reynolds Number Airfoils," *Low Reynolds Number Aerodynamics*, edited by T. J. Mueller, Lecture Notes in Engineering No. 54, Springer-Verlag, 1989.

[35]-Parsons, J., *et al "*Shaping of Axisymmetric Bodies for Minimum Drag in Incompressible Flow", Journal of Hydronautics, Vol. 8, 1974.

[36]-D.Webb, *ALACE Glider—Test Tank Trials*. Falmouth, MA: Report of the Webb Research Corp., 1995.

[37]-Lepech, M., *et al "Long Term Durability Performance of Engineered Cementitious Composites"*, Restoration of Buildings and Monuments, Vol 12, No. 2, 2006.

[38]-*"Analysis of foils and wings operating at low Reynolds numbers"*, Guidelines for XFLR5 v6.03, 2011

[39]-James C. Sivells and Robert H. Neely, "Method for calculating wing characteristics by lifting line theory using nonlinear section lift data", April 1947, NACA Technical Note 1269.

This page has been intentionally left blank
for double side copying

Appendix

This page has been intentionally left blank
for double side copying

Appendix I

Airfoil Upper Surface Coordinates

x	y	x	y	x	y	x	y
100.000	0.00231	0.75207	0.01472	0.27125	0.03238	0.00394	0.00487
0.99983	0.00232	0.74121	0.01529	0.26064	0.03233	0.00257	0.00383
0.99931	0.00233	0.73020	0.01587	0.25018	0.03225	0.00147	0.00281
0.99845	0.00236	0.71906	0.01645	0.23987	0.03214	0.00067	0.00182
0.99725	0.00240	0.70780	0.01705	0.22971	0.03199	0.00017	0.00087
0.99573	0.00248	0.69641	0.01764	0.21972	0.03182	0.00000	-0.00007
0.99388	0.00257	0.68492	0.01824	0.20991	0.03162		
0.99171	0.00266	0.67331	0.01885	0.20027	0.03137		
0.98922	0.00277	0.66162	0.01946	0.19080	0.03109		
0.98641	0.00290	0.64983	0.02007	0.18152	0.03078		
0.98328	0.00305	0.63796	0.02069	0.17244	0.03044		
0.97984	0.00321	0.62602	0.02130	0.16355	0.03006		
0.97610	0.00338	0.61402	0.02191	0.15486	0.02964		
0.97206	0.00358	0.60195	0.02252	0.14636	0.02919		
0.96771	0.00378	0.58984	0.02313	0.13809	0.02871		
0.96306	0.00399	0.57770	0.02374	0.13002	0.02819		
0.95811	0.00422	0.56552	0.02433	0.12216	0.02763		
0.95288	0.00447	0.55332	0.02492	0.11452	0.02704		
0.94735	0.00473	0.54110	0.02549	0.10712	0.02642		
0.94154	0.00500	0.52888	0.02606	0.09993	0.02576		
0.93544	0.00529	0.51667	0.02661	0.09297	0.02506		
0.92907	0.00560	0.50445	0.02713	0.08625	0.02434		
0.92243	0.00593	0.49224	0.02763	0.07976	0.02358		
0.91552	0.00626	0.48005	0.02812	0.07351	0.02279		
0.90835	0.00662	0.46788	0.02858	0.06750	0.02196		
0.90093	0.00700	0.45574	0.02902	0.06173	0.02112		
0.89327	0.00738	0.44364	0.02945	0.05620	0.02024		
0.88534	0.00777	0.43159	0.02985	0.05093	0.01934		
0.87718	0.00818	0.41960	0.03022	0.04590	0.01841		
0.86879	0.00861	0.40766	0.03056	0.04113	0.01746		
0.86017	0.00906	0.39579	0.03088	0.03661	0.01648		
0.85132	0.00951	0.38399	0.03116	0.03234	0.01547		
0.84226	0.00998	0.37226	0.03142	0.02833	0.01445		
0.83299	0.01046	0.36061	0.03164	0.02458	0.01342		
0.82352	0.01096	0.34905	0.03185	0.02108	0.01237		
0.81385	0.01146	0.33760	0.03203	0.01785	0.01130		
0.80399	0.01198	0.32626	0.03217	0.01486	0.01023		
0.79395	0.01251	0.31502	0.03227	0.01215	0.00915		
0.78372	0.01304	0.30389	0.03234	0.00970	0.00807		
0.77333	0.01359	0.29288	0.03239	0.00751	0.00699		
0.76277	0.01415	0.28200	0.03240	0.00558	0.00592		

This page has been intentionally left blank
for double side copying

Appendix II

Fuselage Coordinates

x	z	x	z
0,285	2,325	1425,675	28,695
1,32	7,005	1460,865	27,09
3,345	11,58	1493,64	26,775
6,27	15,99	1500	26,7
9,915	20,205		
19,035	28,17		
43,35	42,945		
75,57	57,27		
94,935	64,515		
141,21	79,35		
168,645	86,97		
199,365	94,725		
233,265	102,45		
267,765	109,56		
302,385	115,995		
354,54	124,5		
406,875	131,73		
459,375	137,79		
511,98	142,74		
564,675	146,7		
617,415	149,715		
670,215	151,905		
723,03	153,36		
775,86	154,2		
828,705	154,59		
881,55	154,68		
934,38	154,365		
969,585	153,15		
1004,685	150,345		
1039,545	145,305		
1056,81	141,84		
1073,925	137,73		
1090,89	132,99		
1124,295	121,8		
1173,33	102,09		
1222,08	81,675		
1271,385	62,655		
1321,725	46,62		
1373,25	35,055		

This page has been intentionally left blank
for double side copying

Appendix III

Stability Coefficients - CG_20% - wing_angle 0º

```
XFLR5 v6.03
20.06.2011  22:23:11
PGW
Lateral_CG_20%_wing_0º
_____________________________________
Performing asymmetric calculation :
Counted 2797 panel elements

Launching 3D Panel Analysis....
Using Dirichlet boundary conditions
Warning: The wing and elevator lie in the same plane z=      0 mm
It is recommended to slightly offset the wing or the elevator to avoid numerical instabilities

Type 7 - Stability polar   Mass=      76.330 kg

   ___Center of Gravity Position - Body axis____
    CoG_x=      0.0000 mm
    CoG_y=      0.0000 mm
    CoG_z=      0.0000 mm

   ___Inertia - Body Axis - CoG Origin____
    Ibxx=   3.861e+06 kg.mm²
    Ibyy=   8.652e+06 kg.mm²
    Ibzz=    1.19e+07 kg.mm²
    Ibxz=        2.35 kg.mm²

   Solving the problem...

      Calculation for control position  0.00
      Creating the influence matrix...
      Performing LU Matrix decomposition...
      Solving LU system...
      Searching for zero-moment angle... Alpha=-0.05121°
      Creating source strengths...
      Calculating doublet strength...
      Calculating speed to balance the weight...VInf = 27.67333m/s

      ___Inertia - Stability Axis - CoG Origin____
      Isxx=   3.861e+06 kg.mm²
      Isyy=   8.652e+06 kg.mm²
      Iszz=    1.19e+07 kg.mm²
      Isxz=        7188 kg.mm²

      Calculating the stability derivatives

      No active control - skipping control derivatives


      Longitudinal derivatives
      Xu=     -102.59          Cxu=   -0.010409
      Xw=      45.397          Cxa=   0.0046062
      Zu=     -54.127          Czu=  -9.921e-07
      Zw=      -40135          CLa=      4.0723
      Zq=      -12003          CLq=      8.1583
      Mu=      2.8279          Cmu=  0.00096105
      Mw=       -8006          Cma=     -2.7209
      Mq=       -7908          Cmq=     -18.004
      Neutral Point position= 199.47688mm


      Lateral derivatives
      Yv=     -3899.8          CYb=    -0.39569
      Yp=     -255.27          CYp=   -0.021858
      Yr=      5422.1          CYr=     0.46426
      Lv=     -3.3674          Clb= -0.00014417
      Lp=      -14530          Clp=    -0.52494
      Lr=      38.597          Clr=   0.0013944
      Nv=      5164.3          Cnb=     0.22109
      Np=      332.85          Cnp=    0.012025
      Nr=       -7149          Cnr=    -0.25828

      Control derivatives
      Xde=           0          CXde=           0
      Yde=           0          CYde=           0
      Zde=           0          CZde=           0
      Lde=           0          CLde=           0
      Mde=           0          CMde=           0
      Nde=           0          CNde=           0


      _____State matrices_____________
       Longitudinal state matrix
             -1.34403            0.594752                   0               -9.81
            -0.709114            -525.812            -129.576                   0
             0.326844            -925.341            -914.006                   0
                    0                   0                   1                   0
       Lateral state matrix
             -51.0915           -3.34435            43.3613                9.81
           -0.0642427            -3763.2            8.87812                   0
              433.973            25.6972            -600.748                   0
                    0                   1                   0                   0
```

Stability Coefficients - CG_20% - wing_angle 2°

```
XFLR5 v6.03
20.06.2011  22:25:19
PGW
Lateral_CG_20%_wing_2°
_____________________________
Performing asymmetric calculation :
Counted 2797 panel elements

Launching 3D Panel Analysis....
Using Dirichlet boundary conditions
Warning: The wing and elevator lie in the same plane z=      0 mm
It is recommended to slightly offset the wing or the elevator to avoid numerical instabilities

Type 7 - Stability polar   Mass=      76.330 kg

   ___Center of Gravity Position - Body axis____
    CoG_x=      0.0000 mm
    CoG_y=      0.0000 mm
    CoG_z=      0.0000 mm

   ___Inertia - Body Axis - CoG Origin____
    Ibxx=   3.861e+06 kg.mm²
    Ibyy=   8.652e+06 kg.mm²
    Ibzz=    1.19e+07 kg.mm²
    Ibxz=        2.35 kg.mm²

   Solving the problem...

      Calculation for control position  0.00
      Creating the influence matrix...
      Performing LU Matrix decomposition...
      Solving LU system...
      Searching for zero-moment angle... Alpha=-0.86611°
      Creating source strengths...
      Calculating doublet strength...
      Calculating speed to balance the weight...VInf = 5.93034m/s

      ___Inertia - Stability Axis - CoG Origin____
      Isxx=   3.863e+06 kg.mm²
      Isyy=   8.652e+06 kg.mm²
      Iszz=    1.19e+07 kg.mm²
      Isxz=   1.215e+05 kg.mm²

      Calculating the stability derivatives

      No active control - skipping control derivatives

      Longitudinal derivatives
      Xu=      -21.484          Cxu=    -0.010172
      Xw=       69.273          Cxa=     0.032799
      Zu=      -252.74          Czu= -0.00010081
      Zw=      -8527.1          CLa=       4.0374
      Zq=      -2565.5          CLq=       8.1373
      Mu=        10.28          Cmu=     0.016303
      Mw=      -1650.3          Cma=      -2.6171
      Mq=      -1681.5          Cmq=      -17.864
      Neutral Point position= 193.53061mm


      Lateral derivatives
      Yv=      -836.28          CYb=     -0.39596
      Yp=      -41.877          CYp=    -0.016732
      Yr=       1160.4          CYr=      0.46363
      Lv=       7.9899          Clb=    0.0015962
      Lp=      -3121.9          Clp=     -0.52631
      Lr=       145.41          Clr=     0.024514
      Nv=       1110.5          Cnb=      0.22185
      Np=      -1.4428          Cnp= -0.00024323
      Nr=      -1534.6          Cnr=     -0.25872

      Control derivatives
      Xde=            0         CXde=            0
      Yde=            0         CYde=            0
      Zde=            0         CZde=            0
      Lde=            0         CLde=            0
      Mde=            0         CMde=            0
      Nde=            0         CNde=            0


      _____State matrices_____________
       Longitudinal state matrix
             -0.281467           0.907543                  0              -9.81
              -3.3112           -111.714           -27.6809                  0
              1.18818           -190.738           -194.347                  0
                    0                  0                  1                  0
       Lateral state matrix
             -10.9561          -0.548635             9.2715               9.81
              5.00577            -808.44            33.5965                  0
              93.3836           -8.37715           -128.637                  0
                    0                  1                  0                  0
```

Stability Coefficients - CG_20% - wing_angle 4º

```
XFLR5 v6.03
20.06.2011  22:27:07
PGW
Lateral_CG_20%_wing_4º
_____________________________________
Performing asymmetric calculation :
Counted 2797 panel elements

Launching 3D Panel Analysis....
Using Dirichlet boundary conditions
Warning: The wing and elevator lie in the same plane z=      0 mm
It is recommended to slightly offset the wing or the elevator to avoid numerical instabilities

Type 7 - Stability polar   Mass=      76.330 kg

   ___Center of Gravity Position - Body axis____
    CoG_x=      0.0000 mm
    CoG_y=      0.0000 mm
    CoG_z=      0.0000 mm

   ___Inertia - Body Axis - CoG Origin____
    Ibxx=   3.861e+06 kg.mm²
    Ibyy=   8.652e+06 kg.mm²
    Ibzz=    1.19e+07 kg.mm²
    Ibxz=        2.35 kg.mm²

   Solving the problem...

      Calculation for control position  0.00
      Creating the influence matrix...
      Performing LU Matrix decomposition...
      Solving LU system...
      Searching for zero-moment angle... Alpha=-1.65293°
      Creating source strengths...
      Calculating doublet strength...
      Calculating speed to balance the weight...VInf = 4.07971m/s

      ___Inertia - Stability Axis - CoG Origin____
      Isxx=   3.868e+06 kg.mm²
      Isyy=   8.652e+06 kg.mm²
      Iszz=   1.189e+07 kg.mm²
      Isxz=   2.318e+05 kg.mm²

      Calculating the stability derivatives

      No active control - skipping control derivatives


      Longitudinal derivatives
      Xu=     -17.577         Cxu=   -0.012097
      Xw=      59.768         Cxa=    0.041135
      Zu=     -367.53         Czu= -0.00030964
      Zw=     -5895.5         CLa=       4.0576
      Zq=     -1780.5         CLq=       8.2091
      Mu=      13.485         Cmu=    0.031086
      Mw=     -1089.8         Cma=     -2.5123
      Mq=     -1148.7         Cmq=      -17.74
      Neutral Point position= 184.85377mm


      Lateral derivatives
      Yv=     -578.88         CYb=    -0.39842
      Yp=      -18.66         CYp=   -0.010838
      Yr=      797.11         CYr=     0.46297
      Lv=      12.818         Clb=   0.0037222
      Lp=     -2168.4         Clp=    -0.53141
      Lr=      205.74         Clr=    0.050421
      Nv=      770.69         Cnb=     0.22381
      Np=      -74.75         Cnp=   -0.018319
      Nr=     -1056.7         Cnr=    -0.25897

      Control derivatives
      Xde=           0        CXde=           0
      Yde=           0        CYde=           0
      Zde=           0        CZde=           0
      Lde=           0        CLde=           0
      Mde=           0        CMde=           0
      Nde=           0        CNde=           0


      _____State matrices_____________
       Longitudinal state matrix
             -0.230275          0.783019                 0             -9.81
             -4.81506          -77.2367          -19.2469                 0
              1.55855          -125.959          -132.772                 0
                    0                 0                 1                 0
       Lateral state matrix
             -7.58393         -0.244467            6.3633              9.81
              7.20592          -561.689           47.9269                 0
              64.9407          -17.2319          -87.9183                 0
                    0                 1                 0                 0
```

Stability Coefficients - CG_20% - wing_angle 6°

```
XFLR5 v6.03
20.06.2011  22:39:49
PGW_tail_inverted
Lateral_CG_20%_tail_inverted_wing_6°
_____________________________
Performing asymmetric calculation :
Counted 2797 panel elements

Launching 3D Panel Analysis....
Using Dirichlet boundary conditions
Warning: The wing and elevator lie in the same plane z=      0 mm
It is recommended to slightly offset the wing or the elevator to avoid numerical instabilities

Type 7 - Stability polar   Mass=      76.330 kg

   ___Center of Gravity Position - Body axis____
    CoG_x=      0.0000 mm
    CoG_y=      0.0000 mm
    CoG_z=      0.0000 mm

   ___Inertia - Body Axis - CoG Origin____
    Ibxx=   3.861e+06 kg.mm²
    Ibyy=   8.652e+06 kg.mm²
    Ibzz=    1.19e+07 kg.mm²
    Ibxz=        2.35 kg.mm²

   Solving the problem...

      Calculation for control position  0.00
      Creating the influence matrix...
      Performing LU Matrix decomposition...
      Solving LU system...
      Searching for zero-moment angle... Alpha=-3.39765°
      Creating source strengths...
      Calculating doublet strength...
      Calculating speed to balance the weight...VInf = 3.90530m/s

      ___Inertia - Stability Axis - CoG Origin____
      Isxx=   3.889e+06 kg.mm²
      Isyy=   8.652e+06 kg.mm²
      Iszz=   1.187e+07 kg.mm²
      Isxz=   4.756e+05 kg.mm²

      Calculating the stability derivatives

      No active control - skipping control derivatives

      Longitudinal derivatives
      Xu=     -11.715         Cxu=  -0.0084229
      Xw=      97.596         Cxa=    0.070171
      Zu=     -383.97         Czu=   -0.000353
      Zw=     -6040.9         CLa=       4.3434
      Zq=     -1797.5         CLq=       8.6575
      Mu=      26.278         Cmu=    0.063282
      Mw=     -1398.3         Cma=      -3.3675
      Mq=     -1185.7         Cmq=      -19.129
      Neutral Point position= 231.47576mm


      Lateral derivatives
      Yv=     -3703.9         CYb=       -2.663
      Yp=     -2553.1         CYp=      -1.5491
      Yr=        5153         CYr=       3.1265
      Lv=     -264.94         Clb=   -0.080375
      Lp=     -2337.8         Clp=    -0.59849
      Lr=      631.31         Clr=     0.16162
      Nv=      5098.8         Cnb=       1.5468
      Np=      3443.5         Cnp=     0.88156
      Nr=     -7092.1         Cnr=      -1.8156

      Control derivatives
      Xde=           0        CXde=           0
      Yde=           0        CYde=           0
      Zde=           0        CZde=           0
      Lde=           0        CLde=           0
      Mde=           0        CMde=           0
      Nde=           0        CNde=           0


      _____State matrices_____________
       Longitudinal state matrix
             -0.153478            1.27861                  0              -9.81
              -5.03037           -79.1421           -19.6435                  0
               3.03718           -161.619           -137.047                  0
                     0                  0                  1                  0
       Lateral state matrix
             -48.5246           -33.4486            63.6038               9.81
             -15.6772           -568.405            89.7102                  0
              428.862            267.286             -593.8                  0
                     0                  1                  0                  0
```

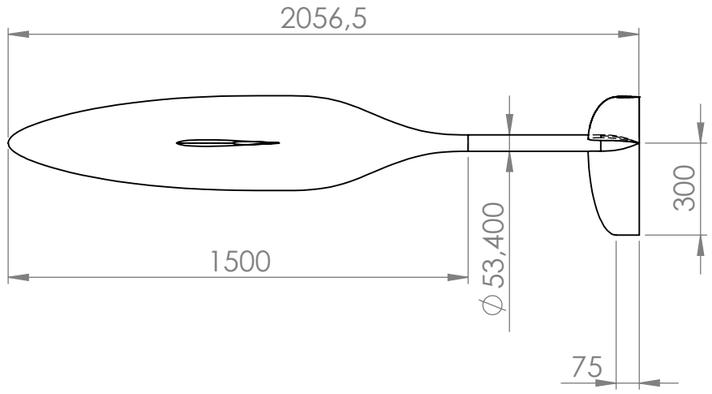

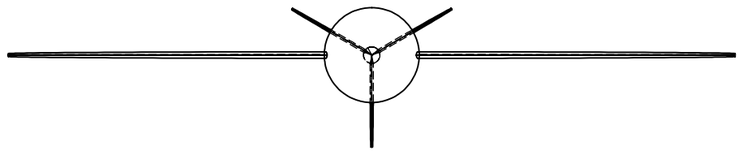

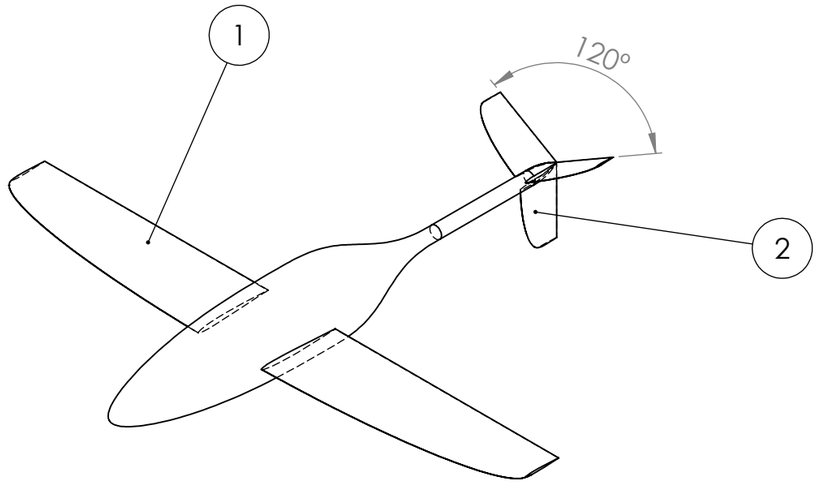

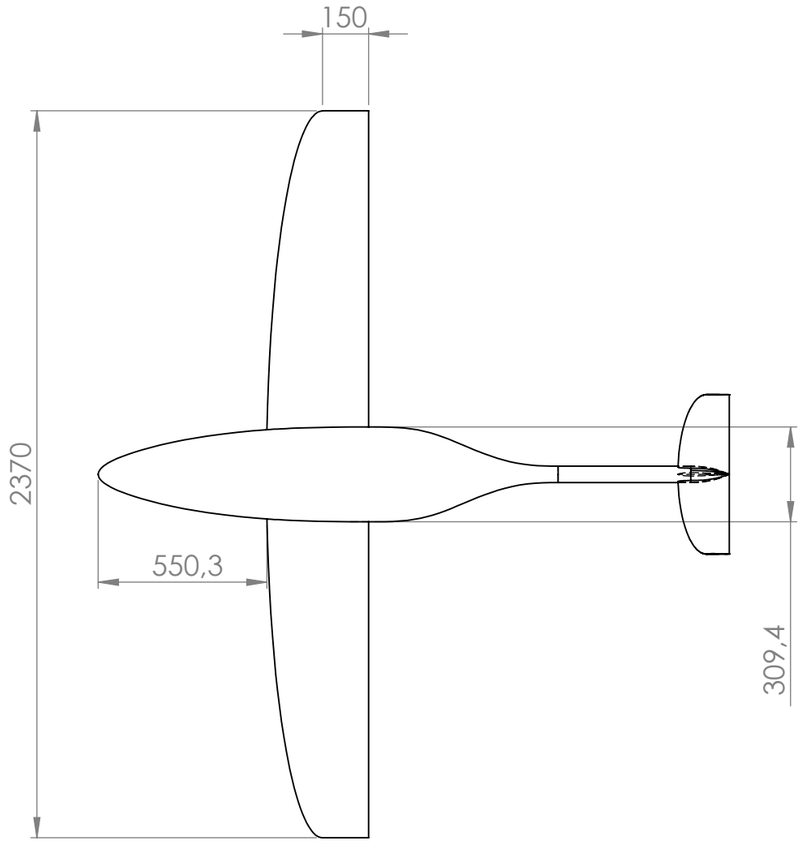

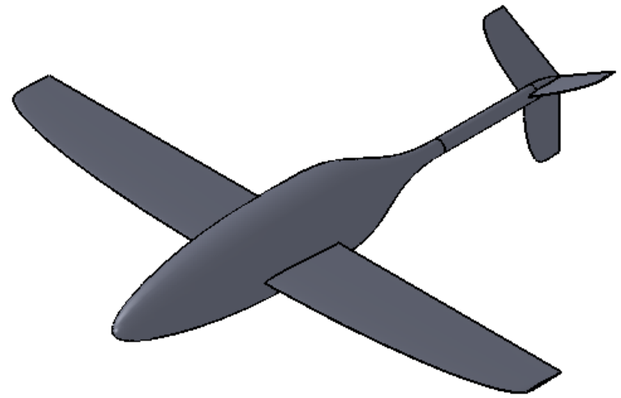

1- Mean chord of wings - 300 mm

2 - Mean chord of tail fin - 150 mm

ALL DIMENSIONS ARE IN MILLIMETERS			
	NAME	DATE	TITLE: PGW_Outer_Shape - General Dimensions
DRAWN	JOAO MORGADO	20/06/2011	
VOLUME: 76,33 dm^3		MATERIAL: N/A	DWG NO. 1 A3
		WEIGHT: N/A	SCALE:1:20 SHEET 1 OF 1

ICEUBI2011
International Conference on Engineering UBI2011
Innovation & Development

Persistent Gliding Waterframe - The Waterframe Conceptual Project

MORGADO, J.[(1)] SILVESTRE, M.[(2)],
[(1)] Dept. of Aerospace Science, The University of Beira Interior, Portugal
[(2)] Dept. of Aerospace Science, The University of Beira Interior, Portugal
email: joaomorgado23@gmail.com

Conference Topic – CT 01

Abstract

Persistent Gliding Waterframe (PGW) is a five year project, in collaboration with University of Saint Thomas, located in USA, whose objective is to develop a small, low cost, efficient autonomous underwater glider. (1) The PGW is a specific type of underwater vehicles which are designed to glide from ocean surface to a programmed depth and back while collect data along a sawtooth trajectory trough the oceans. This vehicle will aid ocean researchers by providing necessary data to predict fish populations, allowing them to provide food for the world. This paper presents the evolution of the waterframe's development which was the responsibility of UBI's team.

Key Words: Persistent gliding waterframe, PGW, autonomous underwater glider, waterframe design

Introduction

Some three-quarters of the Earth's surface is covered by water and only about 0.1% of oceans bottoms have been explored. (2) Historically, the ocean bottoms has been mainly observed using instruments lowered from research ships or, later, suspended from moorings. The relatively high cost of these observation platforms has limited their number and, consequently, the spatial and temporal density at witch oceans has been observed. (3)

To solve this problem began to be developed the Autonomous Underwater Vehicles (AUVs) and in particular the Autonomous Underwater Gliders.

Henry Stommel envisioned a world ocean observing system based on "a fleet of small neutrally-buoyant floats called Slocums" that "migrate vertically through the ocean by changing ballast, and they can be steered horizontally by gliding on wings at about a 35 degrees angle . . . During brief moments at the surface, they transmit their accumulated data and receive instructions . . . Their speed is generally about 0,5 knots." (3)

An underwater glider is a type of buoyancy propelled, fixed wing underwater vehicle without external active propulsion. (4) They alternately reduce and expand displaced volume to dive and climb through the ocean. Unlike floats, gliders additionally carry wings and control their pitch attitude to effectuate a horizontal speed component through the ocean.(5)

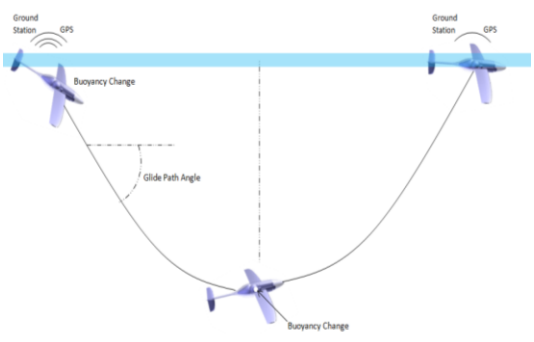

Figure 1 - Diagram of Glider Operation (8)

Buoyancy control, coupled with hydrodynamic lift is a natural choice for a platform designed to both profile and traverse the stratified ocean where gradients are near vertical and the tilt of

surfaces is of key importance. Sensible sampling dictates glide slopes steep compared to isopleths, hence ocean gliders need not attain the shallow slopes of sail planes in the atmosphere. (5)

Gliders must have both long range and high endurance to be an effective alternative to ships. Glider economy stems from long range small size, remote control, and modestly priced data communication. Their small size allows them to be launched from a small boat and recovered few months later for reuse.

Range and endurance are highly dependent on mission objectives and the operating environment. Typically, in battery powered gliders, $80\% - 85\%$ of available energy is intended to power and only $15\% - 20\%$ is devoted to control, sensors and other systems. (3)

The ratio between horizontal and vertical speeds is equal to lift over drag and is typically 2 to 4, much less than for an aeronautical glider but comparable to that of a NASA Space Shuttle.(6)

Nowadays, underwater gliders are entirely autonomous and their operation can be controlled with two-way satellite communications.(7) When are given a set of mission parameters, gliders follow them until they are changed or finished and when return to surface they send the information to main station.

The PGW will be able to locate potential areas in the ocean that would be suitable for sea farming. These farms would provide sources of protein to nations that are in need of food. The PGW will be equipped with an optical sensor that counts the number of blue-green algae in a given area of the ocean. Blue-green algae are at the bottom of the oceanic food chain and counting them allows researchers to estimate and track the fish population in given locations, and make predictions for changes in populations over time. (8) The data collected from the PGW will help researchers monitor the fish population and effectively implement sea farming.

The purpose of this paper is present the development of the waterframe for the PGW.

Design goals and constraints

PGW is a new vehicle, different from the previous vehicles developed and has its own requirements and constraints.

The main objective of the PGW is locate the potential areas in the ocean that would be suitable for sea farming by counting the number of blue-green algae in a given area and due that, the PGW shall be capable of autonomous operation for a minimum period of 4 contiguous months.

The PGW shall be launched and recovered from an ocean going ship or from a dock and the waterframe shall be designed for a deployed useful life of 5 years before reffiting.

The vehicle shall be equipped with a set of sensors so that it will be able to determine its position latitude and longitude, speed progressing forward and determine a new trajectory for the next dive cycle. Moreover, the PGW shall be able to transmitting data for a base station as well as an distress code in case of the vehicle is unable to return to surface.

The glider shall be capable to reach $300\,m$ deep and return to surface with an accuracy of $1000\,m$ left or right.

The PGW shall be capable to cover an horizontal distance of $3000\,km$ in a maximum period of $4\,months$.

Waterframe Design

Design Point

To start the design of the waterframe, it was need to take into account some of the previously presented customer requirements.

The initial estimation of speed was calculated assuming that PGW could take 4 months or just 1 month to cover the total distance.

$$v = \frac{d}{t} \qquad \textbf{Eq. (1)}$$

The range of the values for the speed varies between $0{,}29\frac{m}{s} \leq v \leq 1{,}16\frac{m}{s}$. Operating speed and range are linked to available energy through hydrodynamic drag; higher drag requires higher buoyant forcing to maintain a given speed and thereby uses energy faster. (9)

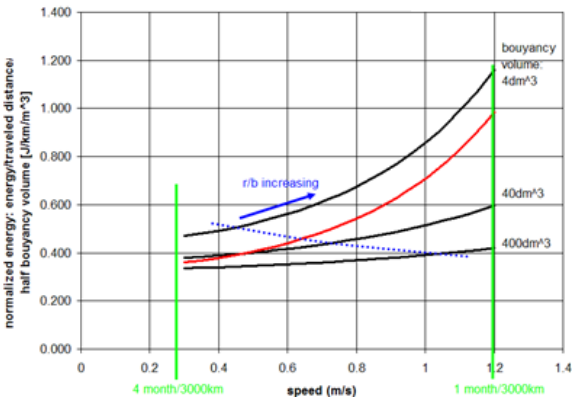

Chart 1 - Initial calculations for size of vehicle. This graph was obtained with an Aspect Ratio of 5 and red curve shows aspect ratio doubled to 10. The dashed line represents the body radius/span=0,1.

An important parameter which determines the performance of the vehicle is glide ratio. Some studies about the influence of the vehicle's size in dimensionless energy consumed by glider.

Obviously, these results are dependent on assumptions like Reynolds influence on wing section or parasite drag coefficient among many other assumptions that were made.

With this chart it was possible to conclude that the necessary battery volume to complete the full range of $3\,000\ km$ is determinant for value of total internal volume of vehicle. In worst case the necessary battery volume is 6 times the total buoyant volume and on average battery volume represents 3 times the total buoyancy volume.

The presented results gives a notion on the influence of buoyancy volume and speed on an effectiveness parameter. The internal volume needed for the PGW was initially estimated from each subsystem team and it was iterated along the design process until final value of $V_{internal} = 33{,}8\ dm^3$. To keep the design process ongoing, was determined the range of possible values to glide ratio. We fixed $c_l = 0{,}4$ (due to symmetric airfoil).

To calculate the L/D we need to calculate first the airfoil's c_{d_0} which is obtained from Mark Drela model's.

$$c_{d_{airfoil}}(c_l, Re) = (0{,}2522 * c_l^3 - 0{,}1511 * c_l^2 + 0{,}0267 * c_l + 0{,}0088) * \left(\frac{Re}{Re_{ref}}\right)^{Re_{exp}} \qquad \textbf{Eq. (2)}$$

The waterframe parasite drag coefficient can be estimated by:

$$c_{d_{0_{waterframe}}} = 1{,}3 * c_{d_{airfoil}} + 0{,}06 * \frac{A_f}{S} \qquad \textbf{Eq. (3)}$$

And the total c_d for waterframe was obtained from:

$$c_{d_{total}} = c_{d_{0_{waterframe}}} + \frac{c_l^2}{\pi * AR * e} \qquad \textbf{Eq. (4)}$$

The L/D can be obtained from:

$$\frac{L}{D} = \frac{c_l}{c_{d_{total}}} \qquad \textbf{Eq. (5)}$$

The variation of the L/D with buoyancy volume is illustrated on Chart 2. Although not the best L/D area, we decided select the smaller buoyancy volumes due the total volume of vehicle is about $0{,}03\ m^3$and as explained before, the volume for the battery is on average, 3 times the buoyancy volume. Thus the buoyancy volume is close to $0{,}006\ m^3$.

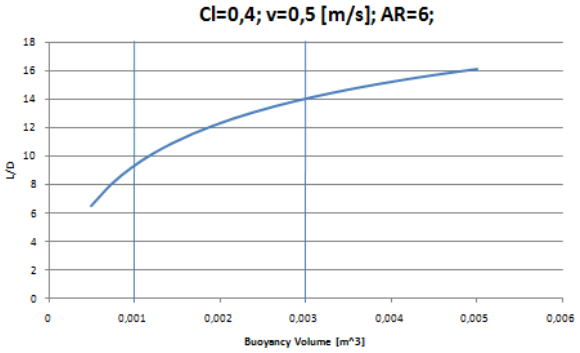

Chart 2 - Variation of L/D due to increasing buoyancy volume. The values on xx axis represent half buoyancy volume.

After select both glide ratio and buoyancy volume ranges, is possible to select the best range to speed which is between $0{,}4 \leq v \leq 0{,}6$ meters per second.

Fixing the speed again, and changing the lift coefficient, it was obtained the Chart 3, which show the best range for glide ratio for a given c_l range and 3 different speeds.

From Chart 3, it is possible to concluded that the best range of values for c_l is $0{,}30 < c_l < 0{,}45$. This is acceptable values, even for a symmetric airfoil. The values lower than $c_l = 0{,}3$ are too low, so they were not considered.

Next step on design process is starting to calculate the influence of wing area on the glide ratio. After some calculations, easily concluded that the maximum glide ratio is almost achieved with an aspect ratio $AR = 8$ and it was decided to use this value.

From wing area and wing aspect ratio is possible to calculate the dimensions of wing, which is presented on

.

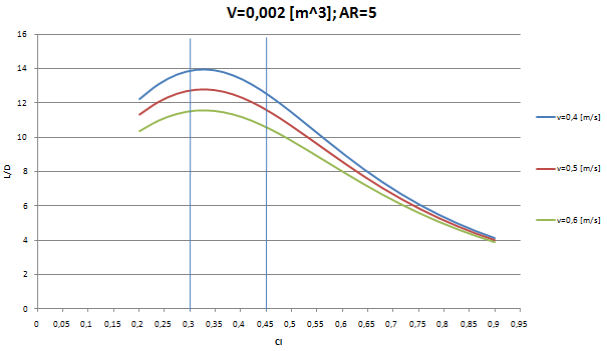

Chart 3 - Glide Ratio for different values of speed. The values were obtained for a fix buoyancy volume of $\boldsymbol{4\ dm^3}$.

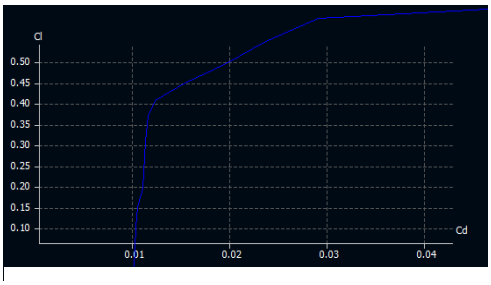

Figure 2 - Drag polar of final airfoil

Since it is a low speed vehicle its Reynolds number also will be small and due this a specific airfoil was developed for application on PGW.

The airfoil was developed based on existing airfoils with low drag to low Reynolds number.

The software used to develop the airfoil was XFLR5, which is an open source software based on X-Foil and allow the inverse design of airfoils.

The drag polar of optimized airfoil is presented on Figure 2 and it is a symmetric airfoil with a $7{,}06\%$ thickness located at $26{,}4\%$ of airfoil chord.

After developed and calculated the dimensions of wing and after optimized the airfoil, it was needed to calculate the tail dimensions.

The horizontal tail area primarily refers to balancing of the moment created by the wing. To calculate the required area to provide the adequate force to balancing the moment produced by the wing were used the tail volume coefficient method. Since the force due to tail lift is proportional to the tail area, the tail effectiveness is proportional to the tail area times the tail moment arm. This method has been used for initial estimation of tail size. The horizontal tail area is given by:

$$S_h = \frac{c_{wing}\, S\, c_h}{l_h} \qquad \textbf{Eq. (6)}$$

For a vertical tail, the wing yawing moments which must be countered are most directly related to the wing span. This means that vertical tail area is given by:

$$S_v = \frac{S\, b\, c_v}{l_v} \qquad \textbf{Eq. (7)}$$

Note that moment arms l_v and l_h is commonly approximated as the distance from the tail quarter-chord to the wing quarter-chord.

The tail volume coefficients both vertical and horizontal need to be assumed. Thus, it was assumed $c_h = 0{,}5$ and $c_v = 0{,}04$.

The chosen concept was an "Y" tail shape. The required tail area is given by:

$$S_{tail} = S_h + S_v \qquad \textbf{Eq. (8)}$$

To decide the necessary tail arm, a chart representing the influence of tail arm length into tail area was drawn.

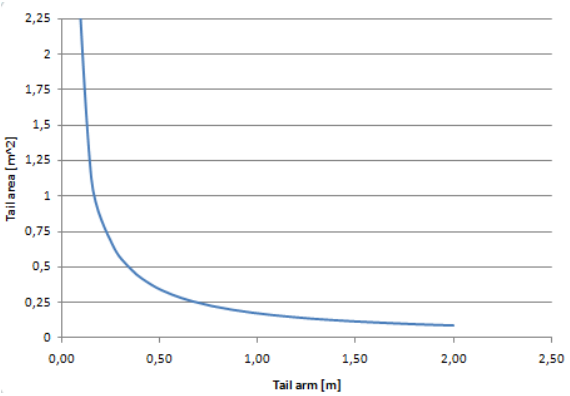

Chart 4 - Influence of tail arm length into tail area

It was decided to fix the tail arm at $1{,}3$ due to lower area needed to perform a stable PGW. The area needed for an arm of $1{,}3\ m$ is about $0{,}132\ m^2$.

After chosen the arm and consequently the required area, as tail has 3 surfaces, the area for each fin was determined by:

$$S_{fin} = \frac{S_{tail}}{3} \qquad \textbf{Eq. (9)}$$

We fixed tail aspect ratio in 2, and since we have area for each fin and its aspect ratio, it is possible to calculate its chord and its span.

The span of the fin is given by:

$$b_{fin} = \sqrt{AR_{fin} * S_{fin}} \qquad \textbf{Eq. (10)}$$

And when span is determined, easily determines the fin's chord by the Eq. (11):

$$c_{fin} = \frac{b_{fin}}{AR_{fin}} \qquad \textbf{Eq. (11)}$$

The general characteristics of the performance and dimensions of PGW are presented on table at

Appendix I.

Mechanical Design

After calculated the performance of the vehicle, it is need to decide the fuselage, wings and tail shapes. As part of an ongoing process the final geometry of the components of the vehicle are dependent of the options taken previously.

In this chapter will be presented the final geometry of fuselage, wings, tail and respective drawings.

Fuselage

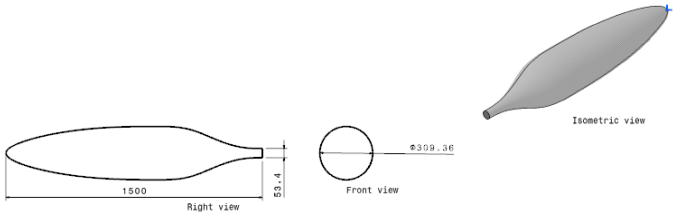

Figure 3 - Fuselage shape. All measures are in millimeters.

Due to the low Reynolds number of the fuselage, an efficient hydrodynamic shape is required to obtain a performance as high as possible. A buoyancy-powered vehicle expends energy against hydrodynamic drag, differential compressibility between the vehicle and seawater and ocean stratification.

Even at slow speeds expected to our model, the drag is the most important, by far. Our approach to counteract this constraint was to adopt a low drag shape developed by Jerome Parsons. (10)

Due to small difference between glider Reynolds number and Reynolds number used on base paper, it was decided to use the same geometry for the fuselage of the vehicle.

The resultant shape of the body of the vehicle can be seen on Figure 3.

To attach the tail at the fuselage, it was necessary develop a tail boom, that is represented on Figure 4. This boom has a constant diameter, with necessary lenght to allow the calculated tail arm and can be used to house an antenna.

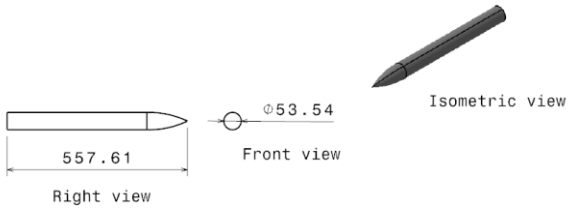

Figure 4 - Tail boom geometry. All measures are in millimeters.

Wings

It was decided to use a mid-wing since it allows a symmetrical configuration in both descent and ascent phases. Minimum induced drag occurs when lift is distributed in an elliptical fashion - i.e. elliptical wing planform without twist or sweep. But elliptical wings in low Reynolds vehicles has not an elliptical lift distribution, since the airfoil change it performance for different chords and this is not an ideal shape for wings which operating in low Reynolds environments. In elliptical wings at low Reynolds environments, parasite drag increases more (due to the low Reynolds wing tip) than induced drag decreases, so, it was adopted a mixture between elliptical and rectangular wing shape. Wing has a taper ratio $\lambda = 0{,}5$, to take the benefits of elliptical wing and be easier and simple to build. The straight

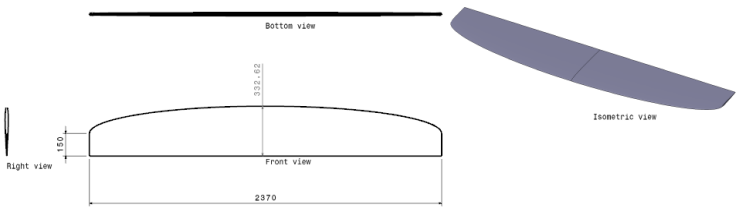

Figure 5 - Geometry of wing and its dimensions. All measures are in millimeters.

trailing edge makes the wing acts as if it has swept, creating dihedral effect, which is useful for lateral stability.

Tail

It was decided to adopt a "Y" tail, because this tail has to lower dihedral effect and vertical fin will improve latero-directional control.

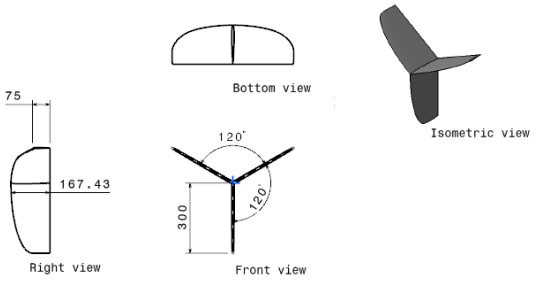

Figure 6 - Geometry of tail and its dimensions. All measures are in millimeters.

When compared with a conventional tail, the "Y" tail has a lower interference drag which is good for performance of the vehicle that is the main objective of the project.

The airfoil used on tail is the same that was developed for wing since it is symmetric and thin. The tail chord distribution along the span of the fin is the same that was used on wings. On Figure 6 it is possible to observe the tail shape and its dimensions.

Main characteristics of the tail can be easily observed in the figure above.

Discussion

An efficient, low drag waterframe for application on PGW was successfully designed respecting the constraints of the project.

A half-scale prototype is being built to conduct some experimental tests which can measure and verify the waterframe performance.

References

(1) Morgado, J., M.Sc. Thesis - "*Persistent Gliding Waterframe - The Waterframe Conceptual Project"*, University of Beira Interior, Portugal, 2011.

(2) Ross, C., *A conceptual design of an underwater vehicle*, University of Portsmouth, Ocean Engeneering 33, USA, 2006.

(3) Davis, R. *et al, "Autonomous Buoyancy-Driven Underwater Gliders"*, Institution of Oceanography, La Jolla, USA, 2002.

(4) http://www.naoe.eng.osaka-u.ac.jp/naoe/naoe7/MUG.html - last visit in 05/11/2010

(5) Eriksen, C., "Autonomous Underwater Gliders - Autonoumous and Lagrangian Platforms and Sensors (ALPS) Workshop", School of Oceanography, University of Washington, Seattle, USA, 2003.

(6) Rudnick, D., et al, "Underwater Gliders for Ocean Research" Mar. Technol. Soc. J., vol. 38, no. 1, pp. 48–59, 2004.

(7) Griffits, G., *et al, "Undersea Gliders"*, ECOR Specialist Panel on Underwater Vehicles, Journal of Ocean Tevhnology, USA, 2007.

(8) - Greene, C., Kleven, J., Deutsch, M., Engen, S., Van Sloun, F., Giancola, J., Korte, J., " *Persistent Gliding Waterframe (PGW) Project -1st year Final Report "*, University of Saint Thomas, USA, 2011.

(9) - Sherman, J., *et al, "The Autonomous Underwater Glider "Spray" "*, IEE Journal of Oceanic Engeneering, Vol. 26, USA, 2001.

(10) - Parsons, J., *et al* "Shaping of Axisymmetric Bodies for Minimum Drag in Incompressible Flow", Journal of Hydronautics, Vol. 8, 1974.

Appendix I

Table 1 - PGW Specifications

Wing Dimensions	
Aspect Ratio (AR)	8
Lift Coefficient (c_l)	0,34
Wing Area (A)	0,70 m^2
Wing Span (b)	2,37 m
Wing mean chord (c)	0,30 m
Tail Dimensions	
Thickness (t)	6,50 %
Maximum thickness point (x_t)	28,20 %
Maximum L/D	32,8
Energetic and Hydrodynamic Performance	
Total Body Volume	76,702 dm^3
Buoyancy Volume	0,004 m^3
Specific Energy	1,48 J/m
Horizontal Speed	0,399 m/s
Forward travel per cycle	8 112,43 m
Trajectory angle	4,23 °
Time per Dive[(1)]	5,66 $hours$
Number of dives	368
Total time for range completion [(1)]	87 $days$
Energy for range	4 452 543 J
Energy per unit length traveled	1,387 J/m